Faculty of Engineering & Information Technology

Finite Element Analysis of Fluid-Structure Interaction in Piping Systems

A thesis submitted for the degree of

Master of Engineering (Research)

Di Cao

CERTIFICATE OF ORIGINALITY

I certify that the work in this thesis has not previously been submitted for a degree nor has it been submitted as part of requirements for a degree except as fully acknowledged within the text.

I also certify that the thesis has been written by me. Any help that I have received in my research work and the preparation of the thesis itself has been acknowledged. In addition, I certify that all information sources and literature used are indicated in the thesis.

Signature of Candidate

ACKNOWLEDGEMENT

I would like to express my everlasting gratitude to the people who provided me support in the successful completion of my master study.

Firstly, I would like to deeply appreciate my principal supervisor, Professor Nong Zhang, for his valuable guidance and support. I am very grateful for the opportunity to further my study as Nong's student. I would also like to thank for his time, patience, and understanding. It has been a great honor to learn from him. I would never complete my research without his engineering profession and continuous inspiration. Moreover, he gave me great encouragement and assistance when my family suffered misfortunes and he helped me to get through all the difficulties.

My appreciation also goes to Dr. Ji, Dr. Luo, Chris, Paul, Cliff and all the other colleagues for their generous help and the friendship. Because of their companionship, I had a good time during my study at UTS.

Finally, I wish to thank my parents for the unconditional love and encouragement. I could not complete my study in Australia without their support and sacrifice.

TABLE OF CONTENTS

LIST OF FIGURES

LIST OF TABLES

ABSTRACT

As a typical fluid-structure interaction (FSI) system, the fluid-filled pipe widely used in industry is investigated in this thesis. It is concerned with two kinds of coupled vibration analysis, in the case of a fluid-filled pipe rigidly bonded to a steel-frame structure at a number of fixed points. One is the fluid-structure interaction analysis in the fluid-filled pipe system while the other is the structural coupling analysis between the pipe and the steel support. Considering the pipe and the steel support as two subsystems, due to the existence of these bonding points, the vibration of one subsystem will force the other to create a new particular vibration pattern. Thus a finite element approach is presented to combine the dynamic models of two subsystems to obtain the natural frequencies and mode shapes of the whole system.

The discretised finite element equation describing the free vibration of the system is deduced in a displacement-pressure format. In order to process both unsymmetrical mass and stiffness matrices due to the FSI coupling, an iterative numerical method is applied to solve the generalized eigenvalue problem and therefore the natural frequencies and model shapes of the coupled system could be obtained. In order to save computation time for modal analysis, the number of degrees of freedom of the full model is significantly reduced by employing dynamic condensation method.

Numerical examples are given to verify the feasibility of the calculation method. The obtained computational natural frequencies are compared with those obtained from experiment. Different parameters influencing the coupled vibration are discussed as well and these results could provide theoretical foundation for the optimization design

of structure-fluid coupled systems such as hydraulically interconnected suspensions fluid-filled pipe systems for vehicle braking, etc.

1 Introduction

Piping systems play a very important role in various industrial and military applications. They are used in many engineering applications for conveying gases and fluids over a wide range of temperatures and pressures. These applications include hydraulics, fluid transfer, cooling water and fuel supply. Unfortunately the pipe shell and contained fluid are also paths for vibrational energy from the pumping devices to the different receiving structures. These vibrations can cause two kinds of problems, mechanical fatigue and radiated noise. Fatigue failure may result in damage to vital parts of the installation. Hence, engineers have been concerned with this problem in power plants, refineries, oilrigs, etc. The radiated noise from pipes contributes significantly to the noise signature of naval ships and submarines besides causing discomfort. As a result, it is in the best interest of the designers to minimize the radiated noise in order to avoid detection of these military vessels. Vibration in pipes produces noise which is a major domestic problem. The noise transmits cross the walls through bathroom and kitchen pipes. Figure 1.1 shows a typical piping system in a ship.

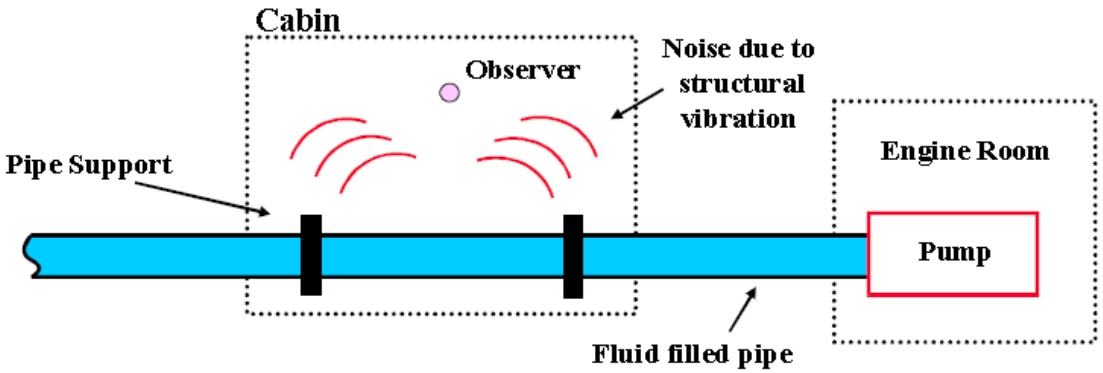

Figure 1.1 Schematic Diagram of a Typical Piping System in a Ship

With the continuous development of science and technology, the research methods of fluid-structure interaction (FSI) become mature and perfect, and an increasing number of researchers pay more attention to this area. However, they have not given enough consideration to the boundary conditions of the pipe systems, which just were simply treated as rigidly anchored constraints in the mechanical models sometimes.

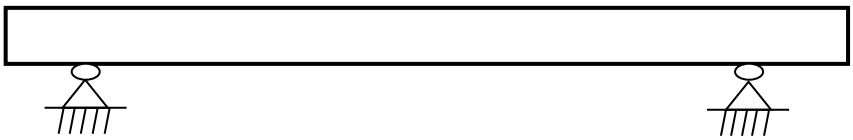

(a) A Pipe with Hinge Supports

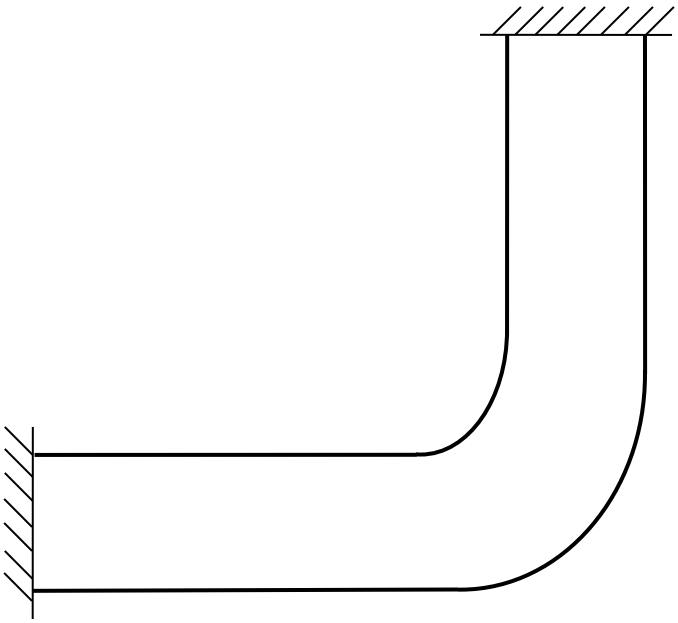

(b) A Pipe with Fixed Supports

Figure 1.2 Two Common Boundary Conditions in the FSI Study

There are some cases not applicative to use these kinds of dynamic models, such as the concrete pump and the hydraulically interconnected suspension (HIS) system. The setup of an HIS system typically comprises of, at each wheel station, a single- or double-

acting hydraulic cylinder that replaces the conventional shock and is designed to greatly reduce vehicular rollover propensity. An accumulator on either side of the vehicle is used to stabilize the flow rate of the hydraulic fluid and minimize fluid fluctuations, and the interconnecting hydraulic pipeline is mounted on the automobile chassis and moves with the car body.

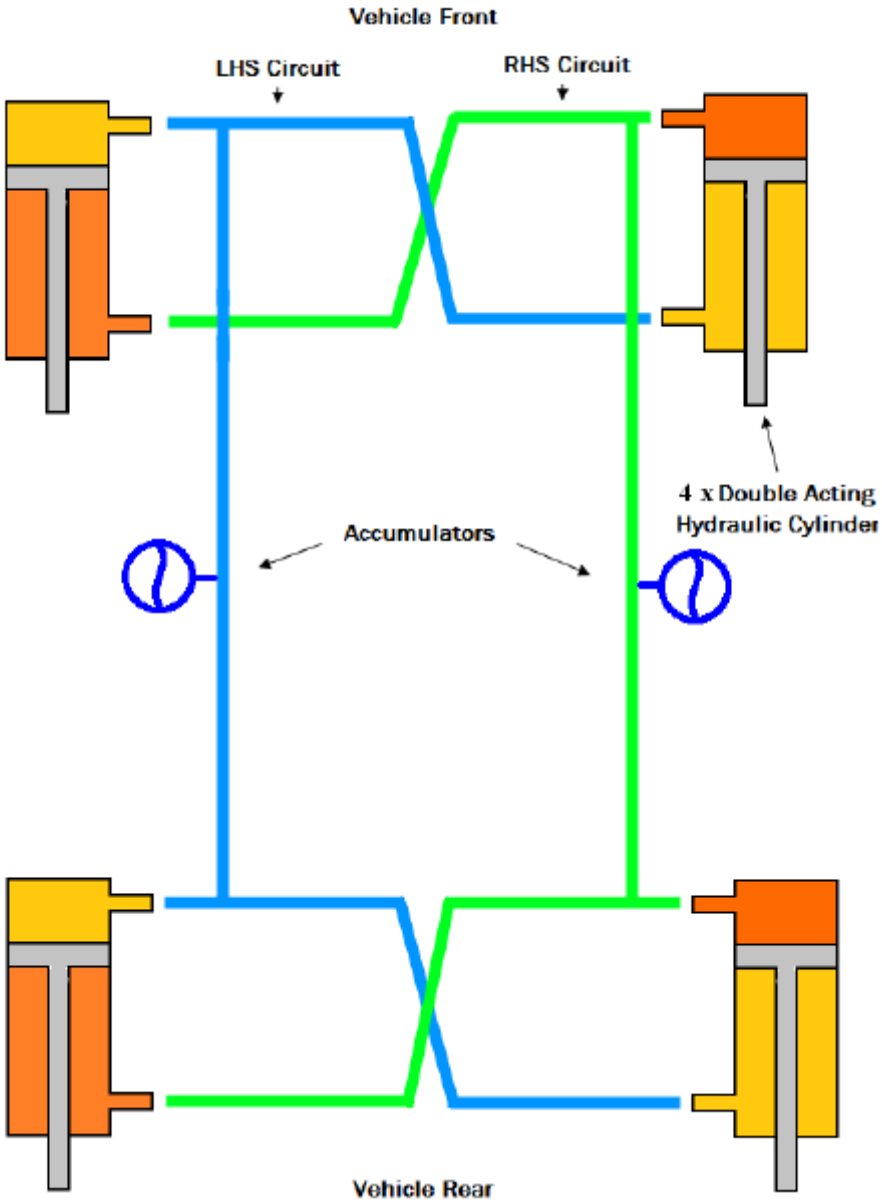

Figure 1.3 Hydraulically Interconnected Suspension System

The concrete pump is a machine used for transferring liquid concrete by pumping. It uses a remote-controlled articulating robotic arm (called a boom) to place concrete with pinpoint accuracy. The tube conveying concrete is mounted on the boom and follows its direction. Unfortunately hose whipping accident is one of the most common accidents associated with operating a concrete pump. “Hose whipping” describes the uncontrolled and rapid motion of the flexible rubber hose on the end of a concrete placement boom or other concrete delivery line. Therefore, it is significant in practice to study the vibration characteristics of the concrete pump in order to prevent and decrease the occurrence of accidents.

Figure 1.4 Construction Site with a Concrete Pump Truck

But in both cases, the boundary conditions of the pipes cannot be easily treated as rigid constraints. Because instead of fully or partly being rigidly anchored, the pipes will vibrate concomitantly with the automobile chassis or the boom which are elastomers

obviously. Only when the boundary conditions are defined properly, their vibration characteristics can be analyzed correctly.

In this thesis report, a generalized dynamic model is proposed to figure out this kind of problems. There are two subsystems constructed in the model: the fluid-filled pipe and the steel support structure. They are tightly bound together at some joint points. Because the displacements and rotations could pass from one to the other by those joint points, when one subsystem is vibrating, the other must be going to be forced to vibrate as well. Then the problems become how to solve coupled vibration responses between two subsystems. Hence in our model, two types of coupling problems need to be resolved ultimately: fluid-structure interaction in the fluid-filled pipe and the coupled vibration between two subsystems. And the finite element method (FEM) is chosen for the theoretical dynamic analysis. Experiments have been performed on laboratory test arrangements that were designed to validate the finite element model.

2 Literature Review

This chapter intends to present the necessary background knowledge to the reader to go through the work presented in this thesis. It begins with a brief background on fluid-structure interaction (FSI) in piping systems and succinctly summarizes the essential mechanisms that cause FSI. In addition, after describing various major research methods to predict FSI, a detailed review of past work on finite element method (FEM) is introduced in particular. This is followed by several model reduction techniques, which will be used for reducing a given dynamic finite element model to one with fewer degrees of freedom while maintaining the dynamic characteristics of the system. At last, a summary of studies about two significant issues related to fluid-piping motion—noise and vibration, and some industrial applications for noise reduction and vibration damping, are then provided.

2.1 Fluid-Structure Interaction

Investigations of researchers in the past make clear that classical waterhammer theory is sufficient and adequate to predict extreme loading on a system, as long as it is rigidly anchored. However, when a piping system has certain degrees of freedom, severe deviations from classical theory may occur due to motion of the system. Pressure waves exert forces which cause a compliant system to move. The motion causes pressure waves in return. This phenomenon is called Fluid-Structure Interaction (FSI) [1].

FSI is presented as an extension of conventional waterhammer theory, as in Skalak's classical article[2]. FSI, and some practical sources of excitation, are shown

schematically in Figure 2.1. Sources of excitation include not only those associated with liquid motion, but also from the structural side.

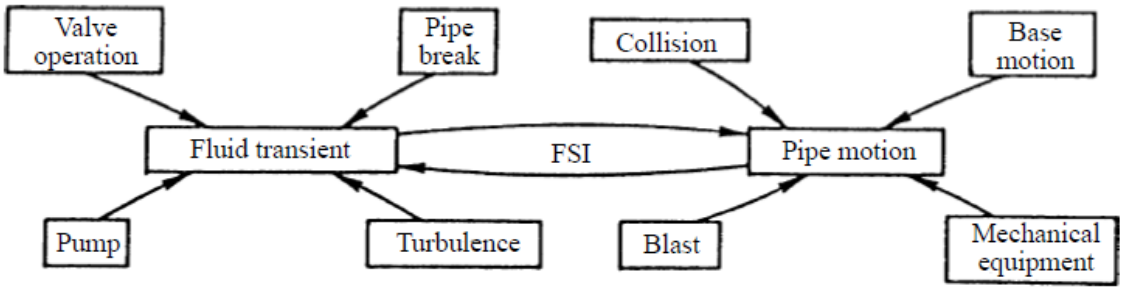

Figure 2.1 Sources of Fluid Transient and Pipe Motion [3]

In flexible piping, waterhammer waves impacting at junctions may set up vibrations that in turn may translate to a variety of structural responses (bending, torsion, shear, axial stresses) at locations distant from the junction. In addition, the vibrating junction will induce fluid transients in the contained liquid column, with acoustic waves traveling away from the junction. The result will be complex interactive motions in both the piping and liquid, with subsequent waveforms highly dependent on the geometry of the piping structure.

Pipe systems experience severe dynamic forces during a waterhammer event. When these forces make the system move, significant FSI may occur, so that liquid and pipe systems cannot be treated separately in a theoretical analysis: interaction mechanisms have to be taken into account [4].

The interaction is always caused by dynamic forces which act simultaneously on fluid and pipe. It is convenient to classify the dynamic forces in to two groups: distributed forces and local forces. The distinguished dynamic forces and their accompanying

coupling mechanisms are diagrammed in Figure 2.4 [1].

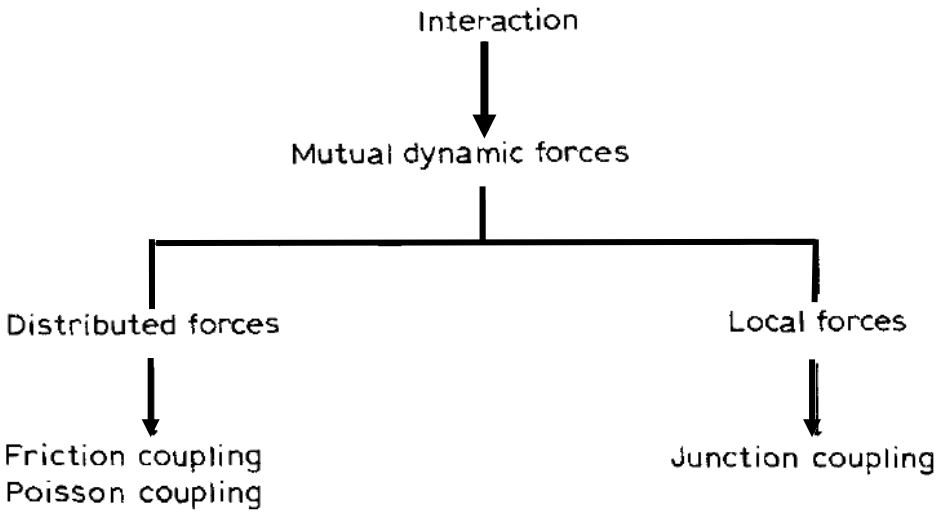

Figure 2.2 Diagram of Forces causing Fluid-Structure Interaction

Three mechanisms are distinguished which couple the dynamic behavior of fluid and piping system[5]: (1) friction coupling, (2) Poisson coupling and (3) junction coupling. Both friction and Poisson coupling are distributed along the axis of a pipe element and act along the entire piping system. The third, and often the most significant, is junction coupling, which results from the reactions set up by unbalanced pressure forces and by changes in liquid momentum only at specific places such as elbows, tees, orifices or valves.

2.1.1 Friction Coupling

Friction coupling is created by the transient liquid shear stresses acting on the pipe wall and represents the mutual friction between fluid and pipe. In most practical systems this coupling is weak.

2.1.2 Poisson Coupling

Poisson coupling relates the pressures in the fluid to the axial (longitudinal) stresses in the pipe via the contraction or expansion of the pipe wall. It is named after Poisson in connection with his contraction coefficient ν, and it is associated with the breathing or hoop mode of the pipe. Poisson coupling leads to precursor waves. These are stress-wave-induced disturbances in the liquid which travel faster than, and hence ahead of, the classical waterhammer waves. The mechanism of Poisson coupling is illustrated in Figure 2.2 [5].

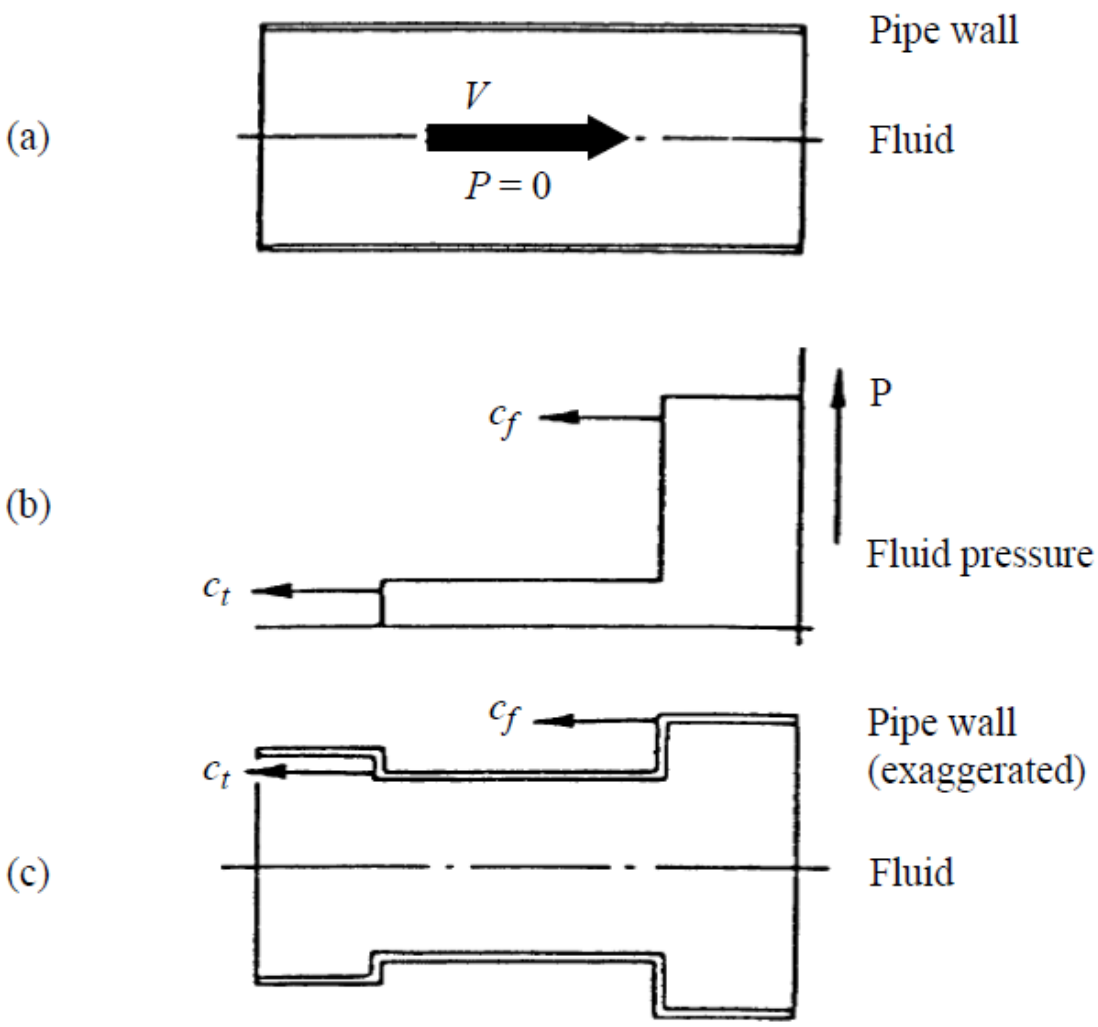

Figure 2.3 Poisson Coupling

In Figure 2.2a, fluid is flowing at velocity V and reference pressure $P = 0$. In Figure 2.2b, the fluid is stopped instantaneously, resulting in a pressure rise which propagates at speed c_f through the fluid. The pressure rise is accompanied by a radial expansion of the pipe wall as shown in Figure 2.2c. Due to this radial expansion the pipe elongates in front of the pressure rise and shortens behind. The elongation reveals itself as an axial stress wave. It propagates at the speed c_t through the pipe and causes a radial contraction of the pipe wall as in Figure 2.2c. The radial contraction causes a secondary pressure rise in the fluid as shown in Figure 2.2b. The secondary pressure rise is often referred to as precursor wave since it propagates at speed c_t , which is generally higher than the propagation speed c_f of the primary pressure rise.

2.1.3 Junction Coupling

Junction coupling describes local forces acting mutually between fluid and piping system. In general it is dominant compared to Poisson and friction coupling. A standard example is the vibrating elbow, which induces pressure waves in the liquid through a combined pumping (compressing) and storage (decompressing) action. Another example is the pipe bridge shown in Figure 2.4 [5].

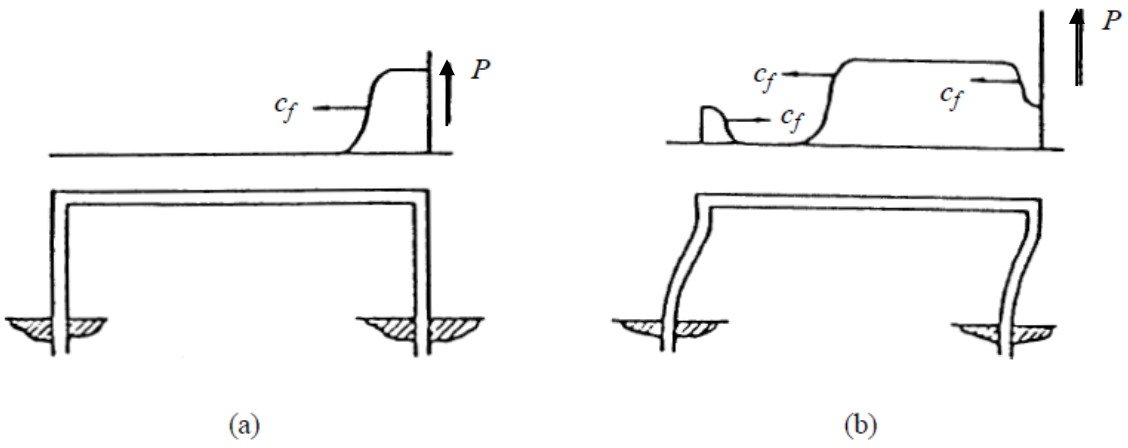

Figure 2.4 Junction Coupling

When a pressure wave has passed the elbow on the right (Figure 2.4a), the net pressure difference between the two elbows causes the pipe bridge to move (Figure 2.4b). Due to the motion the pressure drops at the right and rises at left elbow, as shown simplified in Figure 2.4b. The motion of the pipe bridge induces pressure waves in the fluid, which in return influence the motion of the bridge.

2.2 Problem Categorization of FSI

The main effects of fluid-structure interaction are problem-dependent. When compared to predictions of conventional waterhammer and uncoupled analyses, predictions including fluid-structure interaction may lead to: higher or lower extreme pressures and stresses, changes in the natural frequencies of the system, and more damping and dispersion in the pressure and stress histories.

In practice, pipe systems are never entirely rigid. Indeed, unduly rigid systems may experience extremely high stresses due to temperature effects. The problem is to judge when fluid-structure interaction is of importance. Lavooij and Tijsseling [1] proposed a provisional guideline to answer this question. The guideline is based on the characteristic time-scales of the system under consideration. It says that fluid-structure interaction is important when the time-scale of the structural behavior is: (i) smaller than the time-scale of the liquid behavior and (ii) larger than the time-scale of the excitation. The eigenperiods of the pipe system, the main periods of the waterhammer waves and, for instance, the effective closure time of a valve, provide the relevant time-scales. Uffer [6] emphasizes the importance of pressure rise times.

Calculations with fluid-structure interaction are necessary in situations with high safety requirements, mostly encountered in the nuclear and chemical industry. They may also be useful in post-accident analyses [7-9], in trouble shooting and in the development of design rules.

Fortunately, in practice it is possible to categorize the behavior into groups and in the end various simplifications can be made [10]. In Figure 2.5 we show three classical categories of such problems:

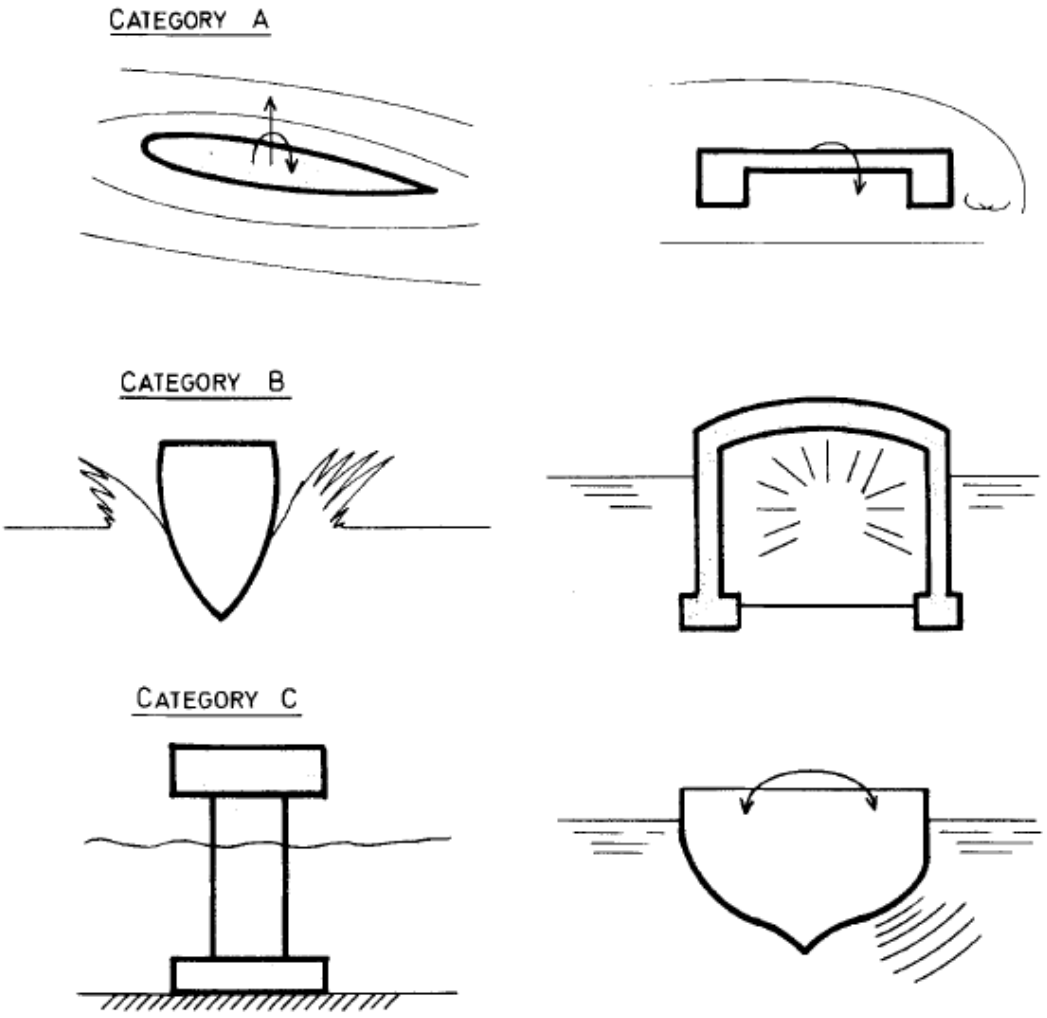

Figure 2.5 Three Broad Categories of Fluid-Solid Interaction [10]

(A) *Problems with large relative motion*——governed by flow characteristics. Here typical is the interaction occurring in flutter of aircraft wings or oscillation of suspension bridges. In such problems compressibility effects are usually non-existent.

(B) *Problems of short duration with limited fluid displacement*——such as are caused by explosions or impact in which configuration changes occur. Here total displacement is limited but compressibility is important.

(C) *Problems of long duration with limited fluid displacement*——here such phenomenon as periodic response of offshore structure to waves or earthquakes, acoustic vibrations or ship motions is characteristic.

2.3 Numerical and Parametric Studies of the Standard FSI Model

2.3.1 Time Domain

The applied research group of engineers and scientists working at Delft Hydraulics Laboratory has conducted an extensive set of numerical experiments that served to enforce the concept of coupled FSI analysis, gain further refinement related to the methods of calculation, and better understand the various mechanisms that constitute the interaction process. Lavooij and Tijsseling [1] reported the use of two different numerical models for FSI: (i) solution of both the liquid and structural governing equations by the method of characteristics (MOC) and (ii) solving the liquid equations by the method of characteristics and the structural equations by finite elements (MOC-FEM). The former utilized the Timoshenko beam theory, and the latter the Bernoulli-Euler beam theory. Both models include all of the basic coupling mechanisms. A provisional guideline was presented that suggests when interaction may be important:

$$T_{cef} < T_s < T_w$$

In which T_{cef} = effective system excitation time, T_s = eigen period of the structure, and T_w = fundamental period of waterhammer. If the structural mode is related to axial motion, then Poisson coupling may be significant. Heinsbroek et al. [11] compared the MOC and MOC-FEM models to two test problems and concluded that for axial vibration the MOC model was preferable since it leads to exact solutions, but that for lateral vibration very fine computational grids were required when compared with the MOC-FEM procedure. Heinsbroek and Tijsseling [12] studied this theme further by applying the solutions to a straight pipe subjected to an impact load and to a single-elbow pipe excited by a rapid valve closure. The effects of rotary inertia and shear deformation were investigated using the two models. It was shown that the Bernoulli-Euler model failed when extreme impact loadings are present, but that for practical pipeline systems, it provides adequate predictions.

Heinsbroek [13] made a comparison between uncoupled and coupled FSI predictions. Using the Delft Hydraulics Laboratory large-scale three-dimensional test rig, he concluded that uncoupled analysis failed to predict properly the dynamic Tresca stresses, and that the coupled model provided more accurate results. Heinsbroek and Tijsseling [14] studied the effect of support rigidity on the predicted waveforms from the Delft test rig. In particular, they focused on two items: the validity of uncoupled FSI, and magnitudes of extreme pressures and pipe stresses. The results showed that for the given test system, uncoupled FSI fails when the rigidity of the bend supports is less than the axial stiffness of one meter of pipe, and that maximum stresses seem to be higher in more flexible pipe systems, but the resulting forces on the supports are lower. They also presented an interesting diagram that shows how the main frequency of the pressure waveform varies with the assumed rigidity of the bend supports, Figure 2.6.

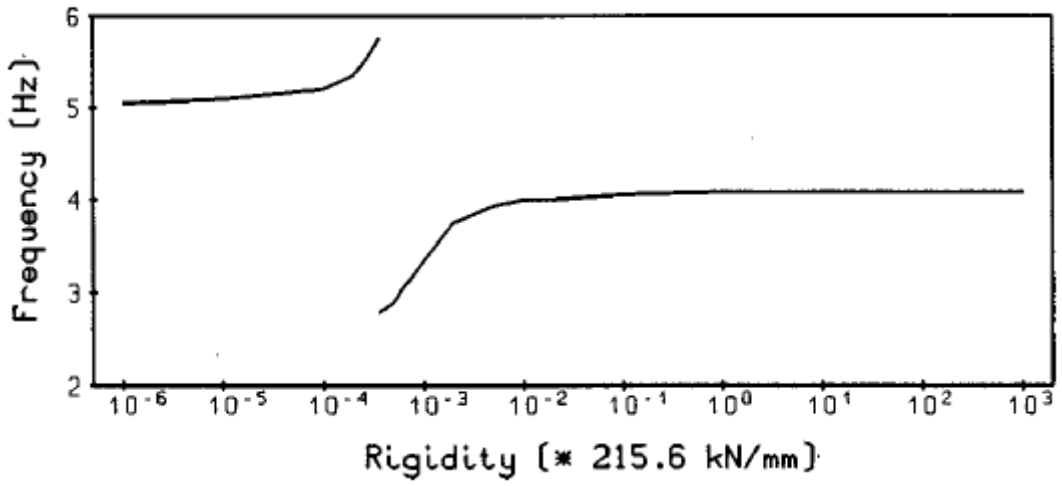

Figure 2.6 Instantaneous Closure of Valve in Reservoir-Pipe-Valve-System: Main Frequency of Pressure Wave versus Rigidity of Bend Supports [14]

Erath et al. [15] explained this behavior in terms of two idealized and coupled mass-spring systems, where one system represented the liquid and the other the solid. Additional parametric analyses were performed by Tijsseling and Heinsbroek [16] using the Delft rig data to determine the effect of bend motion. The contribution of each bend, as well as the effects of combinations of bends, on the predicted pressures and stresses was examined. The study clearly demonstrated how pipe and bend vibrations introduce the now well-established higher frequency components in the classical waterhammer waveform, with resulting pressures up to 100% higher than those predicted by the Joukowsky equation.

Tijsseling [17] revisited the simple four-equation model, with Poisson coupling being the only FSI mechanism. He demonstrated the presence of a beat in the predicted pressure waveform which he termed a Poisson-coupling beat; friction was not included in the formulation, so that damping of the signal did not occur. Bouabdallah and Massouh [18] also utilized the four-equation model to predict axial-mode FSI. In the

study, time-line interpolations were employed for the fluid characteristics; the authors reported that accompanying damping effects were negligible for the conditions posed in their simulations. Gorman et al. [19] revisited the axialcoupled model with an independent derivation that included the effects of radial shell vibration and initial axial tensional stress within the pipe. Using a finite-difference solution for the structural equations combined with the method of characteristics for the liquid, they compared their predictions of oscillatory flow with a simplified model developed by Lee et al. [20]. Both models included lateral as well as axial motions, in contrast to the formerly discussed four-equation axial models; in that respect, they were more inclusive.

2.3.2 Frequency Domain

Several groups have carried out investigations that relate to modeling in the frequency domain. A refined analytic transfer matrix model for axial fluid and pipe vibrations was reported by Charley and Caignaert [21], in which they included the variation of the pipe wall crosssection in addition to axial pipe force and velocity, and fluid pressure and velocity. Their model was compared with the more common model neglecting the area variation, and it showed a better match with measured data up to 2000 Hz. Zhang et al. [22] applied the Laplace transform to the Poisson-coupled axial FSI equations that included quasisteady laminar friction. The accuracy of their model compared favorably with experimental data and earlier developed formulations.

Svingen [23-25] described a finite element model for FSI in piping; the formulation includes axial vibration with Poisson coupling as well as bending, torsion, and junction coupling. The model was verified using laboratory data for a single-elbow vibrating pipe, and simulations were performed showing the effects of various types of coupling

on pressure and displacement spectra. A similar study was performed by Gajic et al. [26, 27], wherein their model included linearized friction damping. Svingen's model was extended (Svingen and Kjeldsen [28], Svingen [29]) to include a novel Rayleigh-like damping term for the fluid motion. By analogy, the mass proportional damping was associated with linearized steady-state friction, and the stiffness proportional term with frequency-dependent friction. Svingen and Gajic compared their methodologies in a joint study (Svingen et al. [30]). Lastly, Moussou et al. [31] analyzed Z-shaped piping that contained two vibrating elbows using both a 3D and a simplified 1D numerical code. They compared two piping/fluid models: one where the mass of the fluid is added to the mass of the pipe wall and the other a fully coupled FSI model. The correct latter approach leads to a description of the coupled modes of vibration (Fig. 2.7) and the development of a transfer function relating the structural displacement to the applied pressure perturbation.

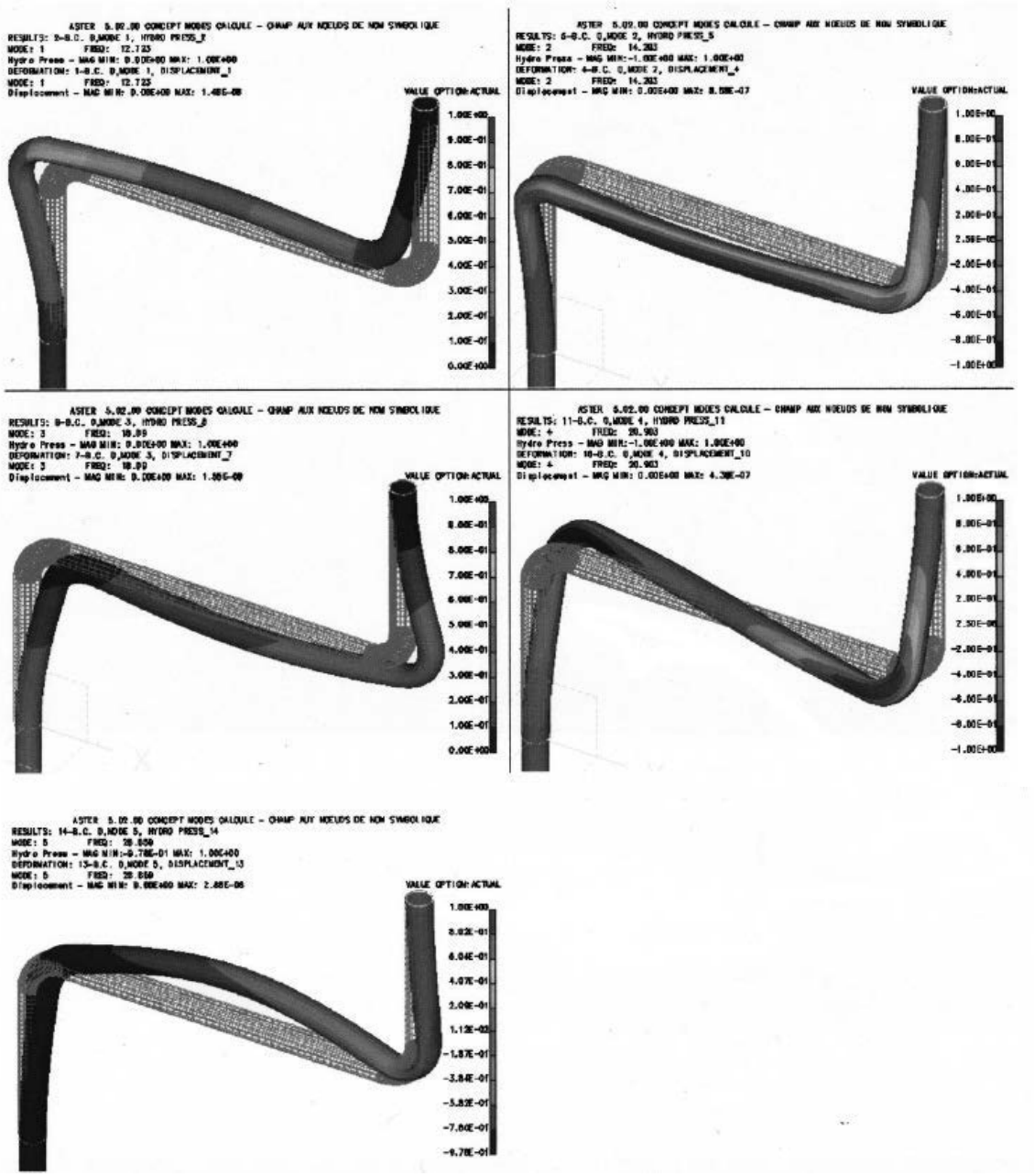

Figure 2.7 Vibration of a Z-shaped Pipe Section: Prediction Showing Fully Coupled Modes

[31]

2.4 Laboratory Measurements of the Standard FSI Model

2.4.1 Time Domain

A number of papers have dealt with the analysis of FSI in the time domain using the standard numerical or analytical methods. Most of the reported studies make use of laboratory-derived data for purposes of verification. In addition to the work of Budny [32], Wiggert et al. [33] verified a method of characteristics solution for both the contained liquid and piping components using data from a piping system that exhibited two-degree-of- freedom motion (Wiggert et al. [34]). It was noted, however, that no significant shear and bending moments were present in the experiment, so that the numerical model was not severely tested in predicting those modes.

Heinsbroek and Kruisbrink [35] validated the hybrid numerical code FLUSTRIN developed by Delft Hydraulics Laboratory using a large-scale three-dimensional test rig, Figs. 2.8 and 2.9. The code makes use of the method of characteristics to solve the fluid equations and finite elements for the Bernoulli-Euler based structural equations. These experimental data are probably the most comprehensive that have been collected for studying FSI in a compliant piping system where junction coupling plays a dominant role. The predictions show excellent correlation with the data, including fluid pressures, structural displacements, and strains—a total of seventy recorded signals (Heinsbroek and Kruisbrink [36]). In related studies, Heinsbroek and Tijsseling [12] and Heinsbroek [37] obtained numerical solutions by coupling the fluid method of characteristics solution with two different beam theories for the piping—Bernoulli-Euler and Timoshenko. In addition, they solved the combined system using only the method of characteristics. It was concluded that the Bernoulli-Euler theory combined with a

method of characteristics/finite element solution is sufficient for analyzing FSI in commercial piping systems.

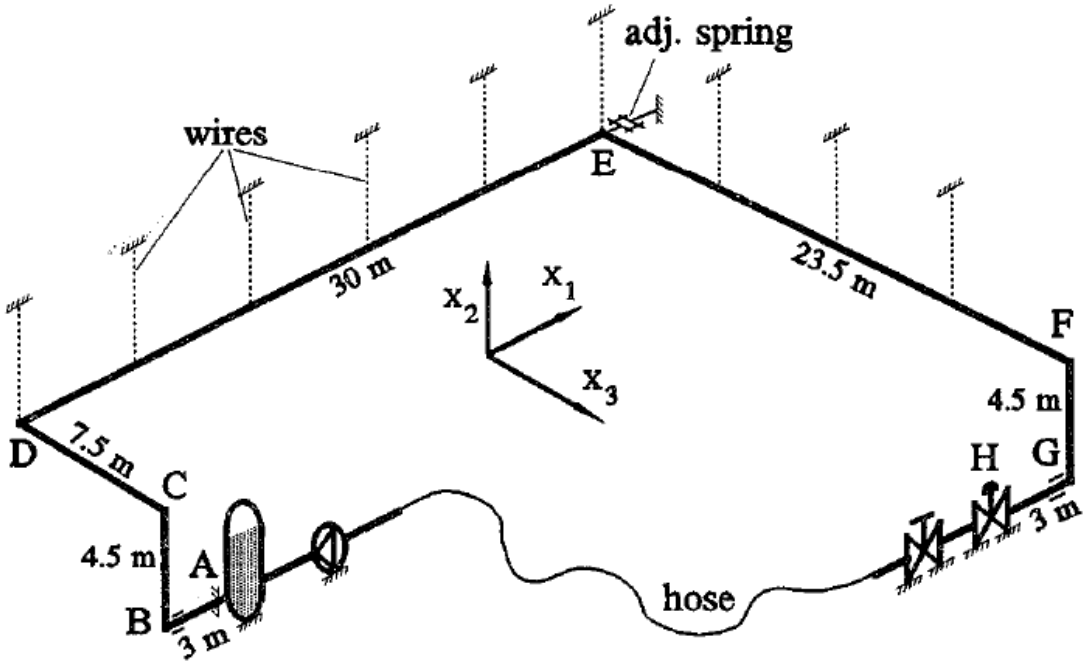

Figure 2.8 Instantaneous Closure of Valve in Reservoir-Pipe-Valve-System: Tested and Simulated Pipeline System [35]

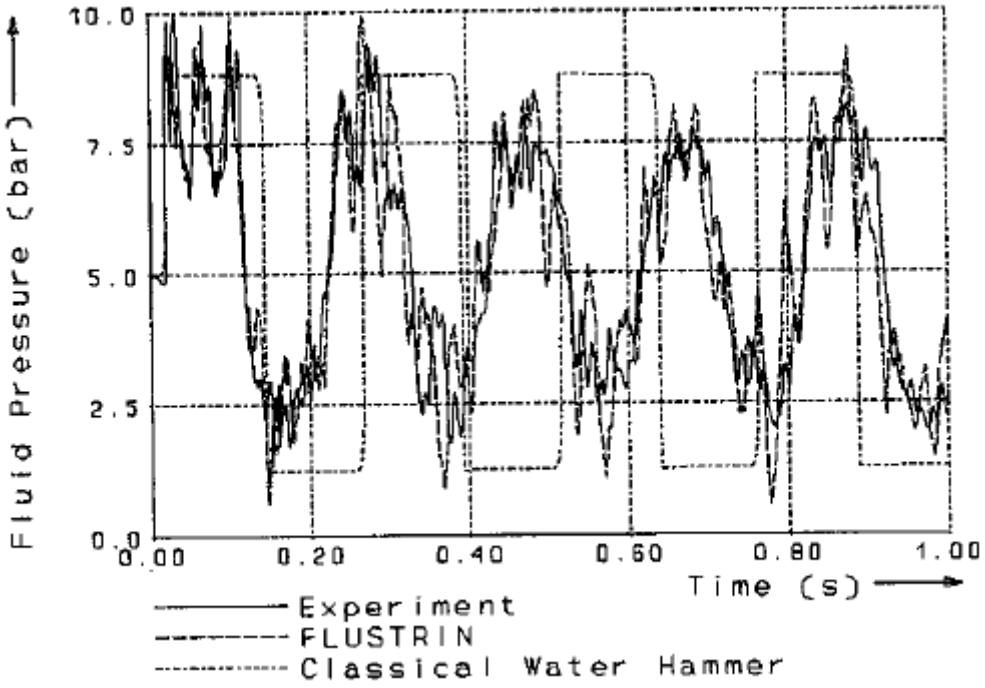

Figure 2.9 Measured and Computed Dynamic Pressure at the Shut-off Valve [35]

Kojima and Shinada [38] performed tests on a thin-walled straight pipe that exhibited axial vibration due to Poisson coupling as well as vibration at the closed-free pipe end. A Lax-Wendroff numerical method (see, eg, Mitchell and Griffiths [39]) was employed to predict the four variables of fluid velocity and pressure, and pipe velocity and strain, with comparisons shown between theory and experiment. Precursor waves were observed in their study. Poisson-coupled FSI in a long horizontal pipe excited by valve stroking was investigated by Elansary et al. [40]. They compared the classic waterhammer solution with the FSI formulation and concluded that the latter gave improved results: Poisson coupling dampened the predicted pressure oscillations. They also concluded that frequency-dependent friction would also contribute to the damping. Vardy et al. [41] isolated a suspended T-section in order to focus on the interactions between stress waves and pressure waves. They demonstrated that coupling at the boundaries might have a major influence on the resulting waveforms. As with many of the studies mentioned herein, they showed that FSI coupling alters the fundamental frequencies of oscillation when compared with those computed by isolating the liquid and structural components.

2.4.2 Frequency Domain

Several investigators over the last decade have undertaken verification of frequency-based FSI models, most of which use analytical solutions rather than numerical ones. In their earlier-mentioned study Tenteralli [42], Brown and Tenteralli [43], and Tenteralli and Brown [44] obtained data from four experiments that were designed to isolate junction, Poisson, Bourdon, and frequency-dependent friction coupling (the latter restricted to the laminar flow regime). A hydraulic servo valve excited the fluid in the piping. In addition, they conducted experiments in a three-dimensional system that combined the junction mechanisms, Figs. 2.10 and 2.11. System responses for

frequencies up to 10,000 Hz were recorded in some of the experiments. Data correlated well with Tenteralli's transmission matrix method of solution. Vibrations in a U-bend piping arrangement was investigated by Lesmez [45] and Lesmez et al. [46] with frequencies up to 32 Hz supplied by an external mechanical vibrator. The data was used to verify an analytical model based on the transfer matrix method. Pressure measurements correlated better than displacement measurements, a result that has been observed in most reported studies. Jezequel et al. [47] conducted a study that focused primarily on experimental data from a U-shaped pipe system. Their results were affected by the presence of cavitation and apparent nonlinear stiffness; consequently a high degree of damping was observed, although similarities were noted between calculated and measured displacement and pressure amplitudes and accompanying frequencies.

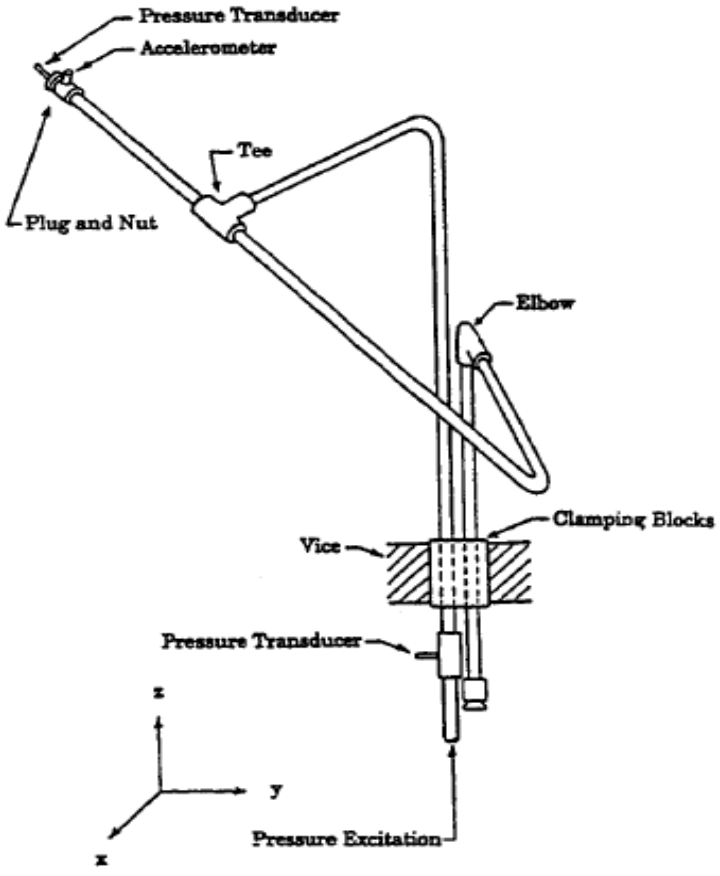

Figure 2.10 Schematic of the Experiment [42-44]

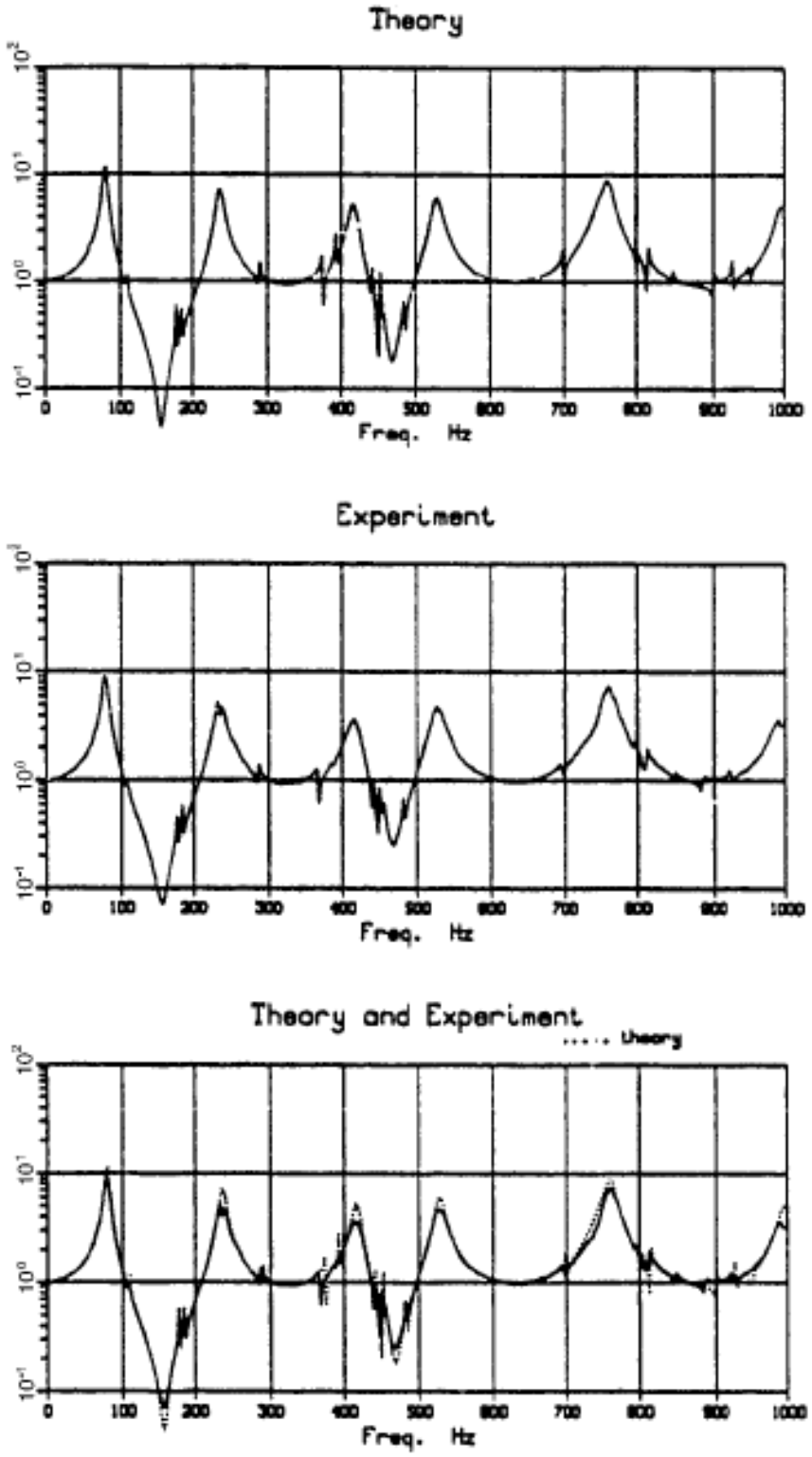

Figure 2.11 Comparison between Theory and Experiment (The ordinate is the pressure)

An experimental study performed by De Jong [48, 49] consisted of vibrating a liquid-filled pipe elbow at frequencies up to 500 Hz. Acceleration and pressure frequency

spectra were used to verify a transfer-matrix analytical model derived from the Timoshenko beam equations and combined with the Poisson-coupled waterhammer relations. The model accurately predicted the spectra up to 250 Hz; beyond that frequency, differences were attributed to inaccurate representation of the flanged connections, the elbow, and lumped masses at the pipe ends. Svingen [23, 24] published vibration data collected in an L-shaped pipe system, with excitation provided by a specially designed oscillating valve that had an operational range up to 1000 Hz, Figs. 2.12 and 2.13. The data showed some discrepancy when compared with a finite-element frequency-domain model. Zhang et al. [50] compared their Laplace transform model with improved data obtained in a repeat of the experiment published by Vardy and Fan [51]. A liquid-filled pipe freely supported in a horizontal plane was subjected to an axial impulsive force that induced junction coupling at each end of the pipe along with distributed Poisson coupling. Good agreement between measured and calculated natural frequencies was noted, especially among the lower fluid and structural modes. Jiao et al. [52] presented experimental frequency spectra obtained in 1D, 2D, and 3D oil-filled steel pipe systems. Their theoretical results included the effects of unsteady laminar friction.

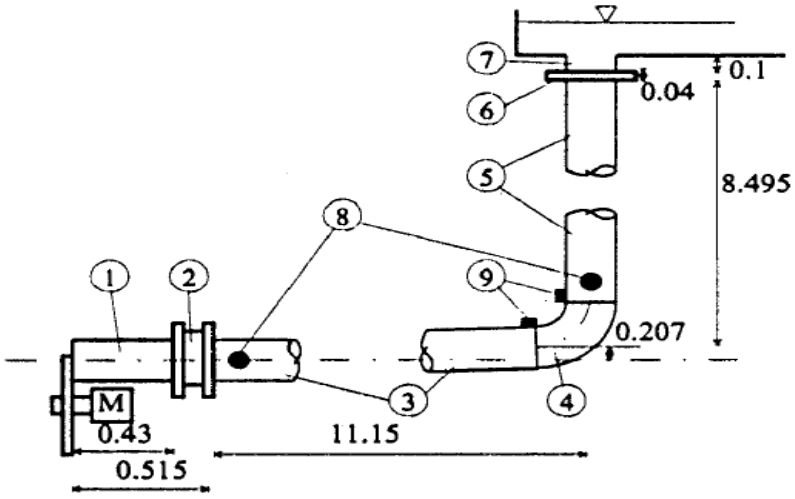

Figure 2.12 Schematic of Experimental Piping System (Dimensions are in meters) [23]

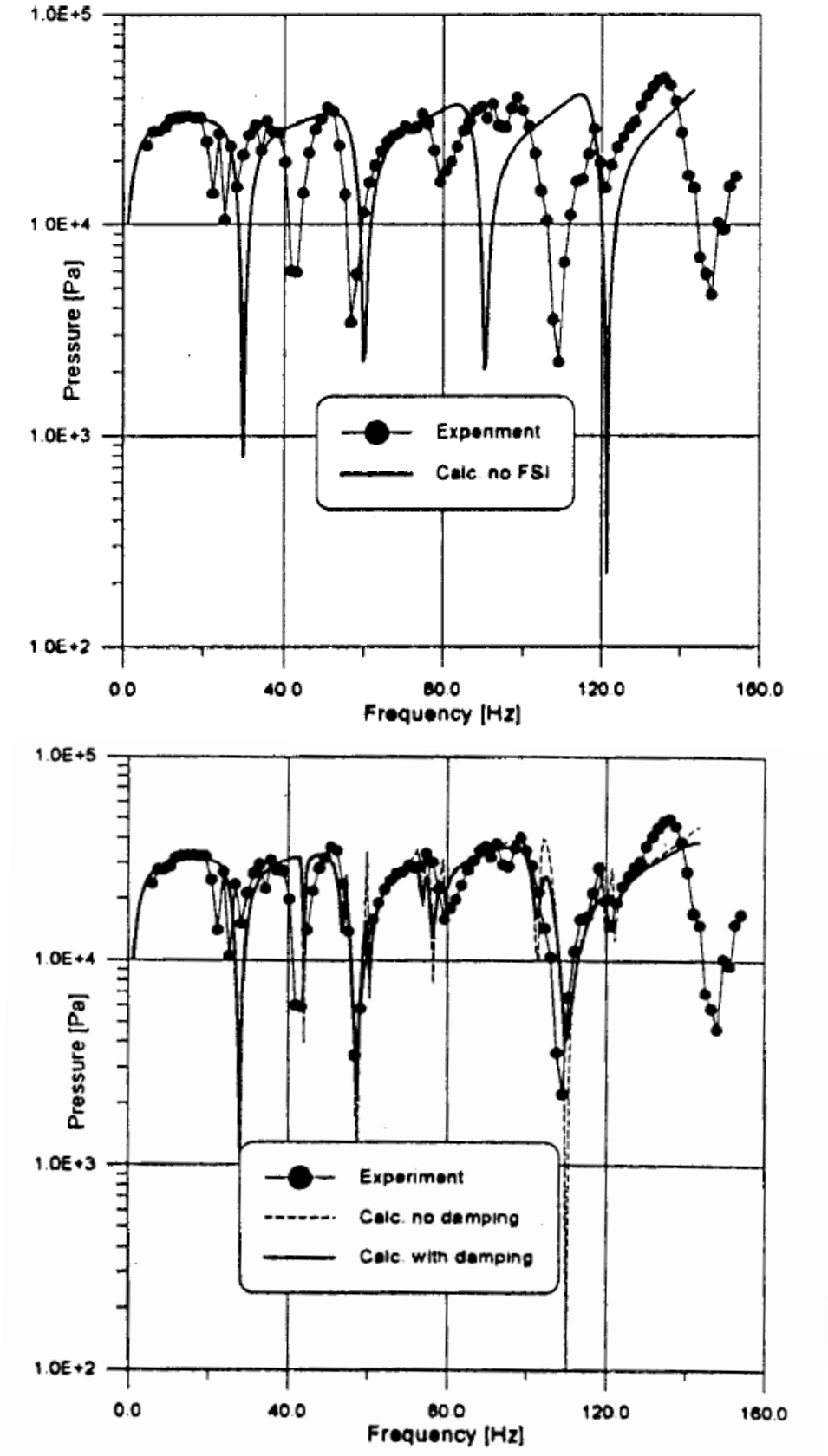

Figure 2.13 Pressure Spectra at Valve: (upper) Calculations without FSI, without damping; (lower) calculations with FSI, with damping and without damping [23]

2.5 Field measurements of the Standard FSI Model

Erath et al. [15, 53] published two related studies that demonstrate FSI in a complex industrial piping system, Fig. 2.14. They provide data for a pipe system with pump shutdown and valve closing from the nuclear power plant KRB II (Gundremmingen, Germany). Six system fluid pressures, nine bending and torsion structural moments, and three structural displacements were numerically predicted and compared with recorded waveforms. Their model consisted of utilizing two solutions in a predictor-corrector mode: a finite-difference waterhammer code coupled with a finite-element structural solution. Even though no Poisson coupling was incorporated, the numerical predictions conform as well as can be expected to the measurements, especially for the first six fundamental periods of system oscillation. Uncoupled FSI calculations were also made, and it was shown that coupled FSI more accurately predicts the true system response. It was noted that in contrast to the conclusions reached by Heinsbroek and Kruisbrink [35], the predicted waveforms are more damped when coupled FSI analysis is employed as opposed to the uncoupled scenario.

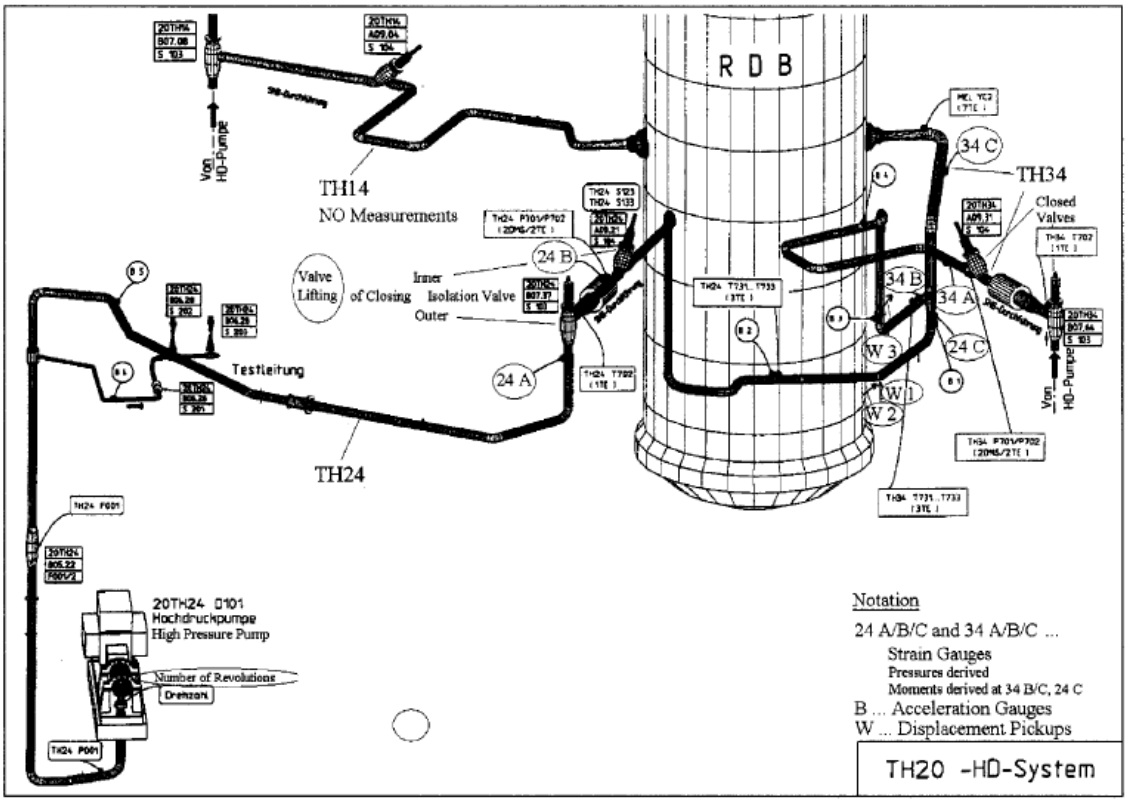

Figure 2.14 Layout of Piping System [53]

Diesselhorst et al. [54] included FSI and unsteady friction in a waterhammer code to obtain a more realistic damping behavior of pressure surges. Data measured during a pump trip in the feedwater system of a nuclear power station confirmed the effects of FSI and unsteady friction. FSI gave increased damping, reduced anchor forces, and changed resonance behavior.

2.6 Industrial Applications of the Standard FSI Model

Though yet in its infancy, interactive FSI analysis is beginning to find a niche in industrial applications. In this section we describe studies that relate to several significant issues related to fluid-piping motion: piping anchors and supports, noise, vibration, and seismic loads.

2.6.1 Anchor and support forces

A limited number of investigations have provided information related to the manner in which waterhammer forces are transmitted from piping to the pipe anchors and support mechanisms and vice versa. Two papers are quantitative while the remaining ones qualitatively deal with the subject matter. An early detailed study by Burmann and Thielen [55] presented measured pressure, strain, and accelerations from a firewater pipeline subjected to transient excitation. They recognized the presence of precursor waves resulting from the Poisson coupling, and successfully modeled the axial waveforms using the extended method of characteristics. Later, Tijsseling and Vardy [56] investigated the effect of a pipe rack on the dynamic axial behavior of a single pipe element. Pressures and velocities were induced by axial impact of a pipe suspended on a rack by a steel rod. Coulomb friction was used to model the resistance between the pipe rack and the moving pipe. The measured forces were very small, yet reasonable agreement was found between measurement and coupled FSI analysis. A simple quantitative design guideline was proposed to assess the possible influence of axial support friction.

Hamilton and Taylor [57], and Locher et al. [58] present qualitative discussions about FSI in a variety of industrial piping systems. They provide evidence of support

performance breakdown caused by a variety of excitations: condensation-induced waterhammer, priming of a liquid pipeline, pump trip on a ship-loading pipeline, and pump startup in a cooling water system that contained vapor pockets. Hamilton and Taylor [59] and Locher et al. [58] respectively give guidelines regarding acceptability criteria and practical approaches and constraints to effective modeling of FSI. Lastly, Chary et al. [60] reported observations in a boiler feed discharge-piping system in which a pipe vibrates off of its supports; they performed a transient FSI analysis using an uncoupled procedure

2.6.2 Noise reduction

Vibrations in liquid-filled piping systems are sources of airborne (audible) noise; consequently FSI analysis plays an important role in the understanding of noise generation and in dealing with means to mitigate such noise. The transfer matrix technique was employed by Kwong and Edge [61] to compare experimental data from two pipe configurations that were excited up to 5000 Hz. They showed that it was necessary to include laminar frequency-dependent friction in their analysis to obtain a better match with the experimental pressure and acceleration data. Subsequently, Kwong and Edge [62] incorporated their analytical method into an optimization procedure using genetic algorithms to determine the position of pipe clamps that minimize noise generation. Experimental results confirmed that significant noise reduction could be obtained by this technique.

De Jong and Janssens [63] describe a procedure to quantify the contribution of fluid-borne sound from machinery in piping. The equivalent-forces technique employs matrix inversion of measured transfer functions from excitation force to pipe response, with subsequent calculation of radiated sound pressure using so-called equivalent-force and

response positions. They note that it is necessary to properly account for seven (instead of six) degrees of freedom in a fluid-filled pipe. Janssens and Verheij [64], using laboratory data from a water-filled pipe system that represented the cooling-water pipe of a ship diesel engine, subsequently employed the methodology. Their predictions of sound pressure spectra trended with the measured spectra and they demonstrated the need for including the correct number of degrees of freedom.

2.6.3 Vibration damping

Experimental studies have been undertaken to reduce the vibrations that may occur due to liquid-pipe coupling. Tijsseling and Vardy [65] fitted a short section of ABS piping to a water-filled steel pipe, and excited axial vibration in the system with an impact rod. They successfully modeled the interactive waveforms using the extended method of characteristics algorithm. From both numerical predictions and experimental data, they concluded that the short plastic extension altered the vibration of the steel pipe by reducing the frequency of response, but not significantly reduced the amplitudes, and noted that a longer plastic section would result in lower amplitudes.

Munjal and Thawani [66] employed the model of Lesmez et al. [46] to calculate the transfer and loss of power in a 500-mm long oil-filled composite-rubber hose; their application was focused on isolating vibrating machinery in the automotive industry. They concluded that Poisson coupling was not of much significance, and that transmission losses in Bernoulli-Euler beams were found to be substantially lower than in Timoshenko beams. Additionally, pipe bends seemed to be beneficial for isolating vibration.

Koo and Park [67] describe a methodology to reduce vibrations in piping by spatially

placing supports in a periodic fashion along a pipe axis. They describe that a pipe constrained in this manner possesses special characteristics known as wave stop and wave propagation frequency bands, or in other words, the system responds with apparent bandpass and band-reject filters. Employing predictive models using transfer-matrix methods combined with experimental data on two piping systems, they conclude that responses can be suppressed with periodically placed supports provided that the excitation frequencies are within wave stop bands.

2.6.4 Earthquake engineering

There have been several studies reported that deal with seismic loadings on liquid-filled piping. Hara [68] analyzed a liquid sodium-filled Z-shaped piping system subjected to a one directional seismic excitation. The bending motion of the piping and the waterhammer were formulated in the frequency domain, and, using modal analysis, a two-degree-of-freedom set of equations was obtained for the fundamental vibration modes of the coupled system. Random, artificially generated, seismic loads were used to determine safety factors for a range of piping configurations. It was concluded that coupling effects were significant when the frequency ratio between the pressure wave and the pipe vibration ranged from 0.5 to 2, and the magnitude of the pressure wave induced by the coupling reached about 0.7 to 1.0 kPa per 1 Gal of excitation. Hatfield and Wiggert [69] conducted a numerical study in which an aboveground 3D pipe system was subjected to simulated earthquake ground motion; the motion was directed to excite the fundamental mode of the piping. The piping was filled with non-moving liquid, and component synthesis was used assuming no Poisson coupling. It was found that allowing the piping to be rigid produced an upper-bound estimate of pressure, and conversely, assuming the liquid to be incompressible resulted in underestimating displacement of the piping.

Bettinali et al. [70] studied the effect of earthquake motion along the axial length of a single pipe. They described the development of a coupled FSI model that includes liquid column separation and Poisson coupling. A calculation of a postulated seismic load on the pipe showed that coupled analysis predicts lower pressure amplitudes than uncoupled analysis. Ogawa et al. [71] applied an analytical model of earthquake-induced fluid transients to an in-place underground piping network. Using an artificially modified earthquake for excitation combined with frequency-domain analysis, they concluded that induced sub-atmospheric pressures in the liquid were possible, and demonstrated how two parallel pipes in the same network could have one fail axially while the other experienced no damage, because of the different waterhammer response in each pipe.

3 Problem Statement and Research Method

3.1 Problem Statement

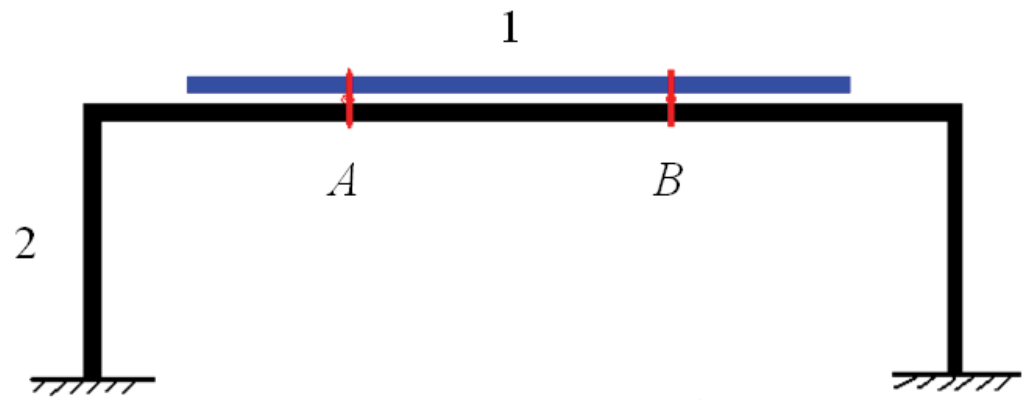

Figure 3.1 A simplified HIS system model

Figure 3.1 is a simplified model of the hydraulic interconnected suspension (HIS) system. When such a system is being installed onto a vehicle, the position where the vehicle and the system are connected has to be chosen carefully in order to avoid the frequency preserve and resonance. Thus, finding the proper parameters of the supporting parts as well as weakening the vibration transmitted from the vehicle body and the fluid would be of much practical usage.

In general, when a fluid-filled pipe is tightly bonded to a steel-frame support structure at a number of fixed points, the HIS system involves two kinds of coupled vibration. One is the fluid-structure interaction in the fluid-filled pipe while the other is the structural coupling vibration that takes place between the pipe and the steel frame structure. Therefore, the fluid-filled pipe and the steel structure are to be considered as two subsystems. The vibration of one subsystem will force the other to create a new particular vibration pattern due to the existence of the fixed bonding points. Thus a

finite element approach is presented in this thesis to combine the dynamic models of the two subsystems and to obtain the natural frequencies and mode shapes of the whole HIS system.

3.2 Finite Element Method

Normally, engineering problems can be solved by mathematical models of physical situations. Mathematical models are different equations with a set of corresponding boundary and initial conditions. However, there are many practical engineering problems for which we cannot obtain exact solutions. To deal with such problems, we resort to numerical approximations, such as the finite element method [72]. The Finite Element Method (FEM) is a numerical procedure that can be used to obtain solutions to a large class of engineering problems, not just vibration analysis. It uses integral formulations to create a system of algebraic equations, so that a solution for each element can be approximated by a continuous function. The global solution is then obtained by assembling all the individual (element) solutions, and results in a seamless or continuous approximation of the entire (global) structure. Hence the finite element method was adopted to create the full order mathematical model of the fluid-filled piping systems in this thesis.

3.3 Fluid-Structure Interaction Analysis

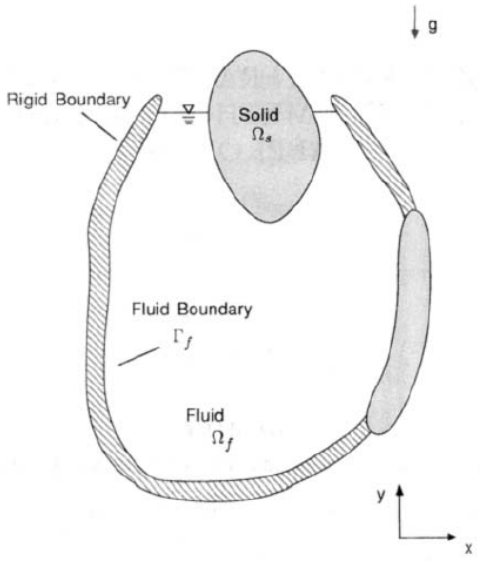

Figure 3.2 . Fluid-structure problem geometry

Numerous physical phenomena provide examples of fluid-structure interaction: the acoustic behaviour of contained fluids, the vibration of submerged and partially submerged structures, sloshing modes of fluids in open containers, etc. Figure 1 illustrates the general geometry under consideration. Many researchers have investigated general finite element methods for use in analyzing the fully coupled fluid-structure interaction problem.

3.3.1 FEM Models for Fluid-filled Pipe

For static analysis of beams considering the effect of shear deformation, a straight forward energy minimization approach was reported by Narayanaswami and Adelman [73], which yields correct finite element characteristics without using additional finite element nodal degrees of freedoms. A traditional cubic polynomial can still be used to describe the transverse displacement. The approach is briefly described below for completeness, with additional consideration of the longitudinal effect for large

deformation analysis in this work. Extension of the approach for dynamic analysis, taking into account the effect of rotary inertia, is presented subsequently.

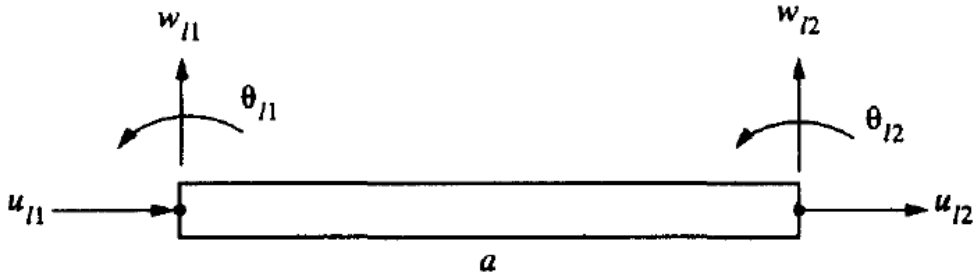

Figure 3.3 A two-node Timoshenko frame element with three degree of freedom per node

We start with the Lagrangian formulation of *Newton's law*

$$\frac{d}{dt}\frac{\partial L}{\partial \dot{x}_i} - \frac{\partial L}{\partial x_i} = F_i \tag{1}$$

$$L = T - V \tag{2}$$

with t the time, x_i the complete and independent generalized coordinates of the system, L the Lagrangian, F_i non-potential force generalized forces, T the kinetic energy and V the potential energy.

Constant shear strain within a cross-section is assumed and is described as [74]:

$$\gamma = \frac{\partial w}{\partial x} - \theta \tag{3}$$

where w denotes transverse displacement of the beam, θ the cross section rotation, and γ the shear strain.

A Timoshenko frame element with two nodes and three degrees of freedom per node is shown in Figure 3.3. The displacement fields within an element are interpolated as

$$w = [N]\{q_l\}_e,\ \theta = [\overline{N}]\{q_l\}_e,\ u = [U]\{q_l\}_e \tag{4}$$

where

$$[N] = [0 \quad N_1 \quad N_2 \quad 0 \quad N_3 \quad N_4]$$

$$[\overline{N}] = [0 \quad \overline{N}_1 \quad \overline{N}_2 \quad 0 \quad \overline{N}_3 \quad \overline{N}_4]$$

$$[U] = [U_1 \quad 0 \quad 0 \quad U_2 \quad 0 \quad 0]$$

$$\{q_l\}_e = \{u_{l1} \quad w_{l1} \quad \theta_{l1} \quad u_{l2} \quad w_{l2} \quad \theta_{l2}\}^T$$

in which

$$N_1 = 1 - \frac{1}{a(a^2 + 12g)}(12gx + 3ax^2 - 2x^3)$$

$$N_2 = \frac{1}{a(a^2 + 12g)}\left[(a^2 + 6g)ax - (2a^2 + 6g)x^2 + ax^3\right]$$

$$N_3 = \frac{1}{a(a^2 + 12g)}(12gx + 3ax^2 - 2x^3)$$

$$N_4 = \frac{1}{a(a^2 + 12g)}\left[-6gax + (6g - a^2)x^2 + ax^3\right]$$

$$\overline{N}_1 = \frac{1}{a(a^2 + 12g)}(6x^2 - 6ax)$$

$$\overline{N}_2 = \frac{1}{a(a^2 + 12g)}\left[a^3 + 12ga - (4a^2 + 12g)x + 3ax^2\right]$$

$$\overline{N}_3 = \frac{1}{a(a^2 + 12g)}(6ax - 6x^2)$$

$$\overline{N}_4 = \frac{1}{a(a^2 + 12g)}\left[3ax^2 - (2a^2 - 12g)x\right]$$

and

$$U_1 = \frac{a - x}{a}, \qquad U_2 = \frac{x}{a}$$

Where

$$g \equiv \frac{EI}{kGA}$$

and $[N]$, $[\overline{N}]$, and $[U]$ denote 1 x 6 row vectors representing shape functions for transverse displacement, cross-section rotation, and longitudinal displacement, respectively; $\{q_l\}_e$ is the element nodal degrees of freedom vector; a is the beam element length; EI is the bending rigidity; k is the shear coefficient; G is the shear modulus; A is the cross-section area of the beam element; and x is the coordinate along the longitudinal direction of the beam element.

The strain energy including the shear effect for a beam element of length a, can be described as:

$$V_e = \frac{1}{2}\int_0^a EI(\frac{\partial \theta}{\partial x})^2 dx + \frac{1}{2}\int_0^a EA(\frac{\partial u}{\partial x})^2 dx + \frac{1}{2}\int_0^a kGA\gamma^2 dx \tag{5}$$

The pipe element stiffness matrix can be obtained directly from the description of strain energy by substitution of eqns (3) and (4) into eqn (5)

$$[k_p]_e = [k_b]_e + [k_a]_e + [k_s]_e \tag{6}$$

where

$$[k_b]_e = \int_0^a EI[\overline{N}_x]^T[\overline{N}_x]dx$$

represents the effect due to bending strain,

$$[k_a]_e = \int_0^a EA[U_x]^T[U_x]dx$$

describes the effect due to axial strain, and

$$[k_s]_e = \int_0^a kGA([N_x]^T - [\overline{N}]^T)([N_x] - [\overline{N}])dx$$

accounts for the effect due to shear strain. The subscript x denotes partial differentiation.

For dynamic analysis of a short, sturdy pipe considering both the effects of shearing deformations and rotary inertia, the mass matrix including these effects needs to be determined in addition to the previous development. Using the shape functions described previously, the kinetic energy of the beam can be written as:

$$T_e = \frac{1}{2}\int_0^a m_p \left(\frac{\partial w}{\partial t}\right)^2 dx + \frac{1}{2}\int_0^a m_p \left(\frac{\partial u}{\partial t}\right)^2 dx + \frac{1}{2}\int_0^a \rho_p I \left(\frac{\partial \theta}{\partial t}\right)^2 dx \qquad (7)$$

where m_p, ρ_p, and I are the mass per unit length, mass per unit-volume, and area moment of inertia of the pipe, respectively. Substituting the shape functions and knowing that they are functions of x only, the pipe element mass matrix can be obtained:

$$[m_p]_e = [m_t]_e + [m_a]_e + [m_r]_e \qquad (8)$$

where $[m_t]_e$ and $[m_a]_e$ represent the traditional mass matrices for transverse and axial inertia effects, whereas $[m_r]_e$ describes the additional rotary inertia effect. These three matrices combined to form the element mass matrix, which can be written as

$$[m_t]_e = \int_0^a \left[N\right]^T m_p \left[N\right] dx$$

$$[m_a]_e = \int_0^a \left[U\right]^T m_p \left[U\right] dx$$

and

$$[m_r]_e = \int_0^a [\overline{N}]^T \rho_p I [\overline{N}] dx$$

Structural damping within the pipe is considered small and hence is neglected. The effects of moving fluid are treated as external forces on the support pipe. The forces turn out to be dependent on the system nodal variables and comprise the centrifugal, Coriolis, and translational inertia forces for a pipe conveying fluid with a constant flowing speed. The element mass, damping, and stiffness matrices for the fluid moving

at a constant speed v can be obtained by considering the virtual work done by the fluid forces [75], with additional consideration of the axial inertia for large deformation analysis of the fluid conveying pipe.

$$[m_f]_e = m_f \int_0^a [N]^T [N] dx + m_f \int_0^a [U]^T [U] dx + \rho_f I_f \int_0^a [\overline{N}]^T [\overline{N}] dx$$

$$[k_f]_e = -m_f v^2 \int_0^a [N_x]^T [N_x] dx \tag{9}$$

where m_f, ρ_f, denote the mass per unit length, mass per unit volume, and area moment of inertia of the fluid, respectively. $v(t)$ is the velocity of the fluid flowing in the pipe. Note that eq. (9) represents a more concise form for fluid element matrices than that shown in the work by Chu and Lin [75] by performing additional integration by parts for the original expressions.

Equations (6), (8), and (9) can be combined to form the dynamic equations of motion in the modal coordinate:

$$[m_l]_e \{\ddot{q}_l\}_e + [k_l]_e \{q_l\}_e = \{f_l\}_e \tag{10}$$

where $\{f_l\}_e$ denotes the external loads on the beam element, respectively, and

$$[m_l]_e = [m_p]_e + [m_f]_e$$

$$[k_l]_e = [k_p]_e + [k_f]_e$$

Then assembling the stiffness and mass matrices of all the elements, the total kinematic and mass matrices can be obtained. The expressions in the modal coordinates can be transformed to the global ones and combined to form the final equations of motion for the entire structure:

$$[M]\{\ddot{X}\} + [K]\{X\} = \{F\} \tag{11}$$

Where

$$[M]=\sum_{i=1}^{n}[T]_i^T[m_l]_e[T]_i\,,\ [\mathrm{K}]=\sum_{i=1}^{n}[T]_i^T[k_l]_e[T]_i\,,\ [F]=\sum_{i=1}^{n}[T]_i^T\{\mathrm{f}_l\}_i$$

in which n is the number of elements used and the coordinate transformation matrix is given as:

$$[T]_i=\begin{bmatrix}\cos\theta_i & \sin\theta_i & 0 & 0 & 0 & 0\\ -\sin\theta_i & \cos\theta_i & 0 & 0 & 0 & 0\\ 0 & 0 & 1 & 0 & 0 & 0\\ 0 & 0 & 0 & \cos\theta_i & \sin\theta_i & 0\\ 0 & 0 & 0 & -\sin\theta_i & \cos\theta_i & 0\\ 0 & 0 & 0 & 0 & 0 & 1\end{bmatrix} \tag{12}$$

3.3.2 Numerical Example 1

Figure 3.4 shows a water-filled straight pipe with two clamped end, and all the parameters as follows: Length= 2m, outer diameter= 22.85mm, inner diameter= 19.65mm; Young's modulus= 210GPa, density of pipe= 7850kg/m3, Poisson's ratio= 0.3; density of pipe= 1000kg/m, bulk modulus= 2.2GPa.

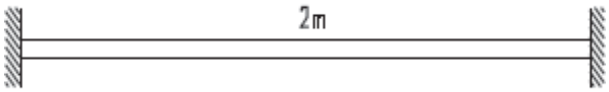

Figure 3.4 A water-filled pipe

Modal analysis for the empty pipe and the fluid only is conducted firstly.

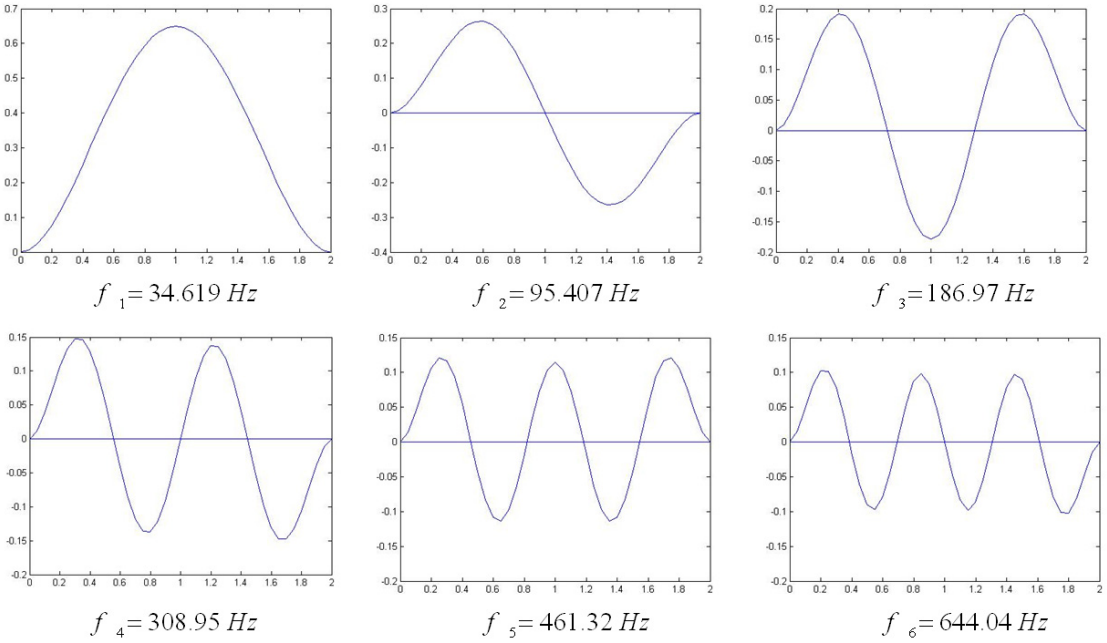

Figure 3.5 First six modes of the empty pipe

For the fluid itself, the natural frequencies and model shapes are as below.

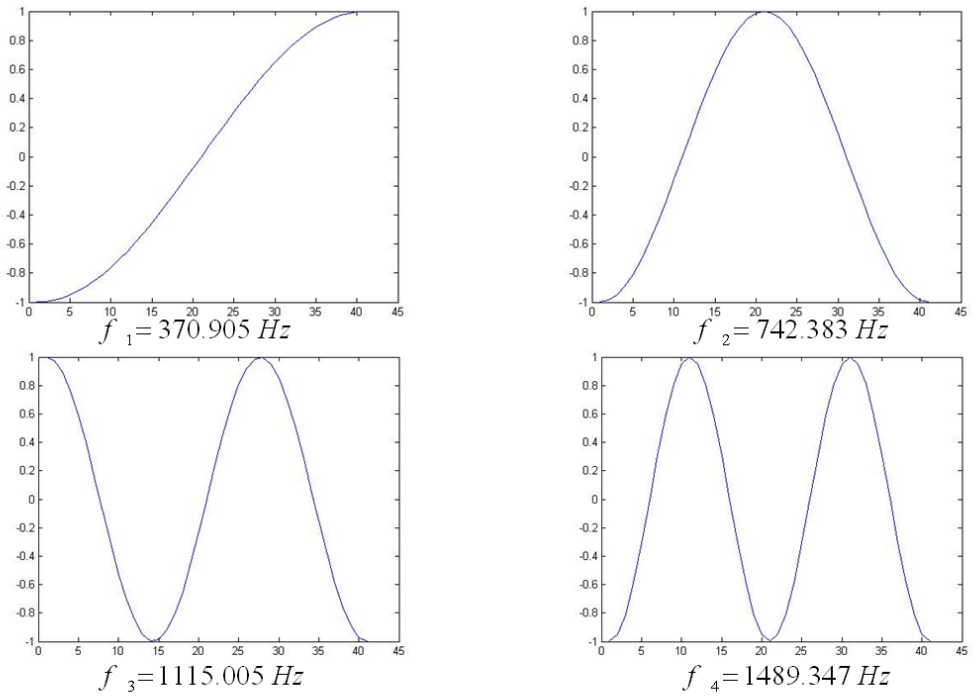

Figure 3.6 First four modes of the fluid

And then the first to sixth order natural frequencies of the water-filled pipe are obtained by equation (11).

Mode	1	2	3	4	5	6
water-filled pipe	28.588	85.344	159.864	290.012	412.36	568.27
empty pipe	34.619	95.407	186.97	308.95	461.32	644.04

Table 3.1 Natural frequencies of water-filled pipe and empty pipe

From table 3.1, it can be found that the natural frequencies of fluid-filled pipe are reduced. This is because water has much bigger density than air. If considering the fluid as added mass, it could easily be understood And this conclusion is consistent with Jaeger's [76]. Hence Because of the fluid-structure interaction, the natural frequencies of the coupled system are reduced. FSI cannot be ignored.

The modal shapes of the fluid-filled pipe system can be shown as structure modal shapes and fluid modal shapes separately. Firstly, the first six orders of structure modal shapes in the fluid-filled pipe can be compared with the modal shapes of the empty pipe.

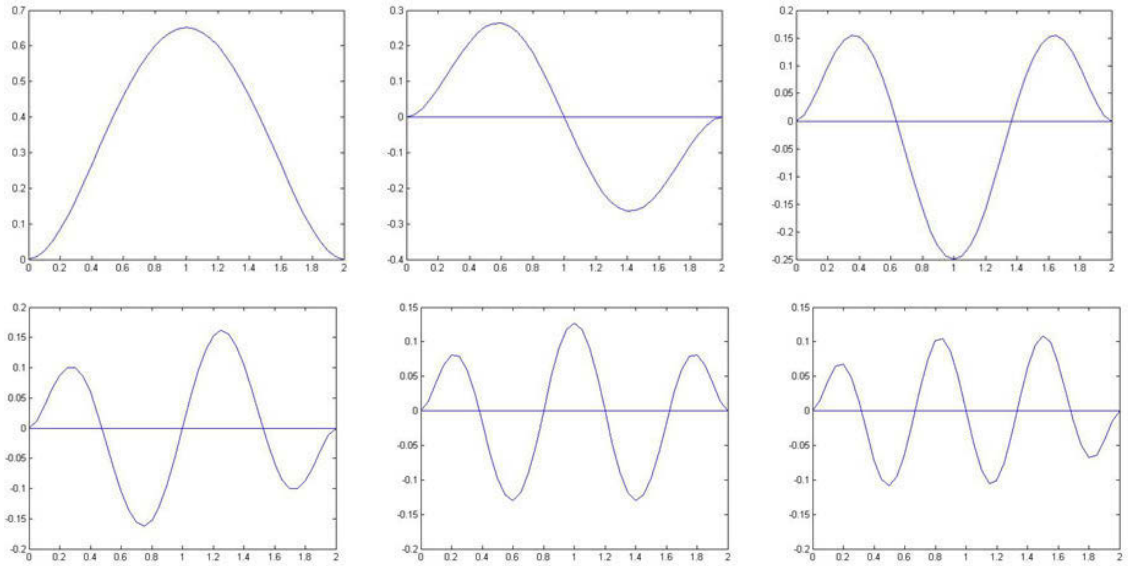

Figure 3.7 First six modal shapes of the fluid-filled pipe

By comparing the previous Figures 3.5 and 3.7, a conclusion could be drawn that the effect of the fluid and FSI to these six modal shapes is not big, since such modal shapes are mainly determined by the structural deformation of the pipe.

Next, the 3rd, 4th order fluid modal shapes in the fluid-filled pipe are shown in Fig. 3.8.

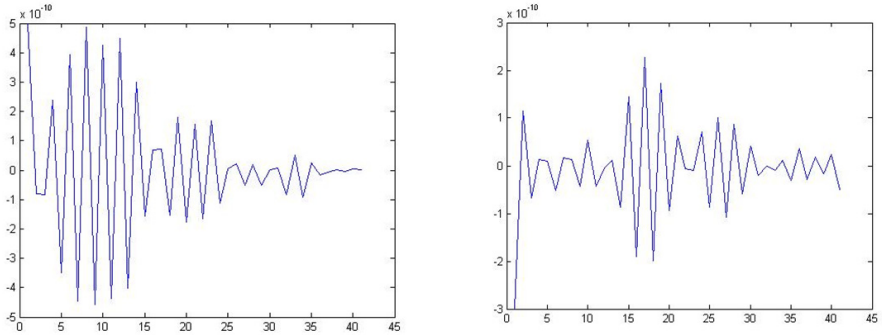

$f_3 = 159.864\ Hz$ $f_4 = 290.012\ Hz$

Figure 3.8 Pressure distribution of fluid induced by the in-plane vibration of structure

Initially, the fluid had no modes at these frequencies. Nevertheless, corresponding modes of fluid, namely “Pressure Distribution”, are generated afterwards due to the fact that the vibration of the pipe structure has changed the pressure of the fluid.

In fact, such influence is exerted in a mutual way. On one hand, the vibration of structure could lead to the pressure change of the fluid inside. On the other hand, the pressure change of the fluid will induce the vibration of the structure. Please refer to Figure 3.9 shown below.

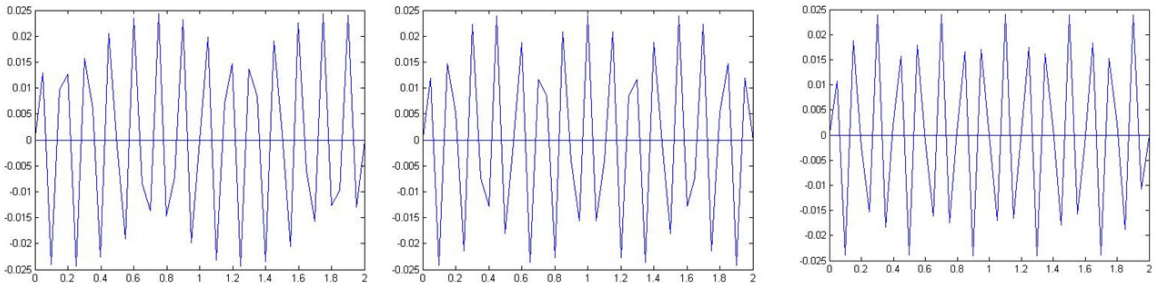

Figure 3.9 Modal shapes of the structure induced by the fluid inside

This proves that due to the FSI, the fluid will make the structure outside generate corresponding vibration of modes.

3.4 Solid Coupling Analysis

3.4.1 Mathematical Model

Now for the hydraulic interconnected suspension system in Fig. 3.10, if the fluid part is ignore, two finite element models for the solid part of the pipe and the steel frame could be obtained via equation (11). Therefore the question becomes how to assemble the two independent FEM models into a whole system?

Here the rigid connection characteristics of those binding nodes need to be utilized. That is, the degrees of freedom belonging to the pipe and the steel frame are the same at binding nodes A and B, which means they have same displacement vectors and acceleration vectors.

For the free vibration equation of the pipe (subsystem 1),

$$M_1\ddot{X}_1 + K_1X_1 = 0 \tag{13}$$

rearrange displacement vector and acceleration vector, to move the degrees of freedom belonging to those binding nodes to the bottom.

$$\begin{bmatrix} M_{11} & M_{12} \\ M_{21} & M_{22} \end{bmatrix}\begin{Bmatrix} \ddot{X}_{1-1} \\ \ddot{X}_{1-2} \end{Bmatrix} + \begin{bmatrix} K_{11} & K_{12} \\ K_{21} & K_{22} \end{bmatrix}\begin{Bmatrix} X_{1-1} \\ X_{1-2} \end{Bmatrix} = \begin{Bmatrix} 0 \\ 0 \end{Bmatrix} \tag{14}$$

For the free vibration equation of the steel frame (subsystem 2),

$$M_2\ddot{X}_2 + K_2X_2 = 0 \tag{15}$$

rearrange displacement vector and acceleration vector as well, to move the degrees of freedom belonging to those binding nodes to the top.

$$\begin{bmatrix} m_{11} & m_{12} \\ m_{21} & m_{22} \end{bmatrix}\begin{Bmatrix} \ddot{X}_{2-1} \\ \ddot{X}_{2-2} \end{Bmatrix} + \begin{bmatrix} k_{11} & k_{12} \\ k_{21} & k_{22} \end{bmatrix}\begin{Bmatrix} X_{2-1} \\ X_{2-2} \end{Bmatrix} = \begin{Bmatrix} 0 \\ 0 \end{Bmatrix} \tag{16}$$

Because the two subsystems are solid coupling at the binding nodes,

$$\ddot{X}_{1-2} = \ddot{X}_{2-1} \qquad X_{1-2} = X_{2-1}$$

After assembling equation (14) and (16), the finite element equation of the whole system is finally gotten.

$$\begin{bmatrix} M_{11} & M_{12} & 0 \\ M_{21} & M_{22}+m_{11} & m_{12} \\ 0 & m_{21} & m_{22} \end{bmatrix}\begin{Bmatrix} \ddot{X}_{1-1} \\ \ddot{X}_{1-2} \\ \ddot{X}_{2-2} \end{Bmatrix} + \begin{bmatrix} K_{11} & K_{12} & 0 \\ K_{21} & K_{22}+k_{11} & k_{12} \\ 0 & k_{21} & k_{22} \end{bmatrix}\begin{Bmatrix} X_{1-1} \\ X_{1-2} \\ X_{2-2} \end{Bmatrix} = \begin{Bmatrix} 0 \\ 0 \\ 0 \end{Bmatrix} \tag{17}$$

which can be written as:

$$M_3\ddot{X}_3 + K_3X_3 = 0 \tag{18}$$

3.5 Numerical Example 2

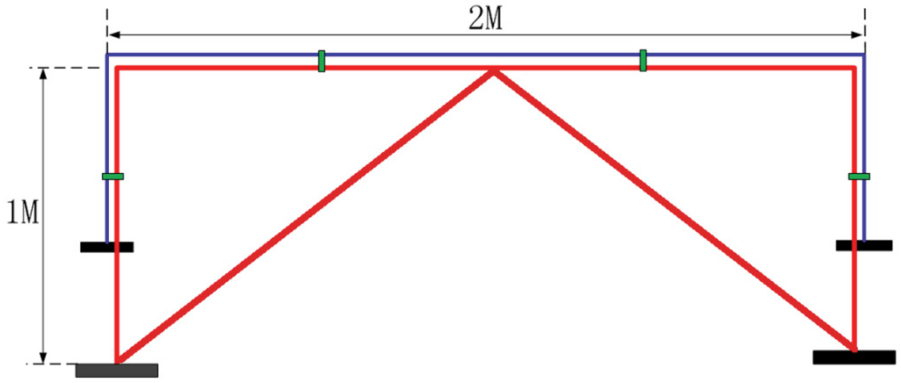

Figure 3.10 A piping system

After solve eigenvalue problem of M_3, K_3, the natural frequencies and model shapes of this piping system can be gotten.

n	1	2	3	4	5	6	7	8	9	10
f(Hz)	82.171	99.838	101.98	131.11	195.38	250.09	278.79	301.25	340.54	343.8

Table 3.2 Natural frequencies of the whole system

Modal shapes analysis for the solid coupling system is conducted next.

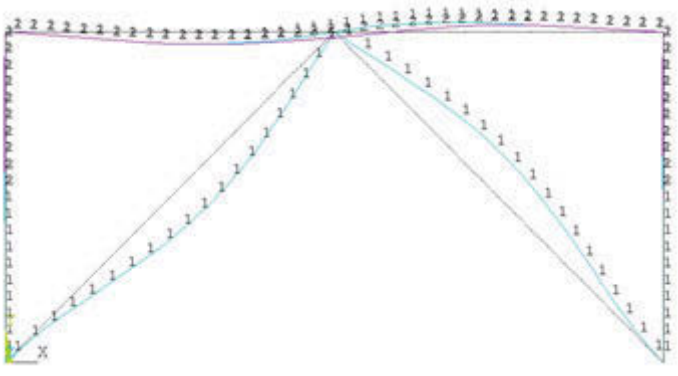

f_1=82.171Hz

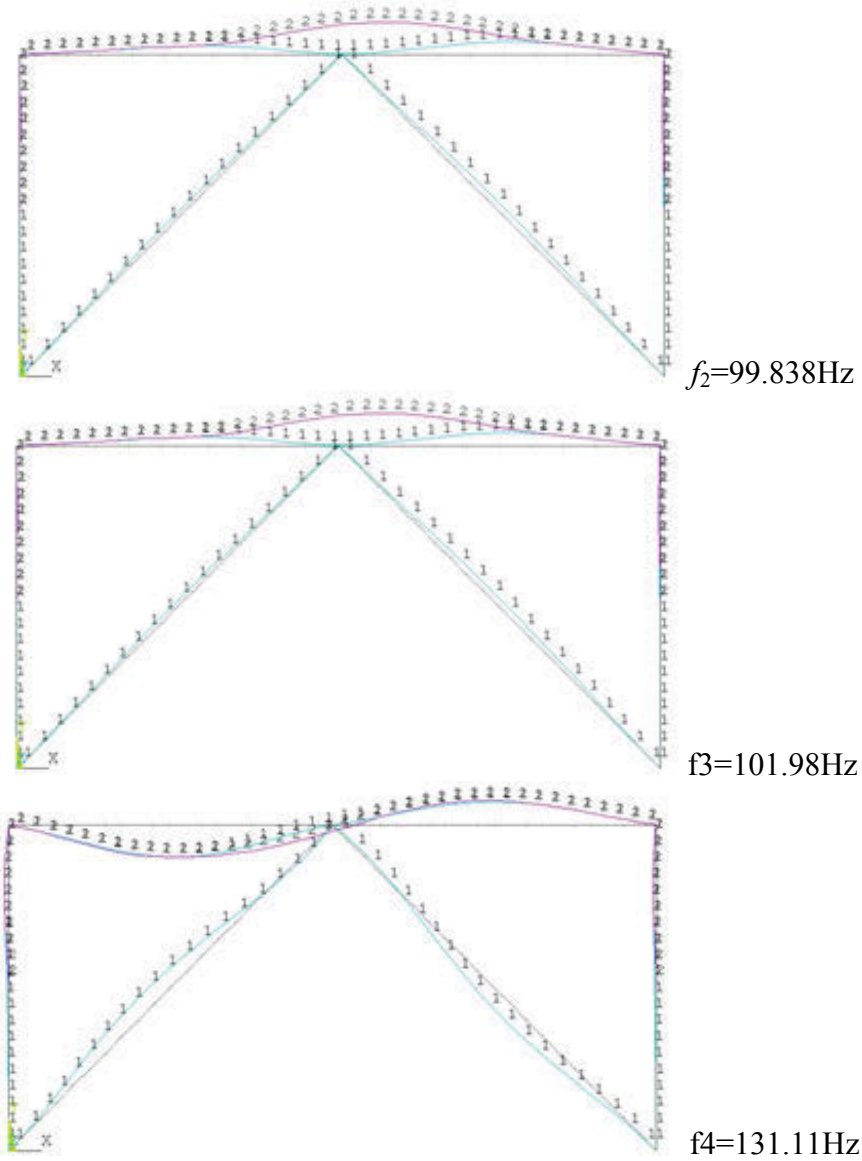

Figure 3.11 First four order modal shapes

Next, some parameters of the pipe will change in turn and modal analysis for the coupled system will repeat again. New modal shapes are going to be compared with the initial results.

① Original parameters

② To reduce the density of the pipe (to 1/5 ρ)

③ To reduce the modulus of the pipe (to 1/5 E)

④ To move the location of one binding node (to left)

By comparing the 1st order modal shapes,

DISPLACEMENT
STEP=1
SUB =1
FREQ=82.171
DMX =.532137

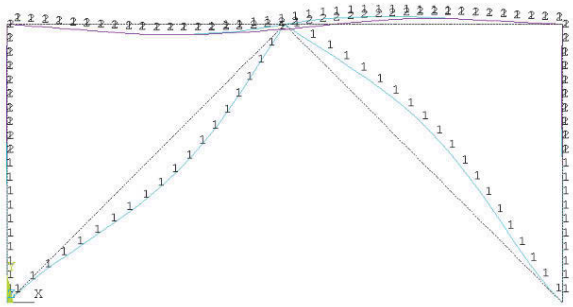

ρ, E
f=82.171Hz,
The pipe and the steel frame vibrate simultaneously.
It is dangerous, and this situation should be avoided.

DISPLACEMENT
STEP=1
SUB =1
FREQ=83.575
DMX =.551466

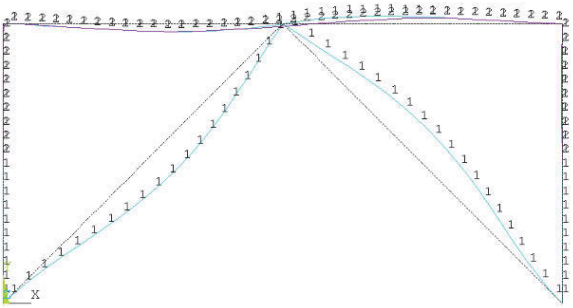

1/5ρ, E
f=83.575Hz,
Because f→K/M,
M↓, f↑
But the change is very small.
K is more useful for this order.

DISPLACEMENT
STEP=1
SUB =2
FREQ=78.034
DMX =.48334

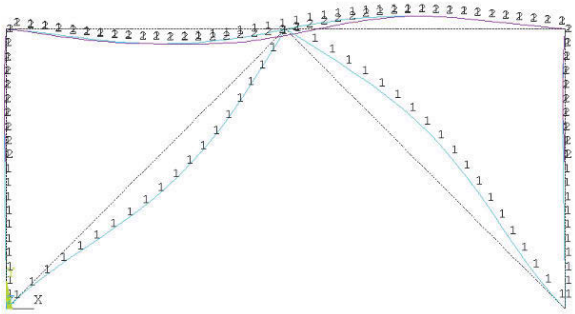

ρ, 1/5E
f=78.034Hz,
Because f→K/M,
K↓, f↓
And the deformation of the pipe is more obvious.

DISPLACEMENT
STEP=1
SUB =2
FREQ=82.194
DMX =.533917

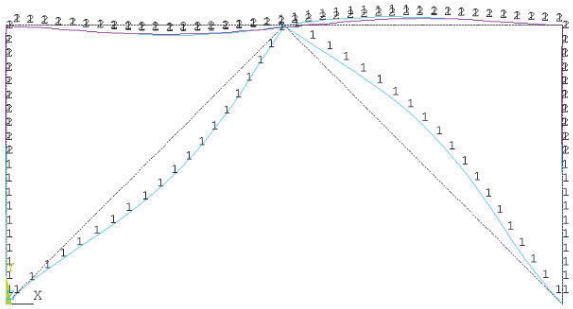

ρ, E, binding node shift left
f=82.194Hz,
There is almost no change.

By comparing the 2nd order modal shapes,

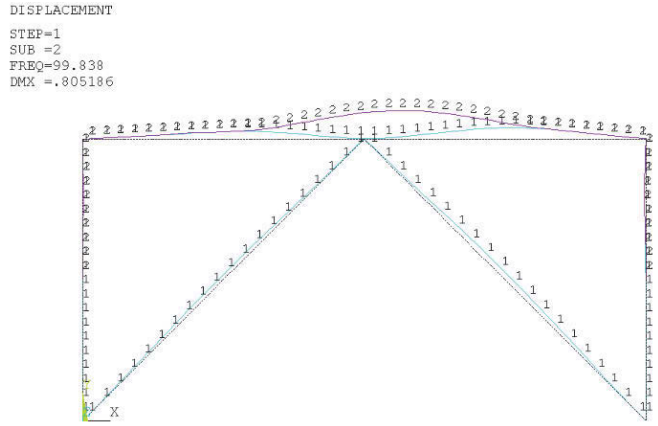

ρ, E
f=99.838Hz,
The vibration of the pipe is primary.
Steel frame almost does not vibrate.

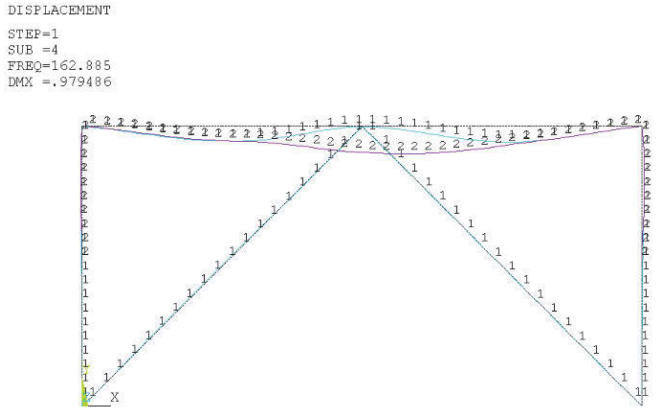

1/5ρ, E
f=162.885Hz,
Because f→K/M,
M ↓ , f ↑
And the deformation of the pipe is large.

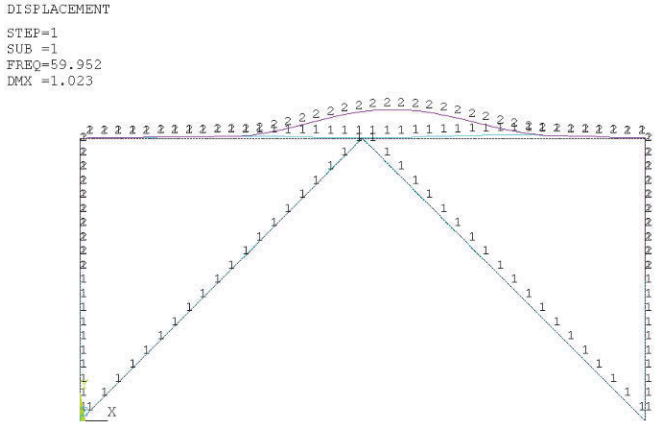

ρ, 1/5E
f=59.952Hz,
Because f→K/M,
K ↓ , f ↓
And the deformation of the pipe is large.

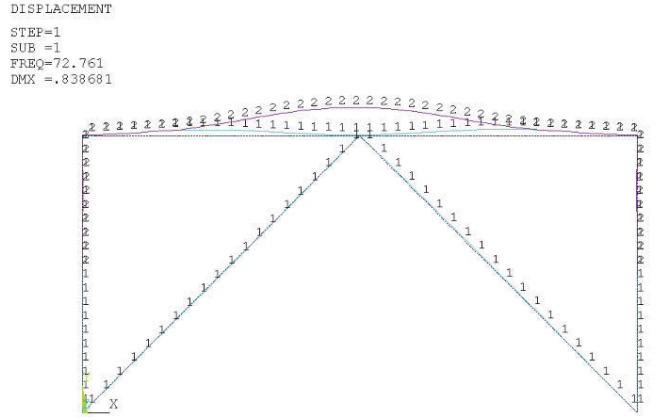

ρ, E, binding node shift left
f=72.761Hz,
Because the vibration of the pipe is primary, after move one binding node to left, both f and deformation change obviously.

By comparing the 3rd order modal shapes,

DISPLACEMENT
STEP=1
SUB =3
FREQ=101.983
DMX =.580734

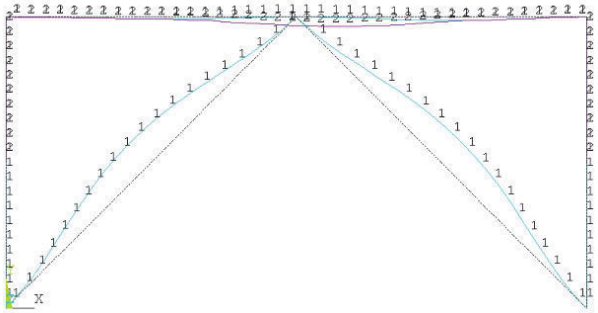

ρ, E
f=101.983Hz,
The vibration of the steel frame is primary.
The pipe almost does not vibrate

DISPLACEMENT
STEP=1
SUB =2
FREQ=101.871
DMX =.591253

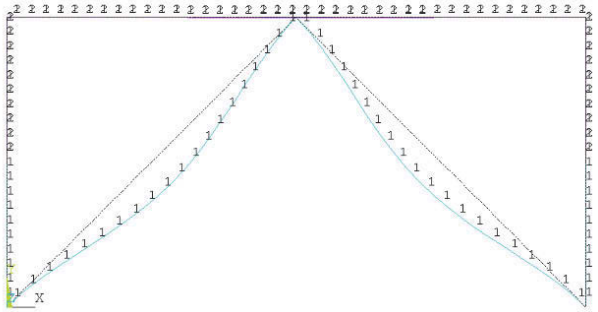

1/5ρ, E
f=101.871Hz,
f and deformation has no change, no matter change M or K of the pipe.

DISPLACEMENT
STEP=1
SUB =3
FREQ=101.871
DMX =.594897

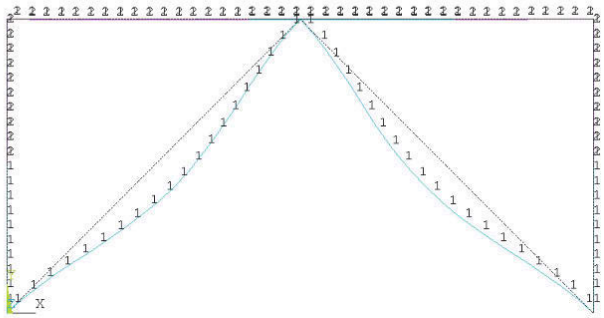

ρ, 1/5E
f=101.871Hz,
f and deformation has no change, no matter change M or K of the pipe.

DISPLACEMENT
STEP=1
SUB =3
FREQ=101.877
DMX =.591075

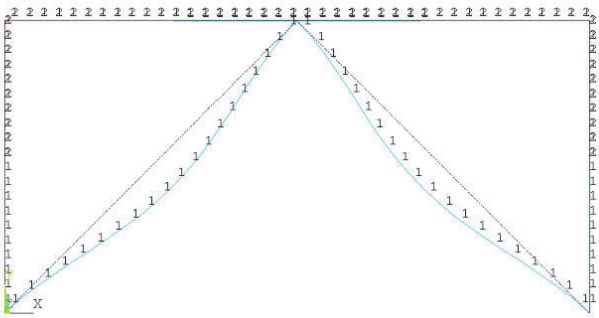

ρ, E, binding node shift left
f=101.877Hz,
Because the vibration of the steel frame is primary, even move one binding node to left, nothing is changed.

By comparing the 4th order modal shapes,

DISPLACEMENT
STEP=1
SUB =4
FREQ=131.108
DMX =.511116

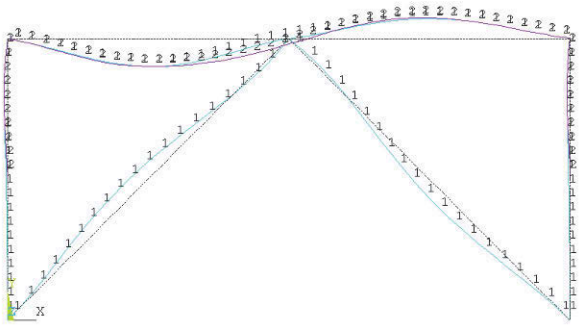

ρ, E
f=131.108Hz,
The pipe and the steel frame vibrate simultaneously.
It is dangerous, and this situation should be avoided.

DISPLACEMENT
STEP=1
SUB =3
FREQ=159.258
DMX =.57325

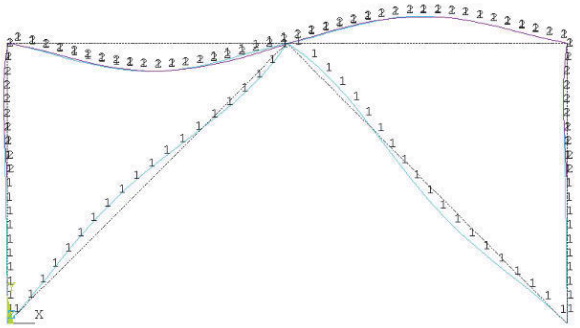

1/5ρ, E
f=159.258Hz,
Because f→K/M,
M↓, f↑

DISPLACEMENT
STEP=1
SUB =4
FREQ=112.698
DMX =.461357

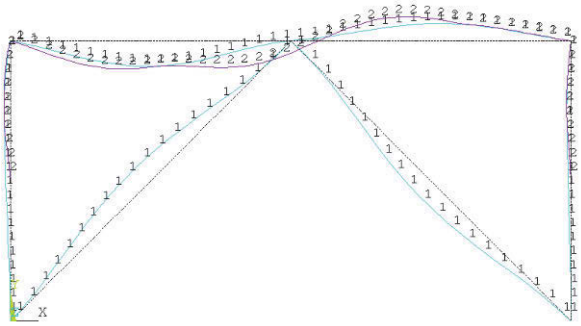

ρ, 1/5E
f=112.698Hz,
Because f→K/M,
K↓, f↓

DISPLACEMENT
STEP=1
SUB =4
FREQ=128.599
DMX =.497764

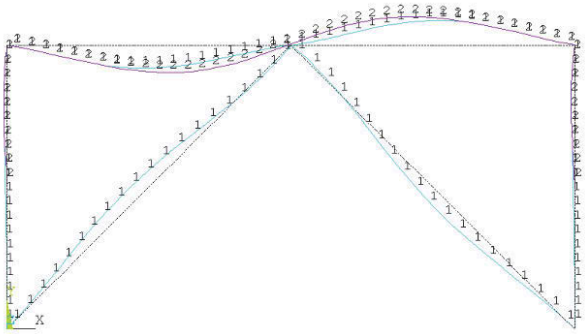

ρ, E, binding node shift left
f=128.599Hz,
There is very small change.

The above discussions provide some ideas to control vibration and reduce noise for the whole structure. If we move the binding nodes (coupled points) to another position, some orders of vibration performance will change obviously, especially for those controlled by the pipe.

However, for ome order modal vibration in which is the steel frame plays a decisive role, it is useless to change the mass matrix or the stiffness matrix of the pipe, or move the position of those binding nodes.

3.6 Model Reduction Method

3.6.1 Procedure of Dynamic Condensation

The dynamic equation of the coupled system can be written as:

$$M\ddot{x} + Kx = F \tag{18}$$

That is:

$$Sx = F \tag{19}$$

where $S = -\omega^2 M + K$, and x is the displacement.

From eq. (18) the dynamic characteristics can be calculated. But for a large scale structural system, if we are trying to find an proper stiffness for some parts of the system, it would cost plenty of time in reassemble the total mass and stiffness matrices before the best fitted stiffness is found. Therefore a condensed model could be of help to this problem. Recently various methods have been tried to strike a balance between the efficiency of finding the proper solutions and the accuracy of the new condensed model. Here a dynamic condensation method proposed by N. Zhang [77] was utilized to act as a more effective way to solve this question. This model reduction method can be expressed as follows:

The modal shapes p of the system can be calculated:

$$K\mathrm{p} = M\mathrm{p}\Lambda \tag{20}$$

Then decompose the modal shapes into low part $\mathrm{p_l}$ and the other part $\mathrm{p_h}$, by multiplying the force F, the result can be divide into $\mathrm{f_l}$ and $\mathrm{f_h}$ corresponding to $\mathrm{p_l}$ and $\mathrm{p_h}$:

$$\begin{pmatrix} \mathrm{p_l^T} \\ \mathrm{p_h^T} \end{pmatrix} \mathrm{F} = \begin{pmatrix} \mathrm{f_l} \\ \mathrm{f_h} \end{pmatrix} \tag{21}$$

To a prescribed frequency ω, if the modal shapes are regularized by S, the above equation can be rewritten as:

$$\begin{pmatrix} \mathrm{p_l^T} \\ \mathrm{p_h^T} \end{pmatrix} \mathrm{F} = \begin{pmatrix} \mathrm{p_l^T} \\ \mathrm{p_h^T} \end{pmatrix} \mathrm{S} \begin{pmatrix} \mathrm{p_l} & \mathrm{p_h} \end{pmatrix} \begin{pmatrix} \mathrm{f_l} \\ \mathrm{f_h} \end{pmatrix} \tag{22}$$

So the equation (23) can be obtained:

$$\mathrm{F} = \mathrm{Sp_l f_l} + \mathrm{Sp_h f_h} \tag{23}$$

So the physical input corresponding to $\mathrm{p_h}$ can be derived:

$$\mathrm{F_h} = \mathrm{F} - \mathrm{Sp_l f_l} = (\mathrm{I} - \mathrm{Sp_l p_l^T})\mathrm{F} \tag{24}$$

According to eq. (19), the complementary displacement vectors can be derived:

$$\mathrm{x_h} = \mathrm{S^{-1}F_h} = \mathrm{S^{-1}}(\mathrm{I} - \mathrm{Sp_l p_l^T})\mathrm{F} \tag{25}$$

Here the complementary vectors can be calculated at two ω, corresponding to the lowest and highest end of the frequency range of interest. The former frequency, can be used to correct the response at the lower frequency side, and the latter is used to correct the response at the higher frequency side.

By combining the low part $\mathrm{p_l}$ and displacement vectors in eq. (25), new modal shapes can be deduced:

$$\mathrm{p_a} = \begin{pmatrix} \mathrm{p_l} & \mathrm{x_h} \end{pmatrix} \tag{26}$$

Here the SEREP method and the dynamic condensation method were combined as a hybrid method to improve the accuracy of the eigenvalues. p_{au} and p_{al} denote the upper and lower part of p_a respectively, so the transition matrix of the SEREP part, when the number of the lower eigenvalues is greater than or equal to the number of the master DOFs, can be expressed as follows:

$$T_s = p_a \left(p_{au}^T p_{au} \right)^{-1} p_{au}^T \tag{27}$$

And if the number of the lower eigenvalues is less than the number of the master DOFs, the transition matrix of the SEREP part can be written as:

$$T_s = p_a p_{au}^T \left(p_{au} p_{au}^T \right)^{-1} \tag{28}$$

Though the SEREP method can give a very accurate result, but the stability of the condensation process relies heavily on the linear dependence of the eigenvalues, sometimes it's not easy to meet this demand, so the dynamic condensation method can be used to fill that requirement.

And from the theory of dynamic condensation, the transition matrix is defined as

$$T_d = \begin{pmatrix} I \\ -S_{ll}^{-1} S_{lu} \end{pmatrix} \tag{29}$$

Then the total transition matrix is formed as:

$$T = T_s + T_d \tag{30}$$

So new modal mass and stiffness matrices can be calculated as shown in eq. (31):

$$M_c = T^T M T \qquad K_c = T^T K T \tag{31}$$

If a perturbation, say mass change or stiffness change on some parts of the system, the change of S can also be derived as δS, so the condensed modal model of the dynamic characteristics equation of the system can be written as:

$$T^T(S+\delta S)T=0 \tag{32}$$

where $\delta S=-\omega^2\delta M+\delta K$.

Then the dimension of the structural system reduces a lot, so the calculating cost reduced a lot.

3.7 Numerical Example 3

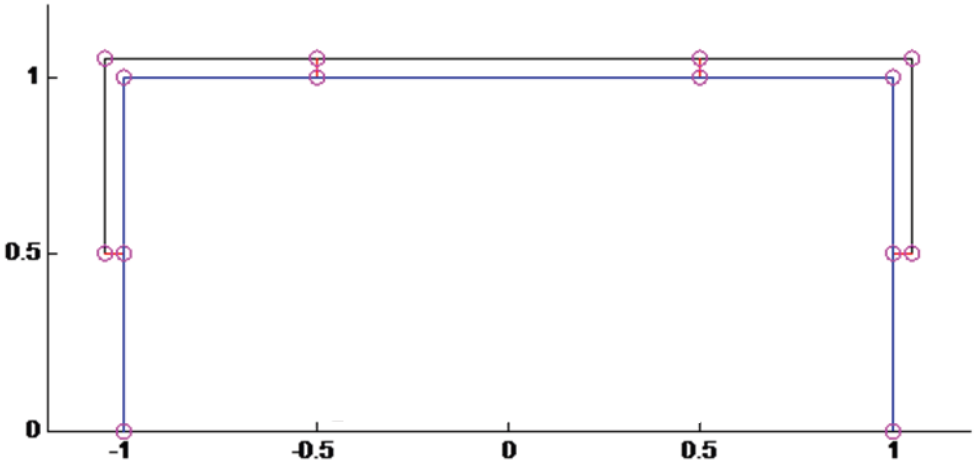

Figure 3.12 A multiple coupling system

Figure above shows a simplified vehicle body rigid connected with a fluid-filled pipe. The system is divided into 411 elements with 409 nodes. The 14 master nodes are chosen mainly on the connecting points or distributed on the pipe and the supporting beam, as shown in Fig.3.12, then the condensed model can be obtained with 10 modal DOFs and 4 displacement vectors on 14 master nodes.

In this model the perturbation on the stiffness of the connecting parts was applied to examine the eigenvalues. The first 10 eigenvalues corresponding to the stiffness changing from 160GPa to 260GPa are shown in Fig.3.13, and the frequencies without perturbation are labeled on the top left, the legend 'Condensed' denotes the stiffness perturbation on the modal condensed model, and the legend 'Original' denotes the stiffness perturbation with the original model:

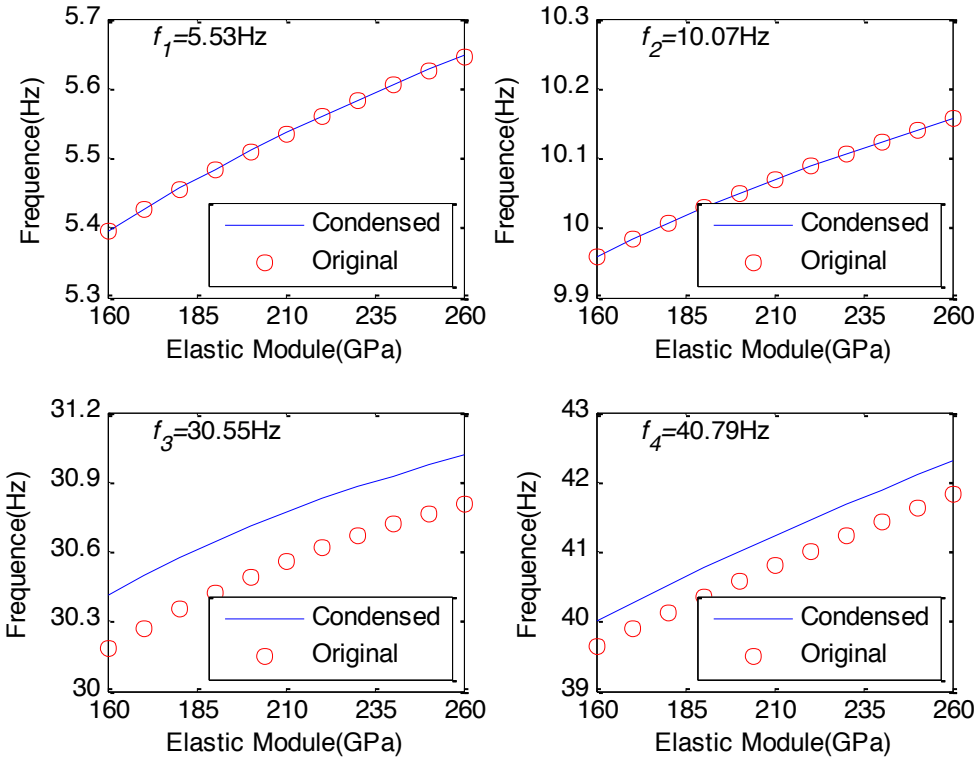

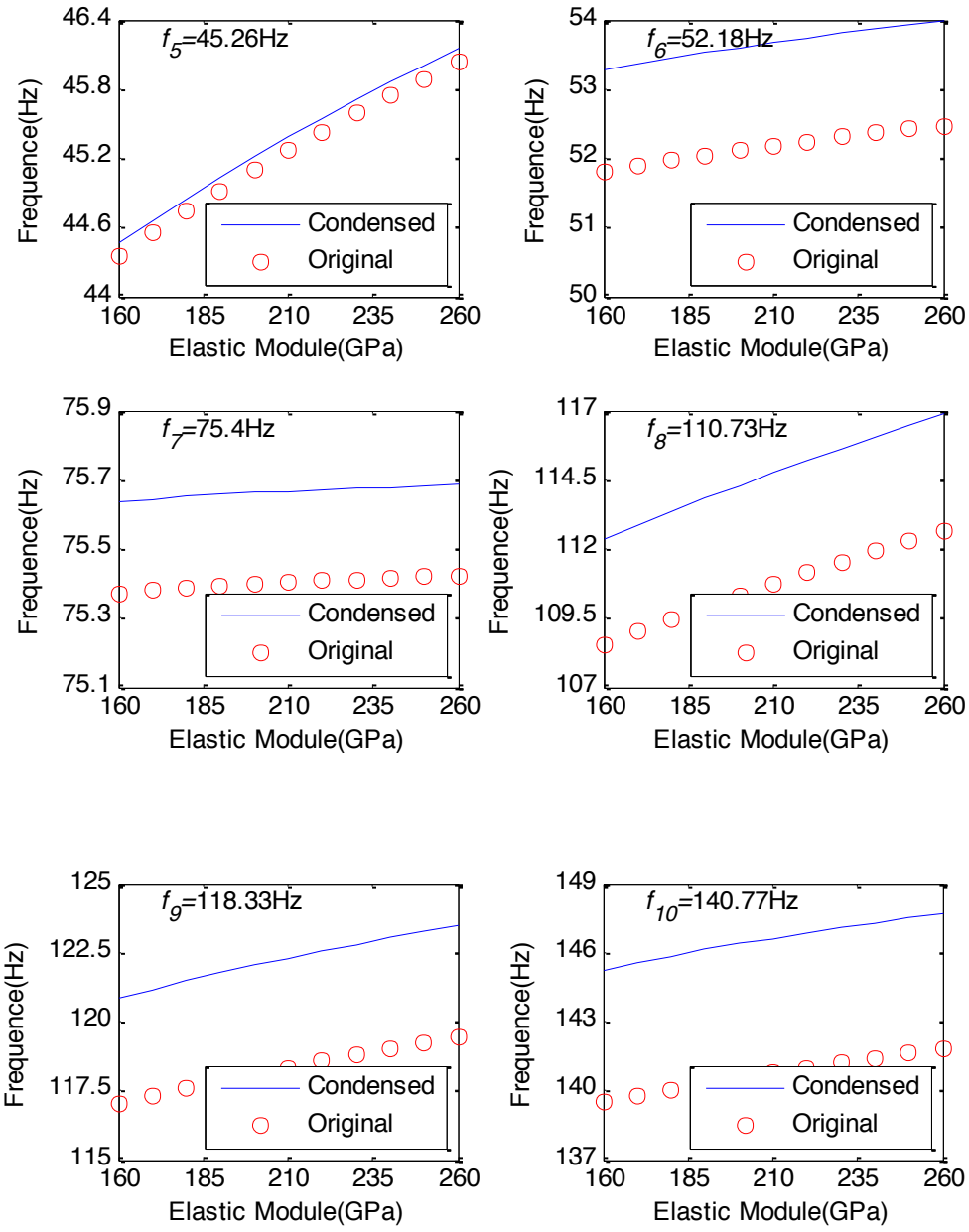

Figure 3.13 the first 10 frequencies with the perturbation on pipe-supporting parts

Fig.3.13 shows the accuracy of the new model which does not decrease after the modal condensation, it means, we can use the new model to predict the response to an excitation while keep the accuracy.

And the error between the variance range of the frequencies after perturbation and the original frequencies can be obtained as Table 3.3:

Frequency	1	2	3	4	5	6	7	8	9	10
Error (%)	0.03	0	0.71	1.06	0.26	2.86	0.35	3.64	3.34	4.15

Table 3.3 The error of the frequencies according to stiffness change

Table 3.3 shows: (1) The change of the frequencies is not proportional to the order of the frequency; (2) With this perturbation method, it is easy to find proper parameters to avoid the natural frequencies, and will of practical usage for the design of HIS system. (3) For a large scale structural system, this model reduction method offers a much smaller matrix to compute the response.

4 Design of Experiment

After obtained those computer simulation results, we will verify the feasibility of the methods proposed in this thesis through the experiments. The whole experiment should proceed according to the following phases:

- Project Planning and Preparation
- Design ——Material Selection and Structure Dimension
- Manufacturing
- Assembly and Installation
- Testing
- Results Analysis and Report

For the design phase, all components or parts need to be manufactured by workshop have been drawn with software SolidWorks, including a steel support structure (25.4mm x 25.4 x 1.2 mm square cross section), a copper fluid-filled pipe (12.7 x 1 mm circular cross section), two steel base plates, six aluminum fixtures for binding the fluid-filled pipe and the steel support structure.

4.1.1 Support structure

The support structure will be made by common steel tube. The cross-section of steel tube is 25.4mm x 25.4mm. And the thickness of this tube is 1.2mm. The density is 7850kg/m3. The material is alloy steel.

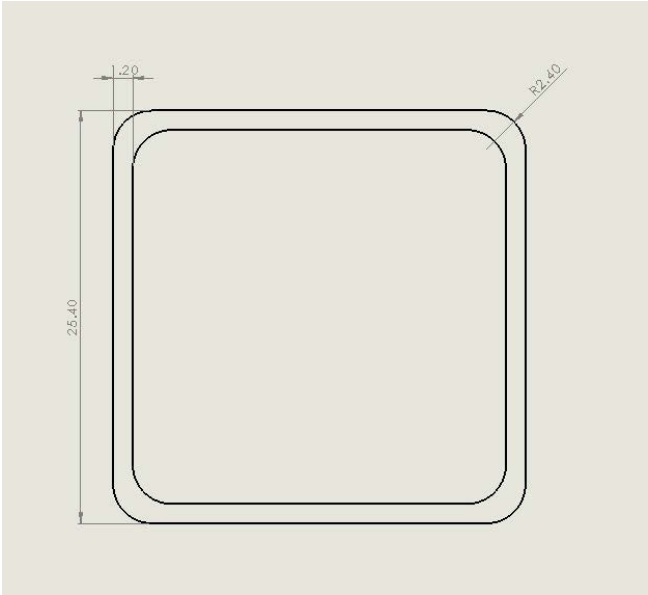	**Size**	**25.4 x 25.4 (mm)**
	Thickness	**1.2 mm**
	Density	**7850kg/m^3**
	Material	**Steel**

Figure 4.1 The cross-section and specification of support tube

The structure of support is a simply equipped structure. The width between the centreline of two vertical side tubes is 1000mm, and its height is 500mm. Two short steel beams are at 45 degree angle between the top support bar and the side tubes. The detailed drawings of structure and components will show in Appendix A.

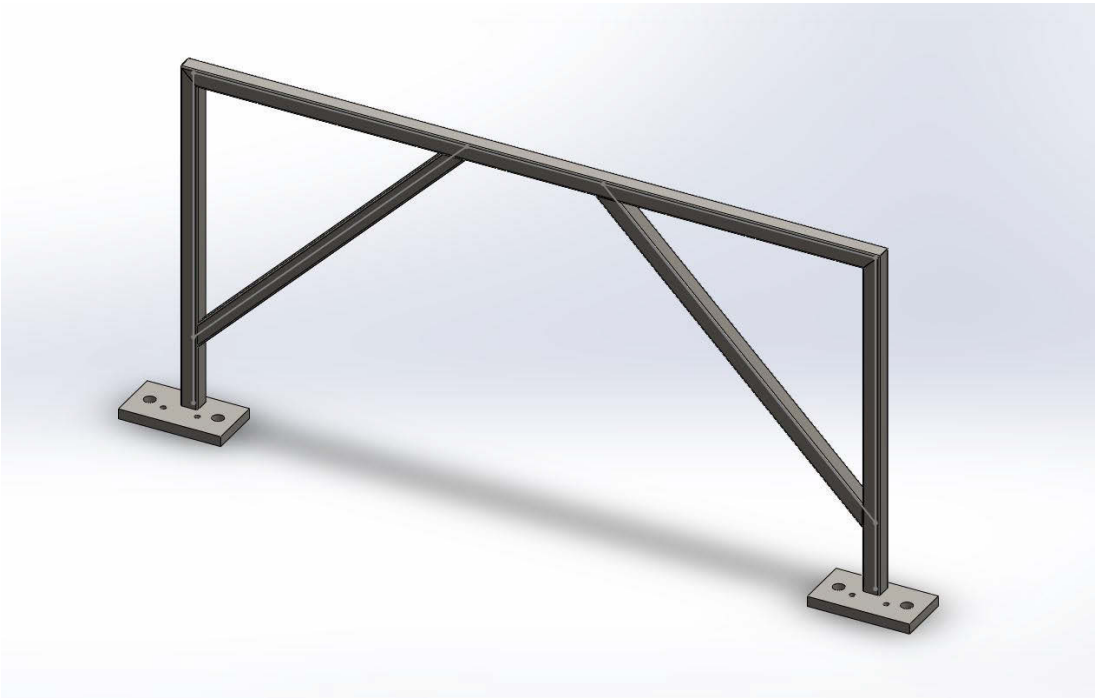

Figure 4.2 Geometry of support structure

Furthermore, there are two base plates under the support structure. These two plates are made of mild steel. Dimension of the base plates for support is 150 x 80 mm and the thickness is 15mm. The plate has two 17mm holes which are used to fix the whole structure on the ground. Also, the plate has two 8mm taps to hookup the pipe. All structure components are connected through welding.

4.1.2 Pipe structure

The fluid-filled pipe structure is made out of common copper pipe. The outer diameter of copper pipe is 12.70mm and the inner diameter is 10.70mm. The thickness of this tube is 1mm and the density is 8900kg/m3.

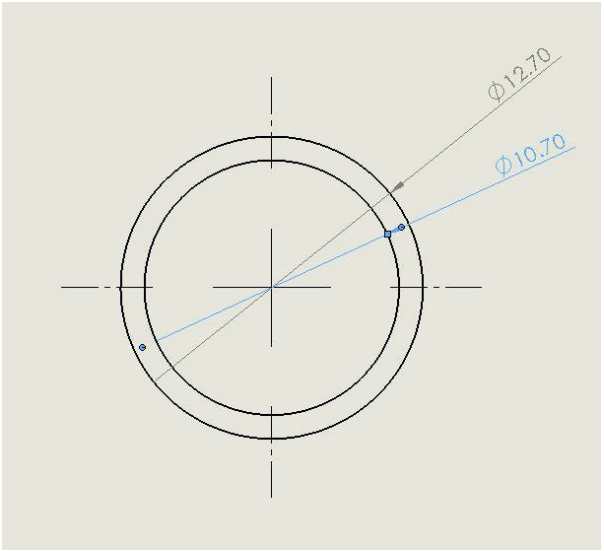

Outer Diameter	**12.70 mm**
Inner Diameter	**10.70 mm**
Thickness	**1mm**
Density	**8900kg/m^3**
Material	**Copper**

Figure 4.3 The cross-section and specification of pipe

The fluid-filled copper pipe is a simple structure as well. The shape of the pipe is similar to that of the support structure.

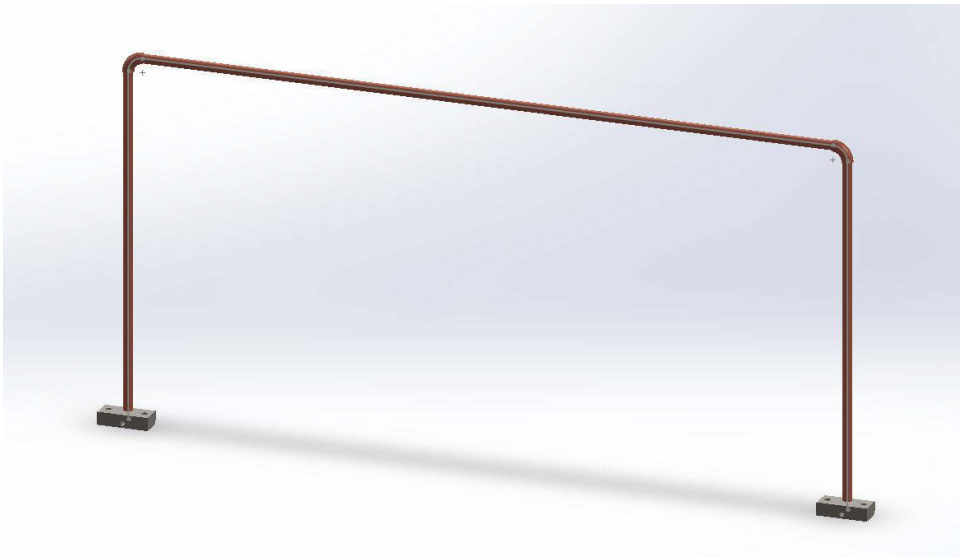

Figure 4.4 Geometry of pipe structure

The size of copper pipe's base plate is 70x30x18mm. Each plate has one 12.7mm hole. The function of these holes is to provide connection between the pipe and the base plate, because such connection cannot be accomplished by welding. At last, the pipe and its base plate will be joined with M6 bolts.

4.1.3 Combined structure

The combined structure is joined by 5 connectors. Each connector is screwed by two 6mm bolts. Hence the pipe and the support structures are bound together tightly.

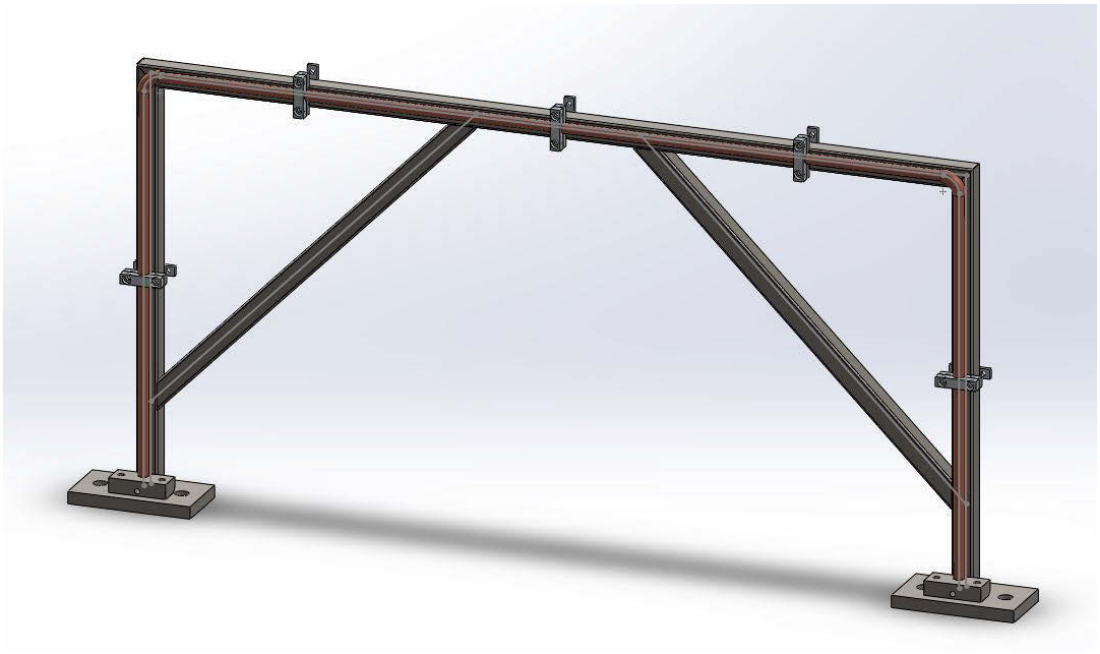

Figure 4.5 Geometry of combined structure

The connectors consisted of 3 components. The size of a connector is 50x12mm made of aluminum. When the connector needs to be used, it will be fixed by M6 bolts to provide strength.

4.2 Experiment Apparatus

This section will explain the necessary apparatus and describe the features for each device. Moreover, impulse hammer, vibration shaker, accelerometer, LabView program will be introduced.

4.2.1 Impulse Hammer

This experiment will use 1 pound impulse hammer. This hammer was made by DYTRAN INSTRUMENTS,INC. The specification of this hammer will provide in Appendix B. The impact hammer is used to shock excite structures or machines with a definable force impulse for the purpose of studying the dynamic behaviour. The

hummer contains a special acceleration compensated piezoelectric force sensor in the head, close to the forward or striking face. An impact tip attached to the force sensor transmits the force of the hammer strike into the sensor and protects the sensor face from damage. The fore sensor in an ordinary hammer will act as an accelerometer picking up the vibration of the hammer head after the strike and adding this vibration to the force/time signal.

Feature:

- Fast
- Good for identifying modal frequencies
- Usually requires averaging to lower noise floor in spectrum
- Hammer mass and impact tip must be suited to the structure.

The impulse hummer will apply soft tip on the head of hammer. This is not only because hard tip may damage to surface of support and copper pipe, but also because the interested modal frequencies are low for structure.

Figure 4.6 MODEL 5805A 1 pound Impulse hammer

4.2.2 Vibration Shakers

Vibration shakers are apparatus commonly used in mechanical vibration experiments. The shaker can create a regular frequency or a special range of frequencies. Shakers are usually electromagnetic, but the electrohydraulic shaker can be used where large forces

are required. The force transducer on the shaker is used to measure vibration stimulus. The vibration of the support structure is created by a shaker. And accelerometers attached on the structure measure the vibration response. Testing by a shaker is slower than by a impulse hammer, but will generally obtain better results. The vibration input signal is usually a swept sine, but other kinds of signals can be applied as well. The benefit of using a shaker is that it is good for identifying the mode shapes and more applicable for structures with large damping. Additional care is to be taken to ensure that the shaker does not become part of the structure.

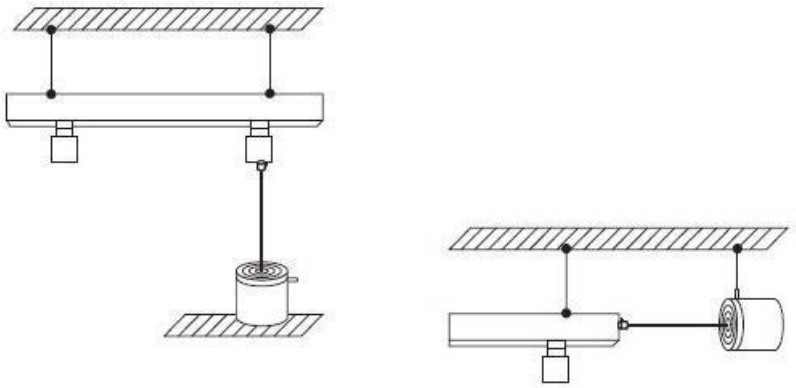

Figure 4.7 Setup method of shaker

In this experiment, the shaker PM50A which is able to create DC 0-10,000 Hz of natural frequency will be used. More specifications are shown in Appendix C.

The shaker is controlled by a computer which makes some signals and then the power amplifier converts and amplifies these signals which are sent to the shaker and Oscilloscope afterwards. The oscilloscope's major function is to monitor the input signals. And the computer receives signals from the measurement sensor attached to the head of the shaker and finally records all the data.

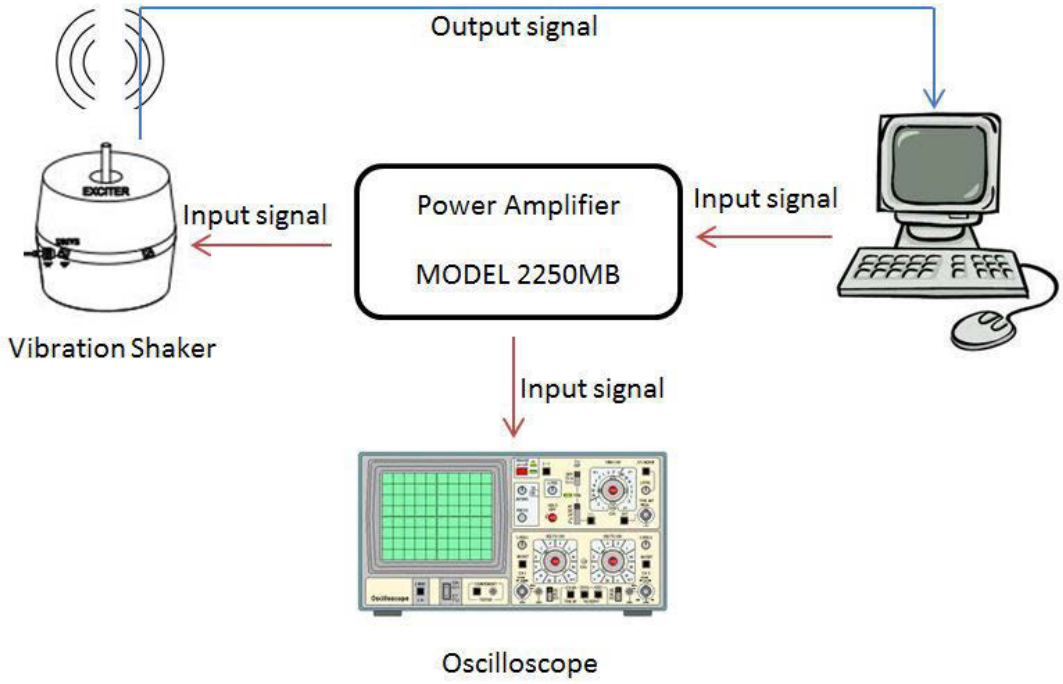

Figure 4.8 Diagram of vibration shaker operation system

4.2.3 Accelerometer

An accelerometer is a device made of piezoelectric materials to measure the vibration or the acceleration of a structure's motion. Such materials produce an electrical charge through the force change in motion. The charge is proportional to the force exerted upon it and since the mass is a constant, the charge is also proportional to the acceleration. The accelerometer must have the ability to measure the range of frequency between 0 and 5000 Hz. Additionally, the size of the accelerometer should be less than 1cm and the weight lighter than 10g. This is because the weight of the accelerometer can influence the result of experiment.

4.2.4 LabView

LabVIEW is a highly productive development environment that engineers and scientists use for graphical programming and unprecedented hardware integration to rapidly design and deploy measurement and control systems. Within this flexible platform, engineers scale from design to test and from small to large systems while reusing IP and refining their processes to achieve maximum performance. In this experiment, LabVIEW 2012 will be used to control the frequency of the vibration shaker. Also, this program will record data of the accelerometer.

4.3 Experiment Procedure

For experimental modal testing to determine natural frequencies, several equipments are basically required and used during the experiment, especially the exciter (shaker), the signal conditioner, the spectrum (FFT) analyzer, the accelerometer, the force transducer and the monitoring system. There are brief descriptions of these equipments. Figure 4.9 represents the schematic illustration of the coupled piping system.

1. The shaker is used as a source of vibration in order to apply a known input force to the system.
2. The transducer is used to convert the physical motion of the system into electrical signals. The piezoelectric sensor (accelerometer) will measure a fraction of the natural frequencies.
3. The signal conditioner is equipped in the system to make the transducer characteristics compatible with the digital storage oscilloscope.
4. The digital storage oscilloscope will execute the task of modal analysis, and acquisition of the data will be displayed by monitoring system using LabVIEW computer software.

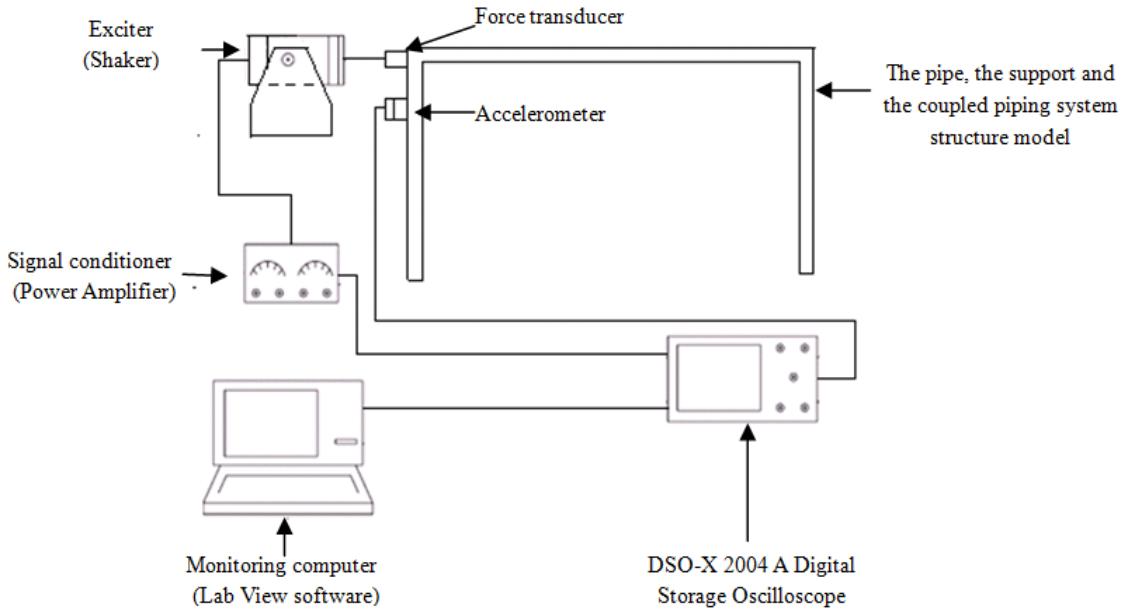

Figure 4.9 The schematic illustration of the coupled piping system

4.3.1 Impulse Hammer

1) The experiment pipe stricture is fixed on the base of support structure.
2) The experiment support structure is fixed on lab floor. This structure is held by 4x16mm bolts and nuts. (Note: 16mm bolts and nuts must be tightened strongly. This point is very important in this experiment.)
3) In support structure experiment, 4 accelerometers are set on 4 points of support experiment structure. Point 1&4 are far from 100mm top frame. And point 2&3 are far from 200mm top frame. (Note: These accelerometers are hold by stick tape tightly. If it is loose, the measurement data will be incorrect.)

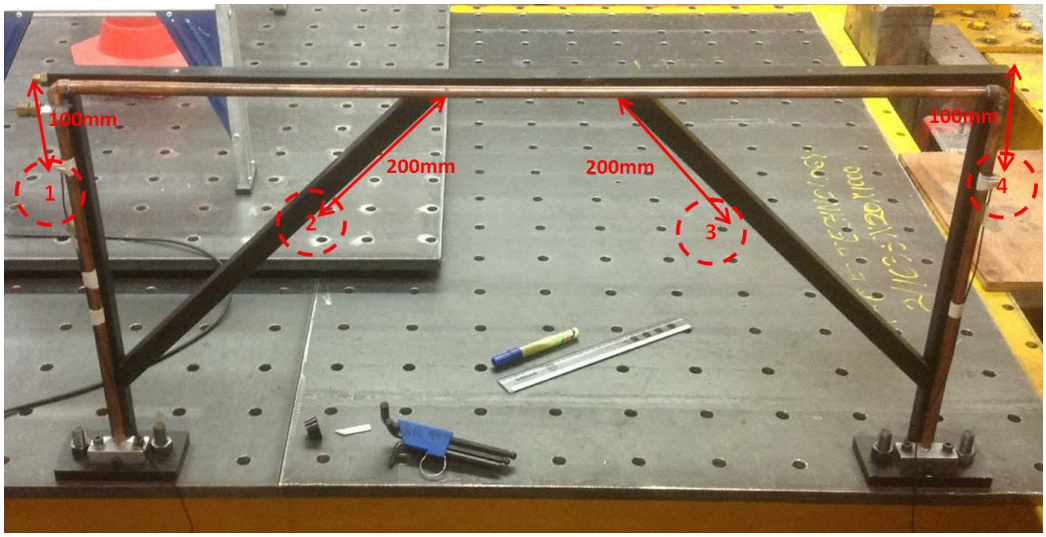

Figure 4.10 Exact setup points of accelerometers on support structure

4) The 25 times of impact is applied to on a point. This point is located from 10 mm of top support frame. (Note: No strong impact. If not, this impact will cause damage or transform this structure.)
5) Record data from 4 accelerometers.
6) In pipe structure experiment, 2 accelerometers are set on 2 points of pipe experiment structure. Point 1&2 are located 100mm both sides from top point of top frame.

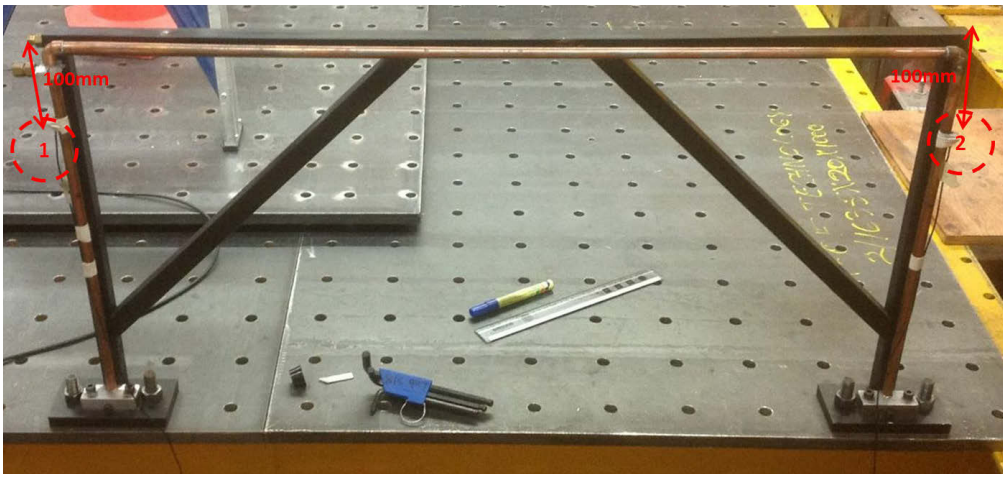

Figure 4.11 Exact setup points of accelerometers on pipe structure

7) The 25 times of impact is applied to on the point which is located from 10mm of top pipe. (Note: weak impacts are applied to this structure. This is because that the pipe experiment structure is made of copper. So, this structure is easy to damage or transform by strong impact.)
8) Record date from 2 accelerometers.
9) In coupled system experiment, support and pipe structure are connected by 5 connecters. This connector is hold by 2 x 6mm bolts. First point is middle of top frame. And then, 2 connectors are located 200mm of top frame from each side frame. Finally, other 2 connectors are hold at middle of point on each side frame. Below figure show exact location of connectors.

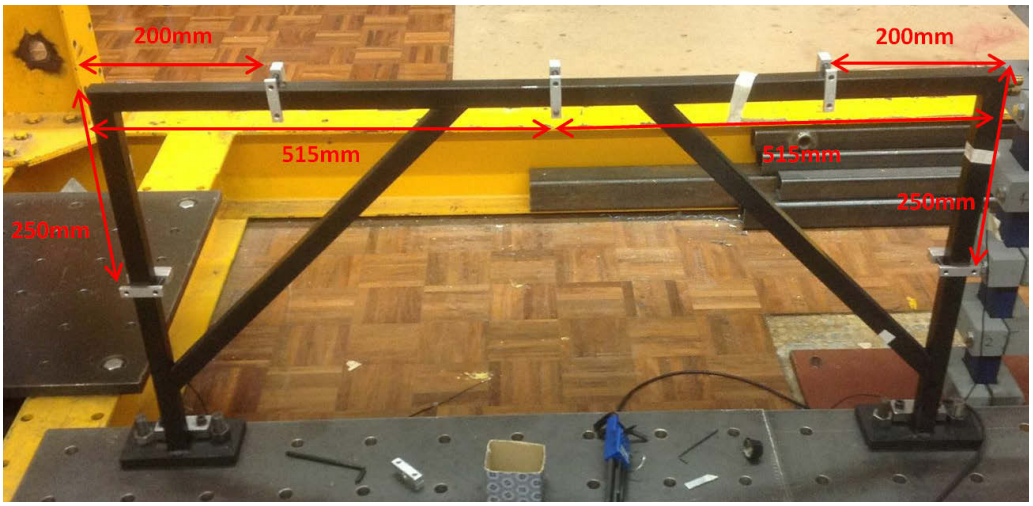

Figure 4.12: Exact connection points of connectors

10) The points of accelerometer is same position with above.
11) First impact point is support structure. The number of impact time is 25 times. The data are recorded. And then, again impact condition which is same with above condition is applied to pipe structure. The data are also recorded.
12) This data is analysed.

4.3.2 Vibration shaker

1) In the shaker experiment, steps from 1 and 3 of the impulse hammer experiment are repeated.
2) The installation of accelerometer is the same point with the impulse hammer experiment.
3) The vibration shaker is hung from roof by steel cable and locate right side frame of support structure. (Note: The shaker was not fixed or attached to a wall. The reason is that if the shaker is fixed or attached to a wall, this natural frequency will be influenced. It means that the shaker was not a part of the experiment structure.)

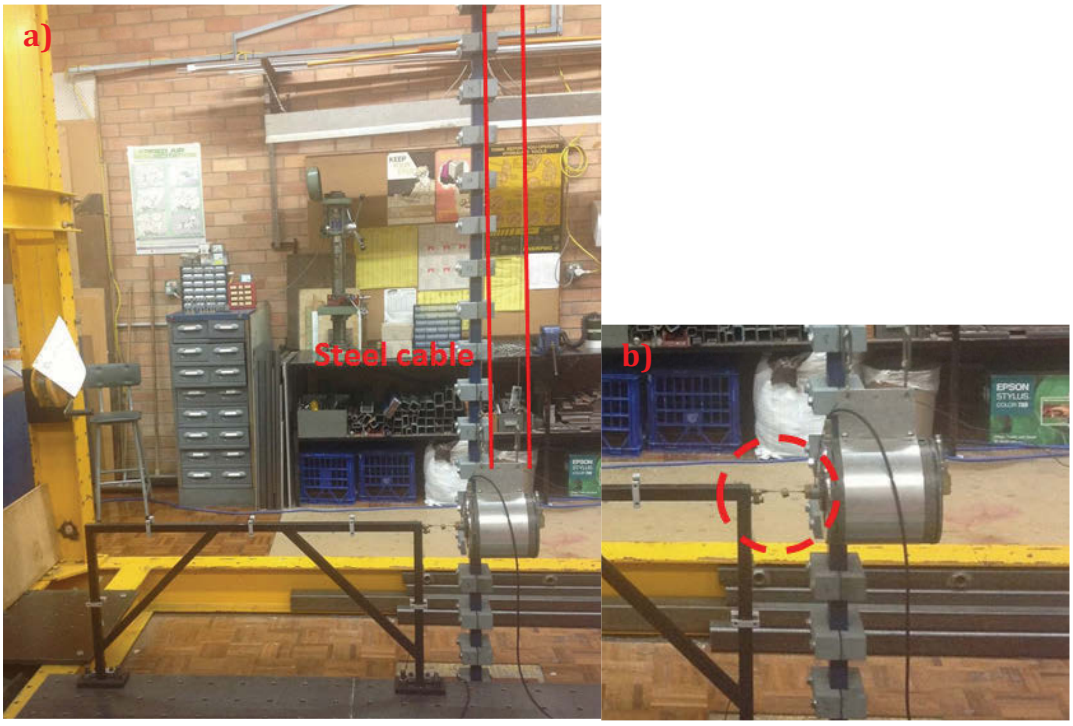

Figure 4.13 (a) the vibration shaker is hung by steel cable. (b) the connection part between the structure and shaker

4) The shaker is connected to the right side frame of support experiment structure by the small steel bar. (Note: This method is to minimise the influence to the system.)
5) The shaker is turned on. The shaker provides the vibration. The range of frequency is from 10 to 5000.
6) Record data from accelerometers.
7) In pipe structure experiment, 2 accelerometers are located at the same point of impulse hammer experiment.
8) The shaker is connected to the right side frame of pipe experiment structure by the small steel bar. (Note. The Tap for connection of shaker cannot be made on pipe structure. So, the shaker is connected to pipe structure by pipe clamp. This clamp is made by Aluminum, so it is light.)

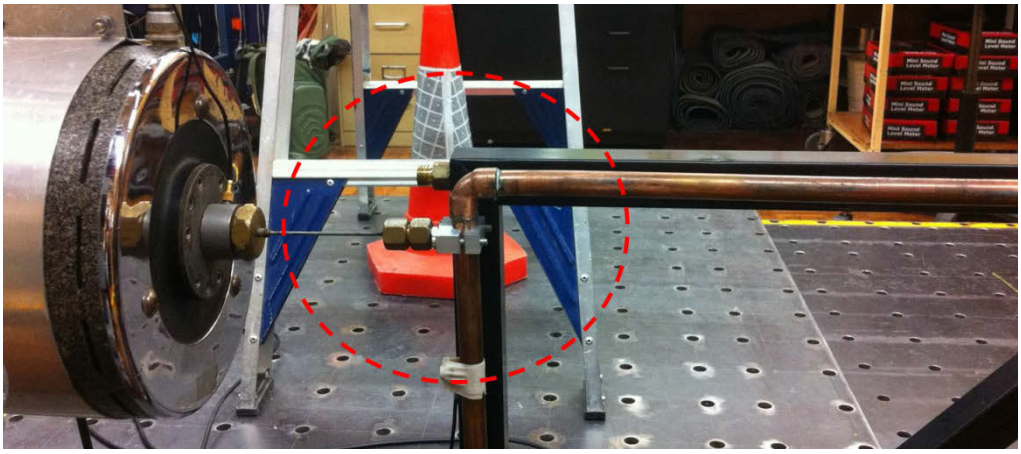

Figure 4.14: Connection between shaker and the pipe experiment structure by pipe clamp.

9) Repeat step5.
10) In coupled system experiment, support and pipe structure are connected by 5 connecters. The points of connector are the same with the impulse hammer experiment.

11) The points of accelerometer is same position with above.
12) First impact point is support structure. The range of frequency is from 10 to 5000. The data are recorded. And then, again impact condition which is same with above condition is applied to pipe structure. The data are also recorded.
13) This data is analysed.

5 Experiment and Simulation Result

This section will be divided by 3 parts. They are the impulse hammer experiment, the vibration shaker experiment and the finite element method simulation. Results from the experiment and simulation will be compared in the end.

5.1 Impulse Hammer Excitation Experiment Results

The result was obtained after 25 impacts conducted by an impulse hammer. The data collected from the four accelerometers attached on the support structure and the other two accelerometers on the pipe structure were analysed. Thus, the corresponding natural frequencies of the support structure and the pipe as well as the combined structure were found in the impulse hammer excitation experiment.

5.1.1 Support Structure in Impulse Hammer Experiment

Firstly, the results for the support structure were analysed in the impulse hammer experiment. Frequency response was plotted versus magnitude as shown in Figure 5.1.

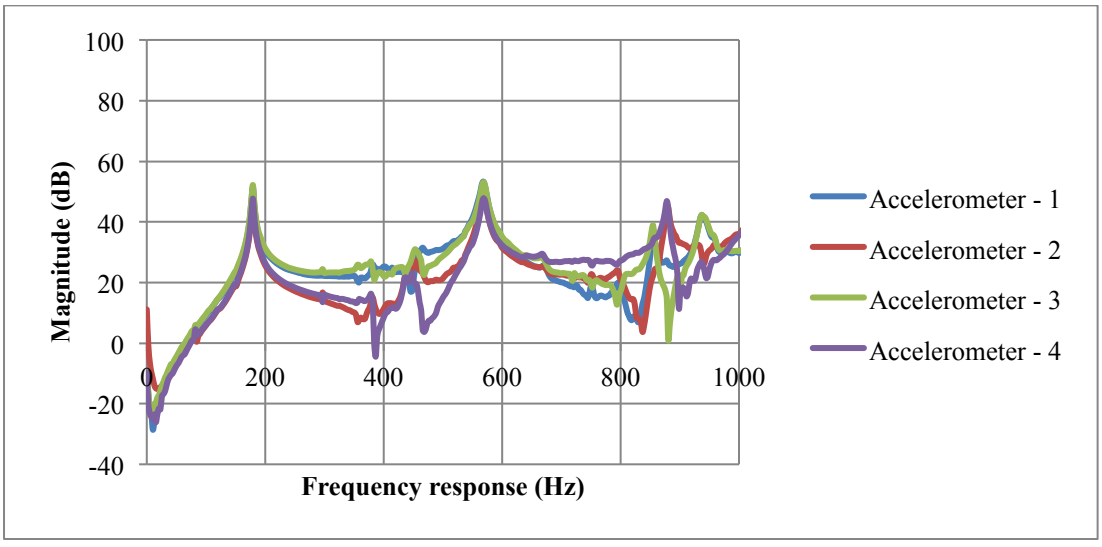

Figure 5.1 FRF of support structure in impulse hammer experiment

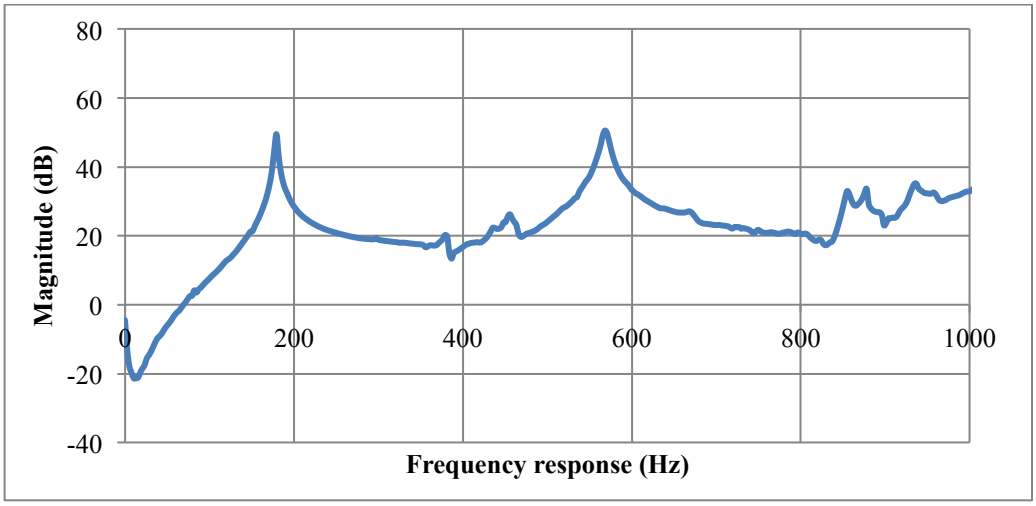

Figure 5.2 Frequency response (Hz) versus Magnitude (dB) 1

Figure 5.2 illustrates the average of the frequency response obtained from the four accelerometers attached on the support structure. The peak points of the graph above are the natural frequencies of such structure. Therefore, the first peak point in the graph is located at 179.2Hz while the second and third frequencies are at 381.44 and 455.68Hz respectively. And then, the next peak point is clear, located at 568.32Hz.

5.1.2 Fluid-filled Pipe in Impulse Hammer Experiment

The graph below demonstrates results of the pipe structure in the impulse hammer experiment. Fig. 5.3 shows the frequency response of the two accelerometers on the pipe structure. Fig. 5.4 was obtained by calculating the average in the two sets of data.

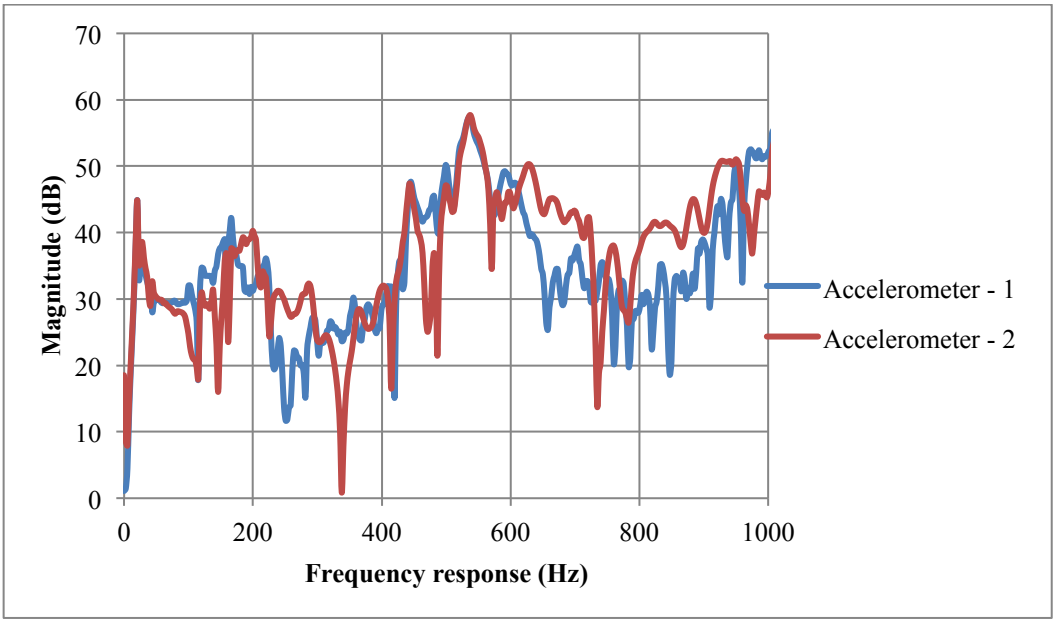

Figure 5.3 FRF of fluid-filled pipe in impulse hammer experiment

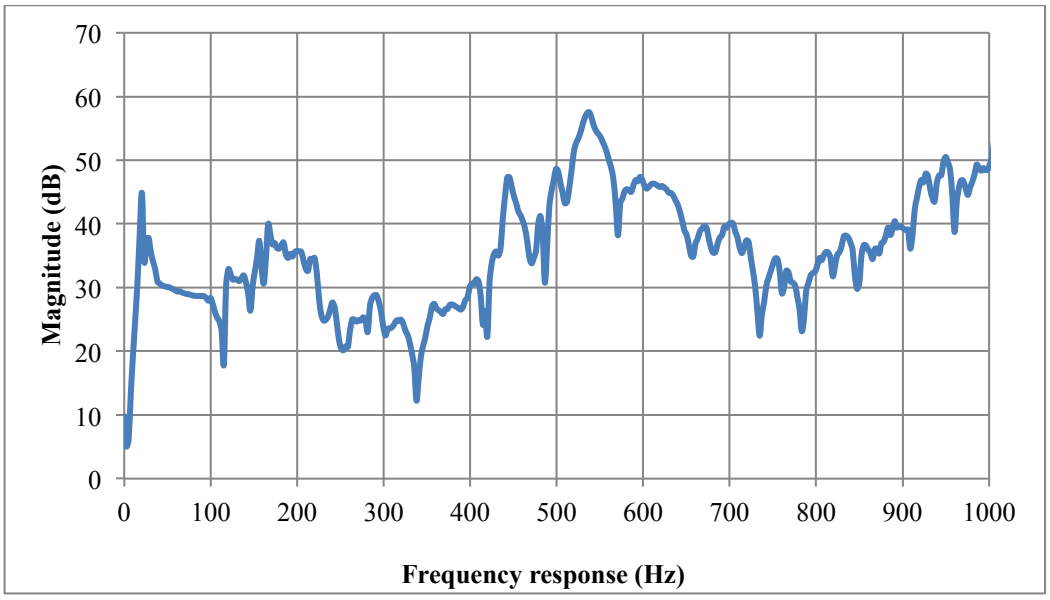

Figure 5.4 Frequency response (Hz) versus Magnitude (dB) 2

The frequency response first peaks at 20.48Hz. The second peak point located at 30.72Hz is very close to the first one, followed by the third, which is 99.84Hz. The next peak point is located at 156.16Hz. It can be seen that the natural frequencies of the pipe structure are lower than those of support structure.

5.1.3 Coupled System in Impulse Hammer Experiment

The results are obtained from accelerometers on both support and pipe structures. Figures 5.5 and 5.7 show the frequency response of every accelerometer in the combined structure, and Figures 5.6 and 5.8 are obtained by averaging each result.

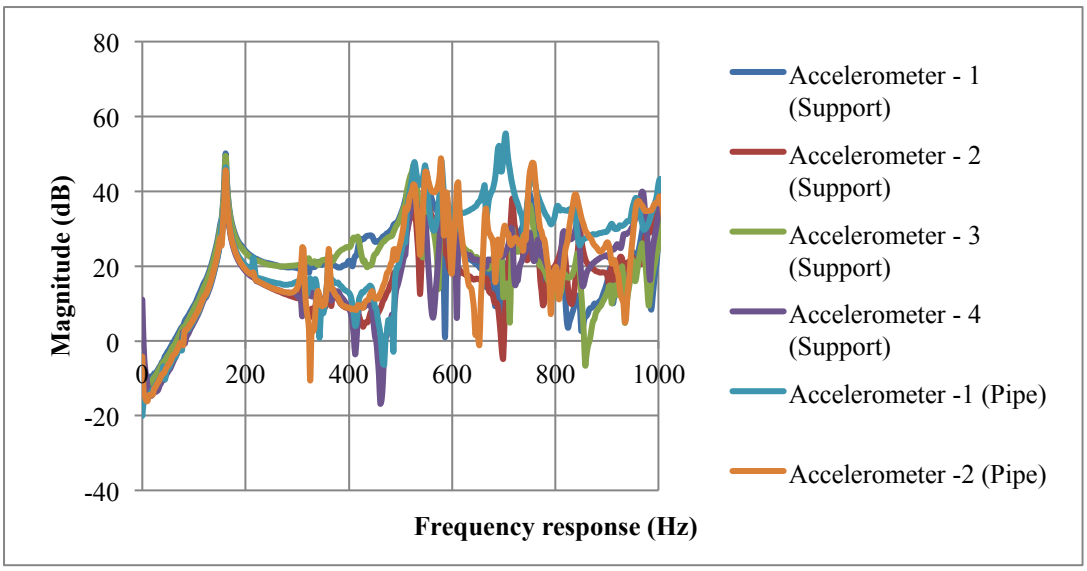

Figure 5.5 FRF of coupled system in impulse hammer experiment 1

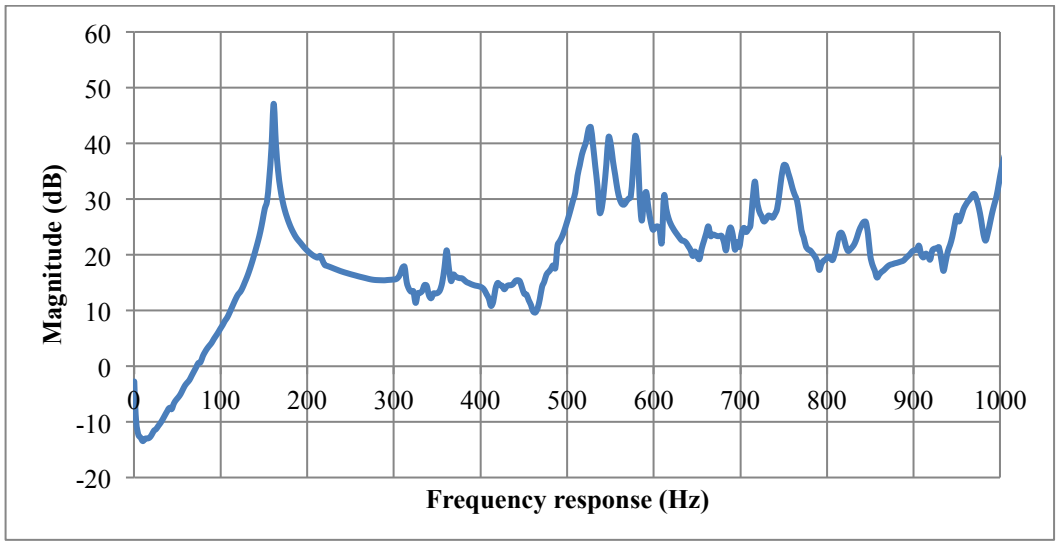

Figure 5.6 Frequency response (Hz) versus Magnitude (dB) 3

The graph above shows the average result obtained after 25 impacts conducted on the support structure of the combined system. The first peak point is located at 161.28Hz, followed by the second peak point at 360.96Hz. But this point is not remarkable. The

next peak point is located at 527.36Hz, which can be easily distinguished. The graph below illustrates results obtained after 25 times of impact on the pipe of the combined structure.

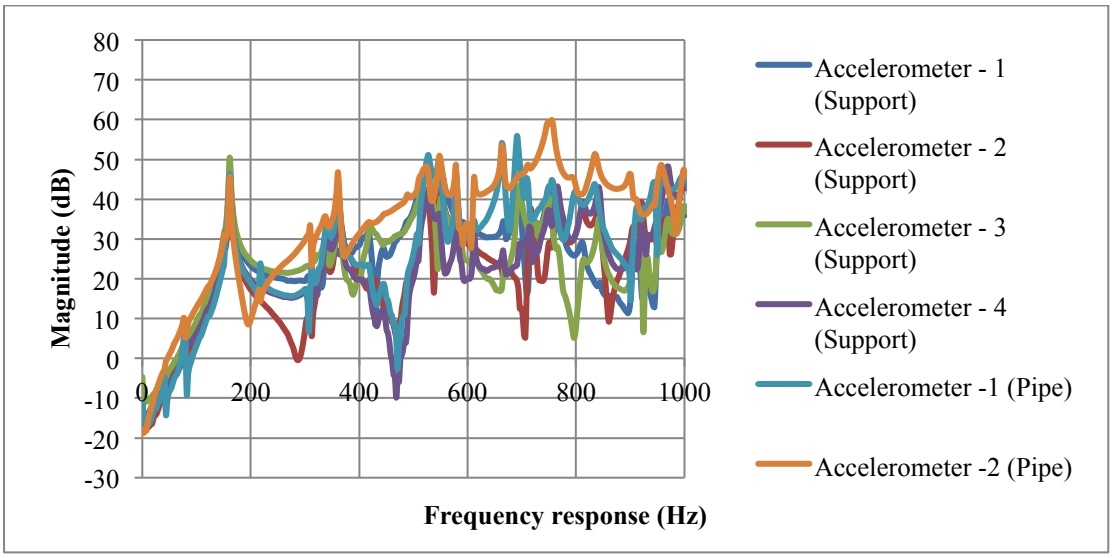

Figure 5.7 FRF of coupled system in impulse hammer experiment 2

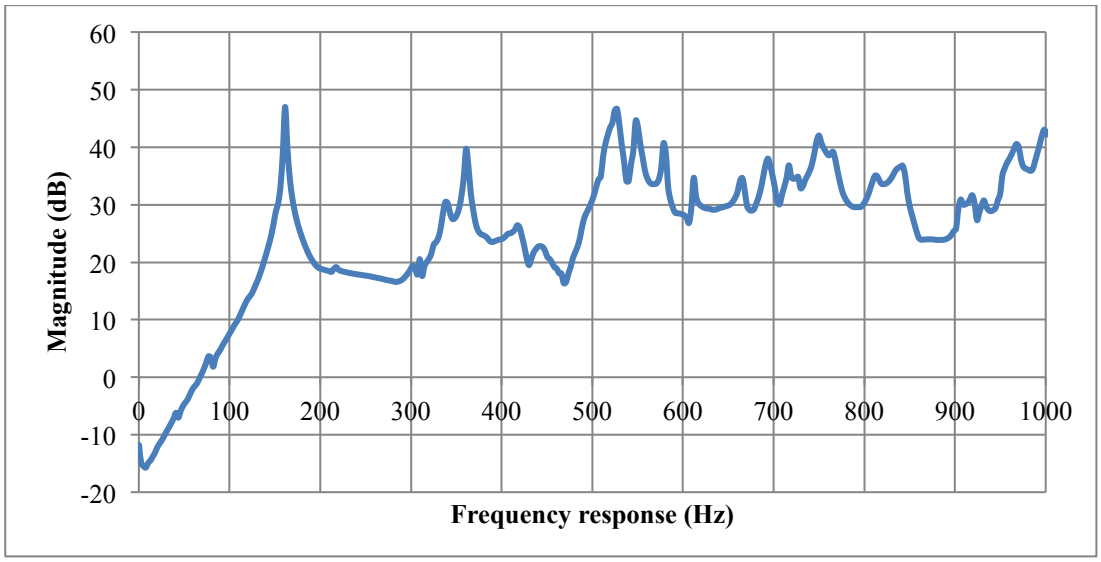

Figure 5.8 Frequency response (Hz) versus Magnitude (dB) 4

The shape of the graph above shows certain similarities with the previous one obtained after 25 times of impact on the support structure. The first peak point in the graphs is located at 161.28Hz, which is the same as before. The second peak point is at 360.96Hz.

This point is more distinguishable and higher than before. The next peak point is located at 527.36Hz.

5.2 Vibration Shaker Excitation Experiment Results

The results were obtained using a vibration shaker. The vibration shaker provided various vibration ranges from 10 to 5000Hz on experiment. The data collected from the four accelerometers attached on the support structure and the other two accelerometers on the pipe structure were analysed. Thus, the corresponding natural frequencies of the support structure and the pipe as well as the combined structure were found in the vibration shaker experiment.

5.2.1 Support Structure in Vibration Shaker Experiment

Firstly, the results for the support structure were analysed in the vibration shaker experiment. Frequency response was plotted versus magnitude as shown in Figure 5.9.

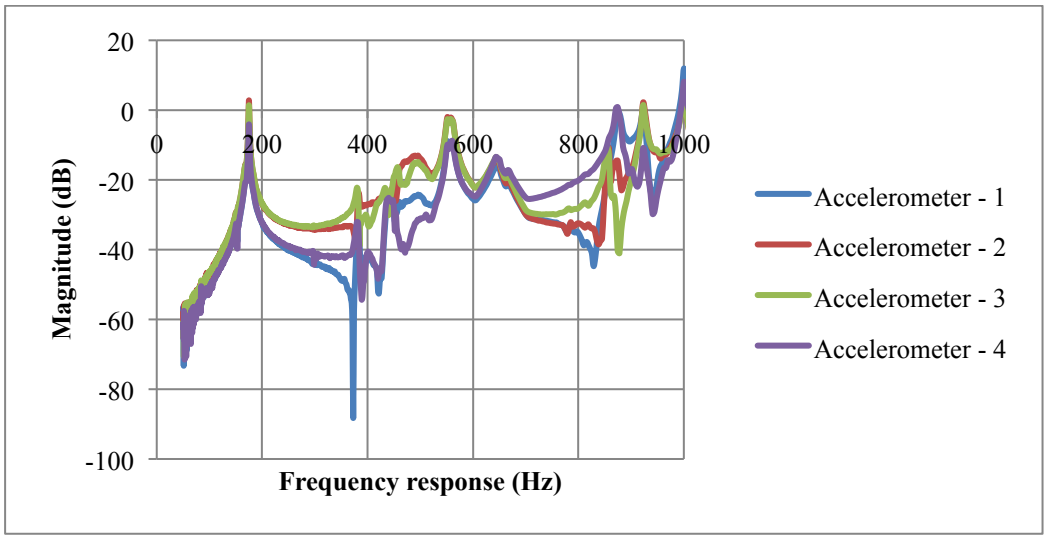

Figure 5.9 FRF of support structure in vibration shaker experiment

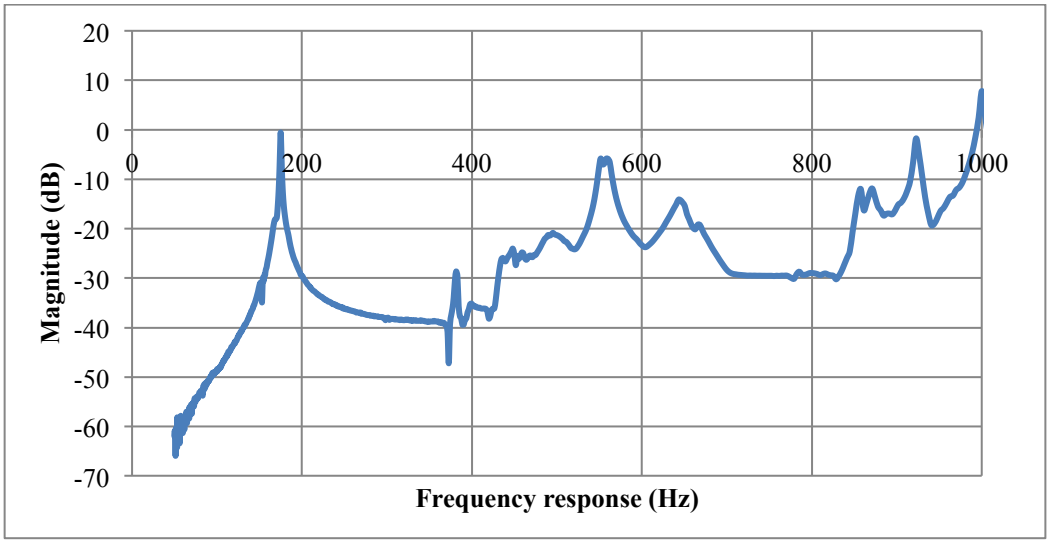

Figure 5.10 Frequency response (Hz) versus Magnitude (dB) 5

Figure 5.10 illustrates the average of the frequency response obtained from the four accelerometers attached on the support structure. The peak points of the graph above are the natural frequencies of such structure. Therefore, the first peak point in the graph is located at 174.89Hz while the second and third frequencies are at 381.39 and 495.22Hz respectively. And then, the next peak point is clear, located at 551.45Hz.

5.2.2 Fluid-filled Pipe in Vibration Shaker Experiment

The graph below demonstrates results of the pipe structure in the vibration shaker experiment. Fig. 5.11 shows the frequency response of the two accelerometers on the pipe structure. Fig. 5.12 was obtained by calculating the average in the two sets of data.

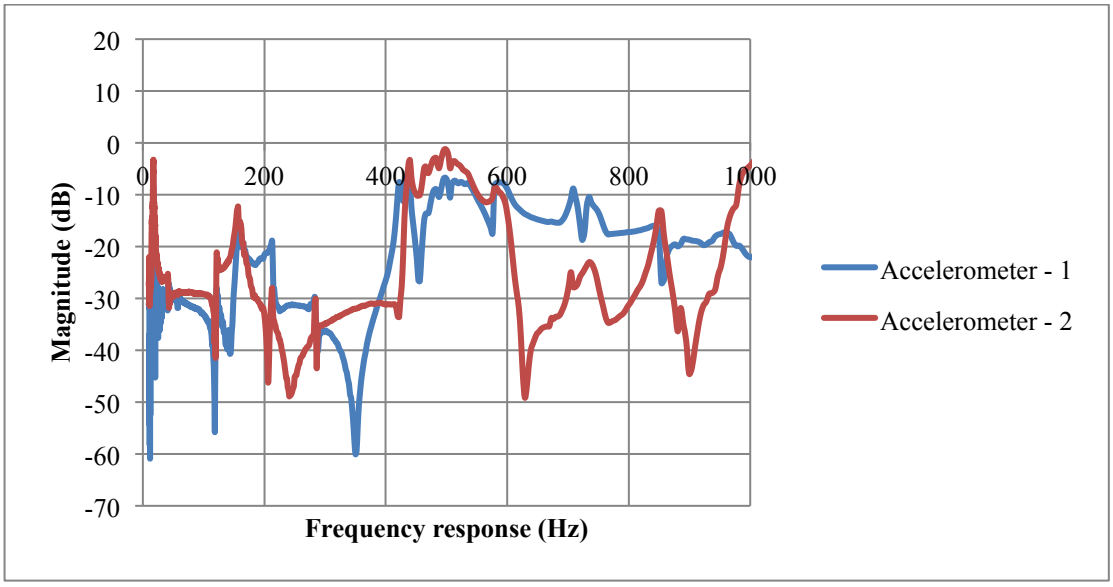

Figure 5.11 FRF of fluid-filled pipe in vibration shaker experiment

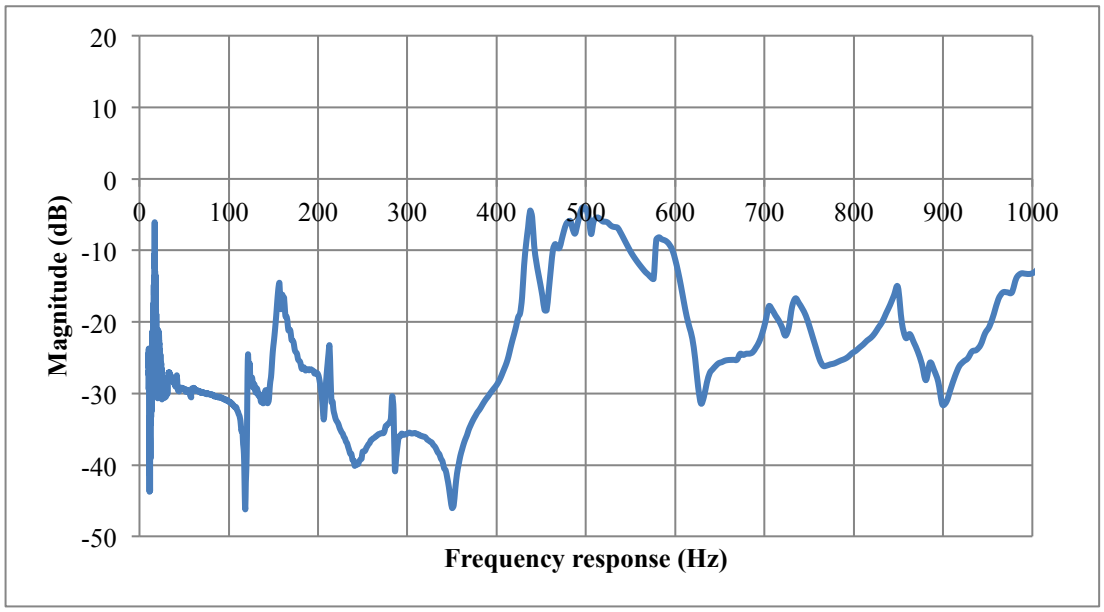

Figure 5.12 Frequency response (Hz) versus Magnitude (dB) 6

The graph was obtained from the data of two accelerometers attached on pipe structure. The frequency response first peaks at 17.06Hz. The second peak point located at 41.81Hz is very close to the first one, followed by the third, which is 121.62Hz. The next peak point is located at 156.78Hz. It can be seen that the natural frequencies of the pipe structure are lower than those of support structure.

5.2.3 Coupled System in Vibration Shaker experiment

The results are obtained from accelerometers on both support and pipe structures. Figures 5.13 and 5.15 show the frequency response of every accelerometer in the combined structure, and Figures 5.14 and 5.16 are obtained by averaging each result.

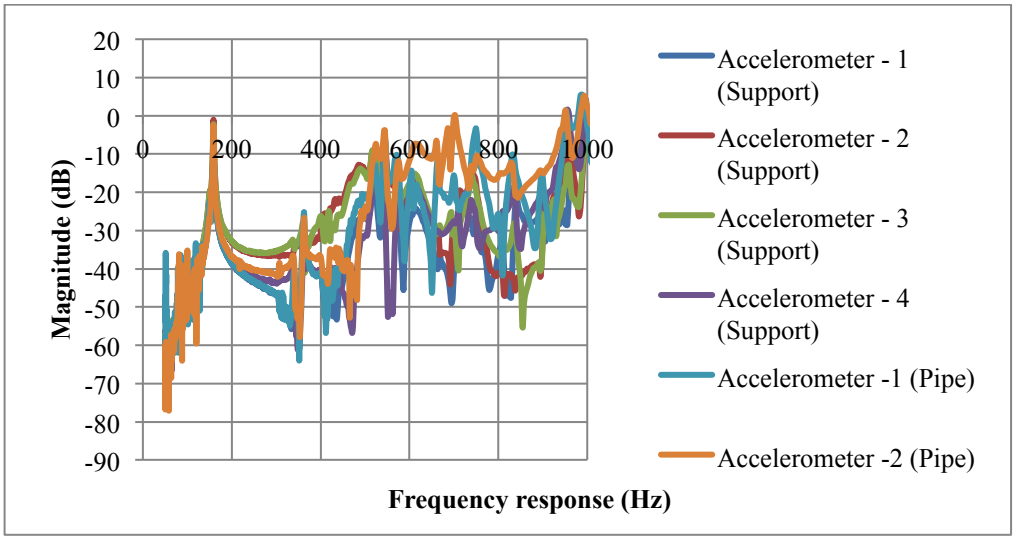

Figure 5.13 FRF of coupled system in vibration shaker experiment 1

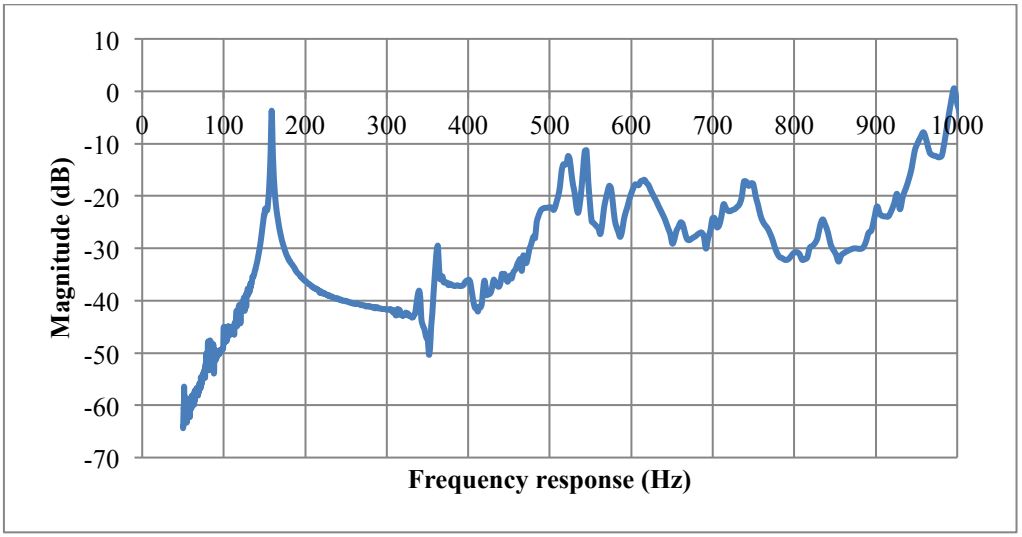

Figure 5.14 Frequency response (Hz) versus Magnitude (dB) 7

The graph above shows the average result obtained the range of frequency between 50 and 5000Hz on support structure of combined system. The first peak point is located at 158.87Hz, followed by the second peak point at 362.82Hz. But this point is not remarkable. The next peak point is located at 545.13Hz, which can be easily distinguished. The graph below illustrates results obtained after providing the range of frequency between 50 and 5000Hz on the pipe of the combined structure.

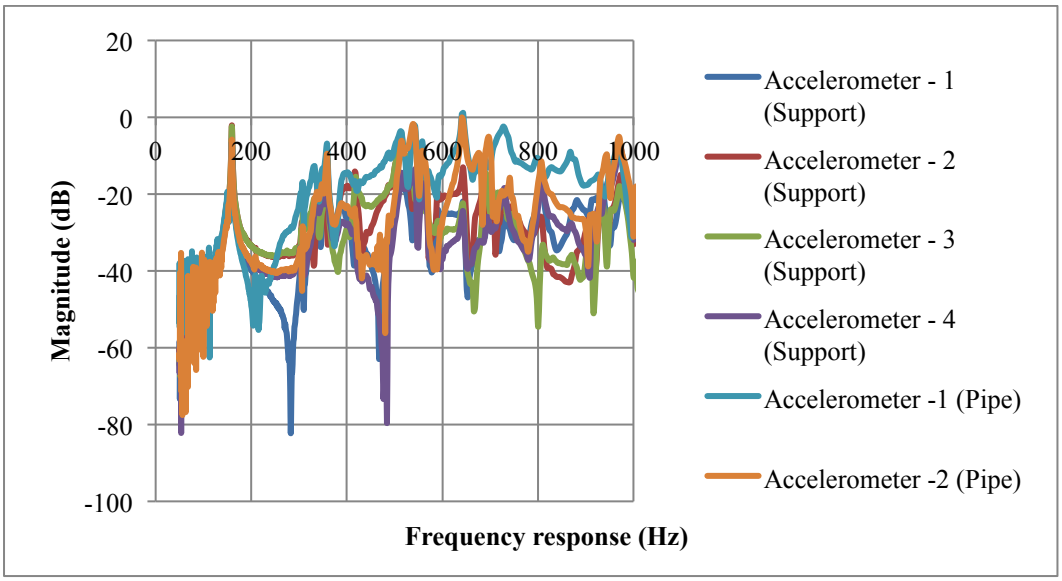

Figure 5.15 FRF of coupled system in vibration shaker experiment 2

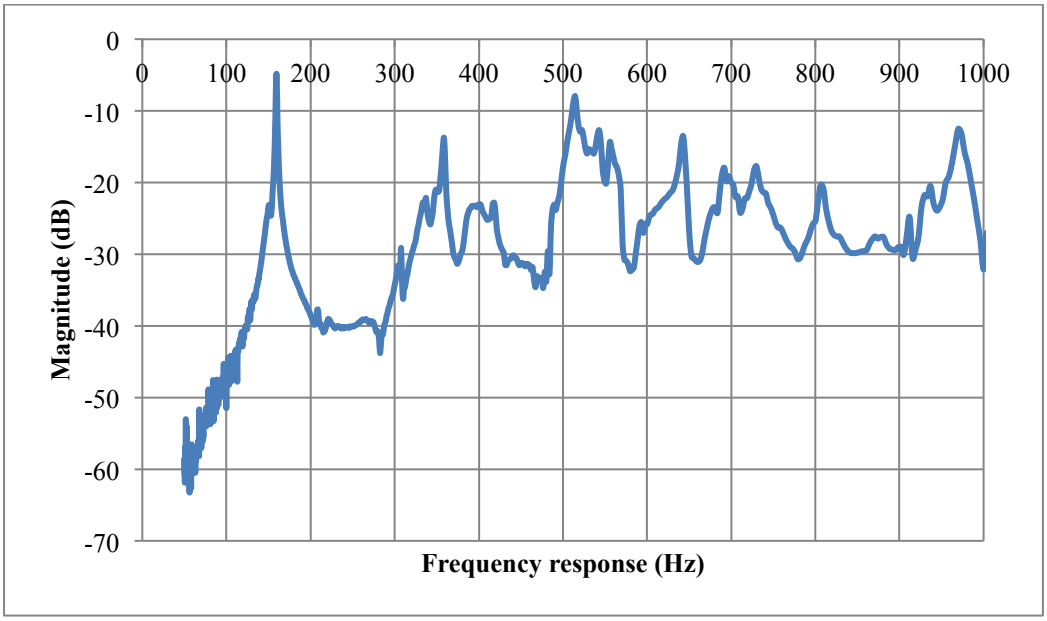

Figure 5.16 Frequency response (Hz) versus Magnitude (dB) 8

The shape of the graph above shows certain similarities with the previous one obtained after the range of frequency between 50 and 5000Hz exerted on support structure of combined system. The first peak point in the graphs is located at 158.87Hz, which is the same as before. The second peak point is at 358.66Hz. This point is more distinguishable and higher than before. The next peak point is located at 514.61Hz.

5.3 FEM Simulation Result

Steel Support Structure	Copper Pipe	Water
D = 25.4 mm	D = 12.7 mm	K = 2.1 Gpa
Thickness = 1.2 mm	Thickness = 1 mm	$\rho = 1000\ kg/m^3$
E = 210 Gpa	E = 100 Gpa	μ = 0.001 Pas
$\rho = 7900\ kg/m^3$	$\rho = 8900\ kg/m^3$	
ν = 0.3	ν = 0.3	

Table 5.1 Geometrical and Material properties of coupled system

The geometrical and material properties of the coupled system in Table 5.1 are applied to the equations introduced in Chapter Three in order to conduct finite element simulations. Hence the first four order natural frequencies and modal shapes of the coupled system can be acquired via equation (18), which are shown in Figure 5.17.

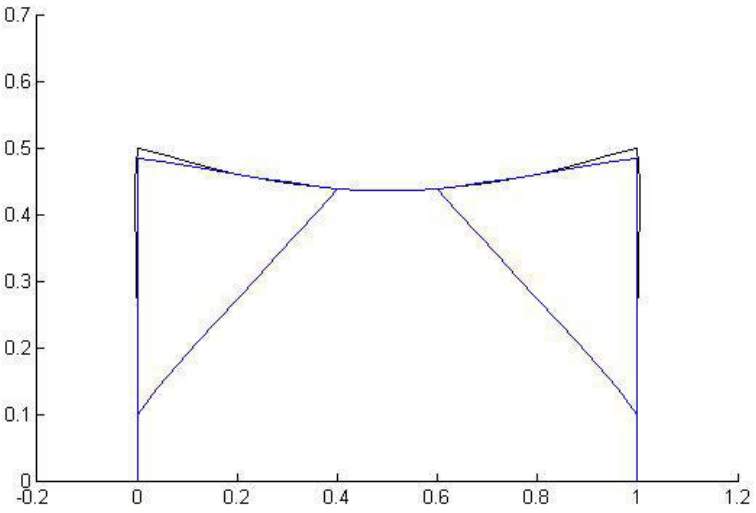

f1 = 165.15 Hz

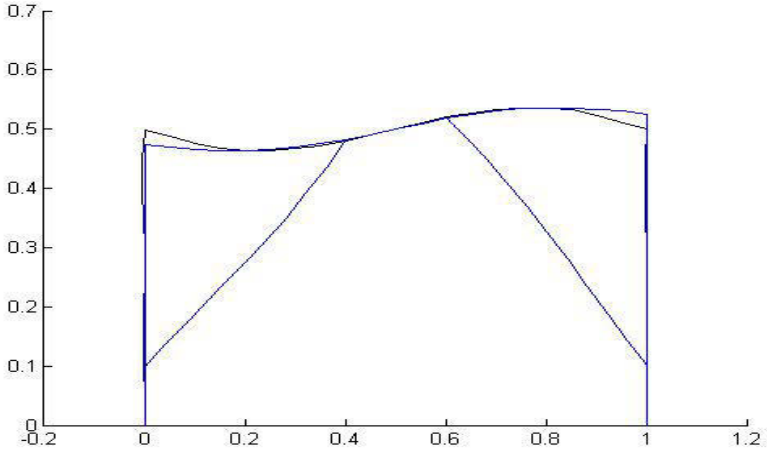

f2 = 387.87 Hz

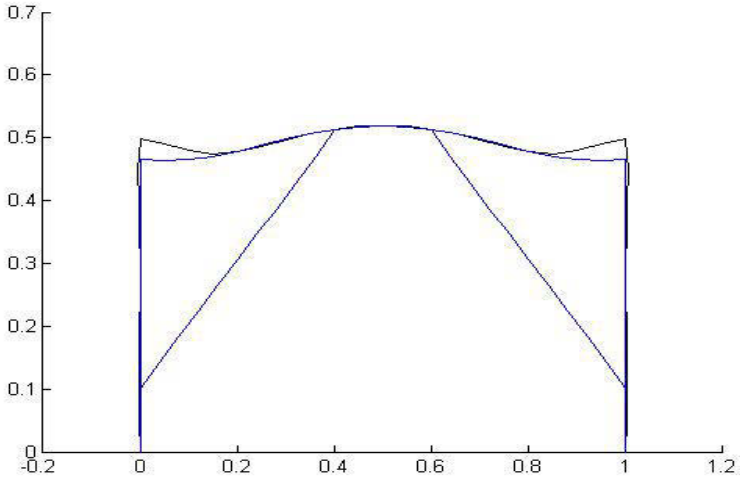

f3 = 406.53 Hz

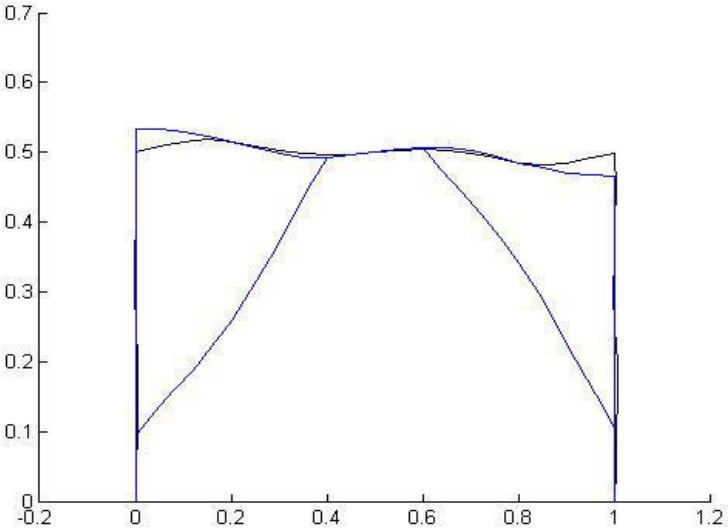

f4 = 480.09 Hz

Figure 5.17 First four order modes of coupled system

6 Discussion

After comparing the natural frequencies of the steel-frame support structure, the fluid-filled pipe and the coupled system, the differences and similarities between the impulse hammer and the vibration shaker experiments will be discussed. Following is the comparison between theoretical and experiment results.

6.1 Comparison of Natural Frequencies between Different Structures

Obviously, the support structure, the fluid-filled pipe and coupled system structure have different natural frequencies. The support structure has the highest natural frequencies. For instance, the first natural frequency of the support structure in the impulse hammer experiment is located at 179.20Hz, which is higher than that of the pipe (20.48Hz) and of the combined structures (161.28Hz). The vibration shaker experiment and FEM simulation share the same conclusion.

Other the other hand, the pipe has the lowest natural frequencies. Therefore, the pipe structure could be excited by low frequencies. All the first natural frequencies of the pipe in impulse hammer and vibration shaker experiment and FEM simulation are approximately 20Hz.

However, the natural frequency of the combined structure differ greatly from that of the pipe, while shares certain similarities with that of the support structure. Despite that the support structure and the pipe are bound by only five connectors, such combination has a huge influence to the pipe on the natural frequencies. As the copper pipe could be excited at low frequencies, the big movement of the vibration may lead to serious

problems on durability and safety of the pipeline. Thus, the pipeline can be protected from some impacts stemming from pumps and valve operation by combining with the appropriate support structure in practice. As a result, the experiment demonstrated that the connection between the support structure and the pipe exerted a positive influence on the pipeline system and that using the support structure was an effective method when it comes to pipeline vibration control.

6.2 Comparison of Natural Frequencies between Impulse Hammer and Vibration Shaker Excitation Experiments

The natural frequencies of each structure were obtained in two different experiments. The two experiments differed in the impact sources, one of which was the impulse hammer and the other the vibration shaker. Figures 6.1 and 6.2 show the frequency response results in the impulse hammer and vibration shaker experiments, respectively.

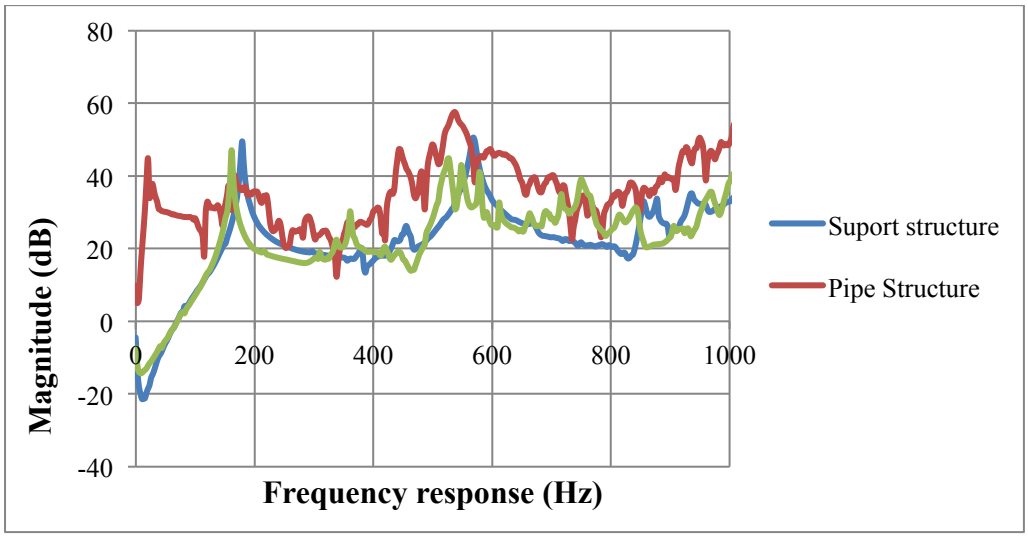

Figure 6.1 Frequency response (Hz) versus Magnitude (dB) in impulse hammer experiment

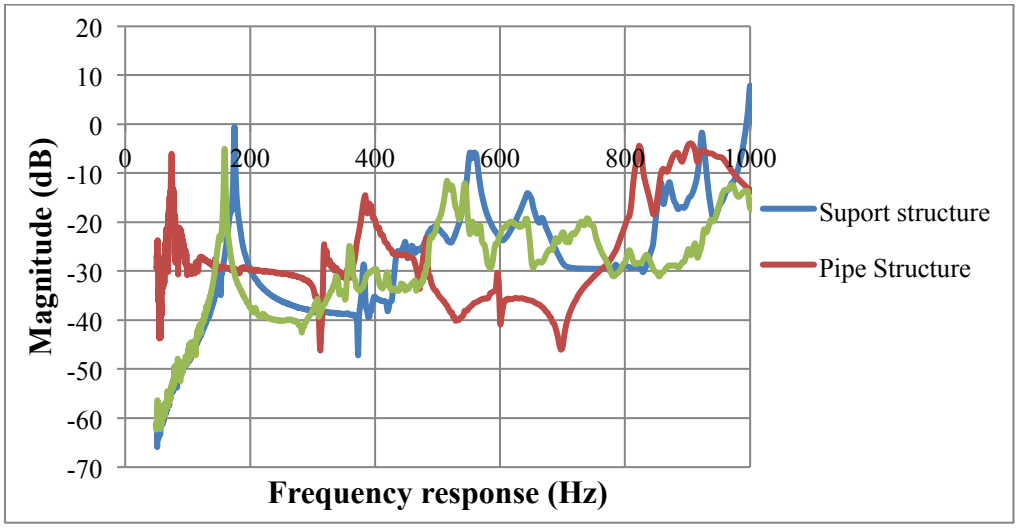

Figure 6.2 Frequency response (Hz) versus Magnitude (dB) in vibration shaker experiment

By comparing the two graphs, it can be observed that the natural frequencies in the impulse hammer experiment are harder to distinguish than those in the vibration shaker experiment that involves less noise. This is because the vibration shaker can provide large input forces, and thus the response can be measured easily. Moreover, the output of the shaker can be easily controlled. The vibration signal is a swept sinusoidal or a random type signal.

Nevertheless, what needs to be taken into consideration is that the effect of the mass of the shaker should be minimized, since it will influence the measured response if the shaker is attached to the structure or the machine being tested. In this thesis, the shaker is attached to the structure by a stringer to isolate the shaker and to reduce the added mass.

Although the impact hammer is simple, portable, inexpensive, and much faster to use than a shaker, it is often not capable of imparting sufficient energy to obtain adequate response signals in the frequency range of interest. It is also difficult to control the

direction of the applied force with an impact hammer. The shape of the frequency response is dependent on the mass and stiffness of both the hammer and the structure or machine. Usually, the useful range of frequency excitation is limited by a cut-off frequency, which implies that the structure does not receive sufficient energy to excite modes beyond. In summary, the vibration shaker experiment acquires better results than the impulse hammer experiment.

6.3 Comparison between Theoretical and Experimental Result

		Theoretical results			**Experimental results**					
		FEM			Impulse hammer			Vibration shaker		
		Support	Pipe	Combined	Support	Pipe	Combined	Support	Pipe	Combined
Natural Frequency (Hz)	1	180.51	18.22	165.15	179.2	20.48	161.28	174.89	17.06	158.87
	2	405.90	38.04	387.87	381.44	30.72	360.96	381.39	41.81	362.82
	3	483.37	109.78	406.53	455.68	99.84	-	495.22	121.62	-
	4	500.64	172.13	480.09	568.32	156.16	527.36	551.45	156.78	514.61

Table 6.1 Natural frequency of each structure in Theoretical and experimental results

By comparing the natural frequencies listed in the table above, the error of the first natural frequencies between finite element analysis and experimental measurement results is less than 5% and the root-mean-square error of modal frequencies is smaller than 10%. That means experiments proved that it is feasible to use the finite element method to develop a multiple coupling system, which is valuable for further study in more depth.

7 Conclusion

The thesis discussed two kinds of coupled vibration analyses in the case of a fluid-filled pipe rigidly bonded to a steel-frame structure at a number of fixed points. And finite element models are built respectively for the fluid-structure interaction analysis and solid structural coupling analysis. The FEM provides an alternative to reported numerical and analytical method. In addition, a dynamic condensation method which could effectively reduce the number of the coupled system's degree of freedom is successfully tested by a summary HIS model. Hence the proposed finite element method allows the efficient computation of many pipe configurations and enables the vibroacoustic optimization.

Numerical examples are given to verify the feasibility of the calculation method. The obtained computational natural frequencies are compared with those obtained from experiments. Different parameters influencing the coupled vibration are discussed as well and these results could provide theoretical foundation for the optimization design of structure-fluid coupled systems, such as hydraulically interconnected suspensions and fluid-filled pipe systems for vehicle braking, etc.

REFERENCES

1. Lavooij, C.S.W. and A.S. Tijsseling, *Fluid-structure interaction in liquid-filled piping systems.* Journal of Fluid and Structures, 1991. **5**: p. 573-595.
2. Skalak, R., *An extension of the theory of waterhammer.* Transactions of the ASME, 1956. **78**: p. 105-116.
3. Wiggert, D.C., *Coupled transient flow and structure motion in liquid-filled piping systems: a survey*, in *Int. Conf. on Computers in Engineering, Pressure Vessels and Piping, ASME*1986: Chicago, U.S.A. p. Paper 86-PVP-4.
4. Tijsseling, A.S., *Fluid-structure interaction in liquid-filled pipe sysems: a review.* Journal of Fluid and Structures, 1996. **10**: p. 109-146.
5. Tijsseling, A.S. and C.S.W. Lavooij, *Waterhammer with fluid-structure interaction.* Applied Scientific Research, 1990. **47**: p. 273-285.
6. Uffer, R.A., *Water hammer conservatisms.* Fluid-Structure Interaction, Transient Thermal-Hydraulic, and Strcutural Mechanics, 1993. **253**: p. 179-184.
7. Almeida, A.B.D. and A.A.M. Pinto. *A special case of transient forces on pipeline support due to waterhammer effects*. in *Proceedings of the 5th International Conference on Pressure Surges*. 1986. BHRA, Hanover, Germany.
8. Wang, C.Y., et al., *Analysis of fluid-structure interaction and structural response of Chernobyl-4 reactor*, in *Transactions of the SMiRT10*1989: Anaheim, U.S.A. p. 109-119.
9. Obradovic, P., *Fluid-strcture interaction: an accident which has demonstrated the necessity for FSI analysis*, in *Transactions of the 15th IAHR Symposium on Hydraulic Machinery and Cavitation*1990b: Belgrade, Yugoslavia. p. Paper J2.
10. Zienkiewicz, O.C. and P. Bettess, *Fluid-structure dynamic interaction and wave forces: an introduction to numerical treatment.* International Journal for Numerical Methods in Engineering, 1978. **13**: p. 1-16.
11. Heinsbroek, A.G.T.J., C.S.W. Lavooij, and A.S. Tijsseling, *Fluid-structure interaction in non-rigid piping——a numerical investigation*, in *Transactions of SMiRT11*1991: Tokyo, Japan. p. Paper B12/1, 309-314.

12. Heinsbroek, A.G.T.J. and A.S. Tijsseling, *Fluid-structure interaction in non-rigid pipeline systems——a numerical investigation II*, in *Transactions of SMiRT12*1993: Stuttgart, Germany. p. Paper J08/2.
13. Heinsbroek, A.G.T.J., *Fluid-structure interaction in non-rigid pipeline systems——comparative analyses*, in *ASME/TWI 12th Int Conf on Offshore Mechanics and Arctic Engineering*1993: Glasgow, UK. p. Paper OMAE-93-1018, 405-410.
14. Heinsbroek, A.G.T.J. and A.S. Tijsseling, *The influence of support rigidity on waterhammer pressures and pipe stresses*, in *Proc of 2nd Int Conf on Water Pipeline Systems, BHR Group*1994: Edinburgh, UK. p. 17-30.
15. Erath, W., B. Nowotny, and J. Maetz, *Simultaneous coupling of the calculation of pressure waves and pipe oscillations.* 3R International, 1998. **37**: p. 501-508.
16. Tijsseling, A.S. and A.G.T.J. Heinsbroek, *The influence of bend motion on waterhammer pressures and pipe stresses*, in *Proc of 3rd ASME & JSME Joint Fluids Engineering Conf, Symp S-290 Waterhammer*, J.C.P. Liou, Editor 1999: San Francisco. p. ASME-FED 248 1-7.
17. Tijsseling, A.S., *Poisson-coupling beat in extended waterhammer theory*, in *Proc of 4th Int Symp on Fluif-Structure Interactions, Aeroelasticity, Flow-Induced Vibration and Noise*1997: Dallas. p. ASME-AD 53-2, 529-532.
18. Bouabdallah, S. and F. Massouh, *Fluid-structure interaction in hydraulic networks*, in *Proc of 4th Int Symp on Fluif-Structure Interactions, Aeroelasticity, Flow-Induced Vibration and Noise*1997: Dallas. p. ASME-AD 53-2, 543-548.
19. Gorman, D.G., J.M. Reese, and Y.L. Zhang, *Vibration of a flexible pipe conveying viscous pulsating fluid flow.* J. Sound Vib., 2000. **230(2)**: p. 379-392.
20. Lee, U., C.H. Pak, and S.C. Hong, *The dynamics of a piping system with internal unsteady flow.* J. Sound Vib., 1995. **180(2)**: p. 297-311.
21. Charley, J. and G. Caignaert, *Vibroacoustical analysis of flow in pipes by transfer matrix with fluid-structure interaction*, in *Proc of 6th Int Meeting of the IAHR Work Goup on the Behavior of Hydraulic Machinery under Steady Oscillatory Conditions*1993: Lausanne, Switzerland. p. 1-9.
22. Zhang, L., A.S. Tijsseling, and A.E. Vardy, *Frequency response analysis in internal flows.* J. Hydrodynam, 1995. **Series B 3(3)**: p. 39-49.

23. Svingen, B., *Fluid structure interaction in piping systems*, 1996, PhD Thesis, The Norwegian Univ of Science and Technology, Faculty of Mechanical Engineering: Trondheim, Norway.
24. Svingen, B., *Fluid structure interaction in slender pipes*, in *Proc of 7th Int Conf on Pressure Surges and Fluid Transients in Pipelines and Open Channels, BHR Group*1996: Harrogate, UK. p. 385-396.
25. Svingen, B., *A frequency domain solution of the coupled hydromechanical vibrations in piping systems by the finite element method*, in *Proc of 17th IAHR Symp on Hydraulic Machinery and Cavitation*1994: Beijing, PR China. p. 1259-1269.
26. Gajic, A., et al., *Fluid-structure interaction analysis in frequency domain*, in *Proc of 7th Int Meeting of the IAHR Work Group on the Behavior of Hydraulic Machinery unfer Steady Oscillatory Conditions*1995: Ljubljana, Slovenia. p. Paper F5.
27. Gajic, A., S. Pejovic, and Z. Stojanovic, *Hydraulic oscillation analysis using the fluid-structure interaction model*, in *Proc of 18th IAHR Symp on Hydraulic Machinery and Cavitation*1996: Valencia, Spain. p. 845-854.
28. Svingen, B. and M. Kjeldsen, *Fluid structure interaction in piping systems*, in *Proc of Int Conf on Finite Elements in Fluid——New Trends and Applications*1995: Venice, Italy. p. 955-963.
29. Svingen, B., *Rayleigh damping as an approximate model for transient hydraulic pipe friction*, in *Proc of 8th Int Meeting of the IAHR Work Group on the Behavior of Hydraulic Machinery unfer Steady Oscillatory Conditions*1997: Chatou, France. p. Paper F2.
30. Svingen, B., et al., *Two numerical methods of hydraulic oscillations analysis in piping systems including fluid-structure interaction*, in *Proc of Int Conf on Fluid Engineering*1997, JSME Centennial Grand Congress: Tokyo, Japan. p. 1601-1606.
31. Moussou, P., et al., *Coupling effects in a two elbows piping system*, in *Proc of 7th Int Conf on Flow Induced Vibrations*2000: Lucerne, Switzarland. p. 579-586.
32. Budny, D.D., *The influence of structural damping on the internal fluid pressure during a fluid transient pipe flow*, 1988, PhD Thesis, Michigan State Univ, Dept of Civil and Environmental Engineering, East Lansing MI.
33. Wiggert, D.C., F.J. Hatfield, and S. Stuckenbruck, *Analysis of liquid and structural transients by the method of characteristics.* ASME J. Fluids Eng., 1987. **109**: p. 161-165.
34. Wiggert, D.C., R.S. Otwell, and F.J. Hatfield, *The effect of elbow restraint on pressure transients.* ASME J. Fluids Eng., 1985. **107**: p.

402-406. (Discussed by R. E. Schwirian and J. S. Walker in 108, 121-122).
35. Heinsbroek, A.G.T.J. and A.C.H. Kruisbrink, *Fluid-structure interaction in non-rigid pipeline systems——large scale validation experiments*, in *Transactions of SMiRT12*1993: Stuttgart, Germany. p. Paper J08/1.
36. Heinsbroek, A.G.T.J. and A.C.H. Kruisbrink, *FLUSTRIN Phase 3 Validation Experiments and Simulations*, 1991, Delft Hydraulics: Delft, The Netherlands. p. Research Report J 526.
37. Heinsbroek, A.G.T.J., *Fluid-structure interaction in non-rigid pipeline systems.* Nucl. Eng. Des., 1997. **172**(123-135): p. Paper J08/1.
38. Kojima, E. and M. Shinada, *Dynamic Behavior of a finite length straight pipe subject to water-hammer (2nd report, for a very thin-walled pipe).* Trans. Jpn. Soc. Mech. Eng., 1988. **Ser. B 54**: p. 3346-3353.
39. Mitchell, A.R. and D.F. Griffiths, *The Finite Difference Method in Partial Differential Equations* 1980: John Wiley and Sons.
40. Elansary, A.S., W. Silva, and M.H. Chaudhry, *Numerical and experimental investigation of transient pipe flow.* J. Hydraul. Res., 1994. **32**: p. 689-706.
41. Vardy, A.E., D. Fan, and A.S. Tijsseling, *Fluid/structure interaction in a T-piece pipe.* J. Fluids Struct., 1996. **10**: p. 763-786.
42. Tenteralli, S.C., *Propagation of noise and vibration in complex hydraulic tubing systems*, 1990, PhD Thesis, Lehigh Univ, Dept of Mechanical Engineering, Bethlehem PA.
43. Brown, F.T. and S.C. Tenteralli, *Dynamic behavior of complex fluid-filled tubing systems——Part 1: Tubing analysis.* J. Dyn. Syst., Meas., Control, 2001. **123**: p. 71-77.
44. Tenteralli, S.C. and F.T. Brown, *Dynamic behavior of complex fluid-filled tubing systems——Part 2: System analysis.* J. Dyn. Syst., Meas., Control, 2001. **123**: p. 78-84.
45. Lesmez, M.W., *Modal analysis of vibrations in liquid-filled piping systems*, 1989, PhD Thesis, Michigan State Univ, Dept of Civil and Environmental Engineering, East Lansing MI.
46. Lesmez, M.W., D.C. Wiggert, and F.J. Hatfield, *Modal analysis of vibrations in liquid-filled piping-systems.* ASME J. Fluids Eng., 1990. **112**: p. 311-318.
47. Jezequel, L., A. Khamlichi, and F. Tephany, *Interpretation of fluid-structure interaction experiment in a frame pipe.* Sloshing, Fluid-Structure Interaction and Structural Response due to Shock and Impact Loads, 1994: p. ASME-PVP 272 1-12.

48. Jong, C.A.F.D., *Analysis of pulsations and vibrations in fluid-filled pipe systems*, 1994, 2000, PhD Thesis, Eindhoven Univ of Technology, Dept of Mechanical Engineering, Eindhoven, The Netherlands (Errata: April 2000).
49. Jong, C.A.F.D., *Analysis of pulsations and vibrations in fluid-filled pipe systems*, in *Proc. of 1995 Design Engineering Tech. Conf.*1995, Boston. p. ASME-DE 84-2, Vol 3, Part B, 829-834.
50. Zhang, L., A.S. Tijsseling, and A.E. Vardy, *FSI analysis of liquid-filled pipes.* J. Sound Vib., 1999. **224(1)**: p. 69-99.
51. Vardy, A.E. and D. Fan, *Flexural waves in a closed tube*, in *Proc. of 6th Int. Conf. on Pressure Surges, BHRA*1989: Cambridge, UK. p. 43-57.
52. Jiao, Z., Q. Hua, and K. Yu, *Frequency domain analysis of vibrations in liquid-fiiled piping systems.* Acta Aeronaut. Astronaut. Sinica, 1999. **20(4)**: p. 1-18(in Chinese).
53. Erath, W., B. Nowotny, and J. Maetz, *Modelling the fluid structure interaction produced by a waterhammer during shutdown of high-pressure pumps.* Nucl. Eng. Des., 1999. **193**: p. 283-296.
54. Diesselhorst, T., R. Schmidt, and W. Schnellhammer, *Realistic calculation of pressure surges. Inclusion of dynamic friction and fluid/structure interaction,.* 3R International, 2000. **39**: p. 678-682.
55. Burmann, W. and H. Thielen, *Measurement and computation of dynamic reactive forces on pipes containing flow.* 3R International, 1988. **27**: p. 434-440.
56. Tijsseling, A.S. and A.E. Vardy, *Axial modelling and testing of a pipe rack*, in *Proc of 7th Int Conf on Pressure Surges and Fluid Transients in Pipelines and Open Channels, BHR Group*1996: Harrogate, UK. p. 363-383.
57. Hamilton, M. and G. Taylor, *Pressure surge-Case studies*, in *Proc of 7th Int Conf on Pressure Surges and Fluid Transients in Pipelines and Open Channels, BHR Group*1996: Harrogate, UK. p. 15-27.
58. Locher, F.A., J.B. Huntamer, and J.D. O'Sullivan, *Caution——Pressure surges in process and industrial systems may be fatal*, in *Proc of 8th Int Conf on Pressure Surges, BHR Group*2000: The Hague, The Netherlands. p. 3-18.
59. Hamilton, M. and G. Taylor, *Pressure surge-Criteria for acceptability*, in *Proc of 7th Int Conf on Pressure Surges and Fluid Transients in Pipelines and Open Channels, BHR Group*1996: Harrogate, UK. p. 343-362.

60. Chary, S.R., et al., *Transient response of a boiler feed pump discharge pipeline-A case study*, in *Proc of 16th Int Modal Analysis Conf*1998: Santa Barbara CA. p. 1-10.
61. Kwong, A.H.M. and K.A. Edge, *Structure-borne noise prediction in liquid-conveying pipe systems*, in *Proc of Institution of Mechanical Engineers Part I-J. Syst. Control Eng.*1996. p. 189-200.
62. Kwong, A.H.M. and K.A. Edge, *A method to reduce noise in hydraulic systems by optimizing pipe clamp locations*, in *Proc of Institution of Mechanical Engineers Part I-J. Syst. Control Eng.*1998. p. 267-280.
63. Jong, C.A.F.D. and M.H.A. Janssens, *Numerical studies of inverse methods for quantification of sound transmission along fluid-filled pipes*, in *Proc of Internoise 96*1996: Liverpool, UK. p. 3203-3206.
64. Janssens, M.H.A. and J.W. Verheij, *The use of an equivalent forces method for the experimental quantification of structural sound transmission in ships.* J. Sound Vib., 1999. **226(2)**: p. 305-328.
65. Tijsseling, A.S. and A.E. Vardy, *On the suppression of coupled liquid/pipe vibrations*, in *Proc of 18th IAHR Symp on Hydraulic Machinery and Cavitation*1996: Valencia, Spain. p. 945-954.
66. Munjal, M.L. and P.T. Thawani, *Prediction of the vibro-acoustic transmission loss of planar hose-pipe systems.* J. Acoust. Soc. Am., 1997. **101**: p. 2524-2535.
67. Koo, G.H. and Y.S. Park, *Vibration reduction by using periodic suppots in a piping system.* J. Sound Vib., 1998. **210(1)**: p. 53-68.
68. Hara, F., *Seismic vibration analysis of fluid-structure interaction in LMFBR piping systems.* J. Pressure Vessel Technol., 1988. **110**: p. 177-181.
69. Hatfield, F.J. and D.C. Wiggert, *Seismic pressure surges in liquid-filled pipelines.* J. Pressure Vessel Technol., 1990. **112**: p. 279-283.
70. Bettinali, F., et al., *Transient analysis in piping networks including fluid-structure interaction and cavitation effects*, in *Transactions of SMiRT 11*1991: Tokyo. p. Paper K35/5, 565-570.
71. Ogawa, N., T. Mikoshiba, and C. Minowa, *Hydraulic effects on a large piping system during strong earthquakes.* J. Pressure Vessel Technol., 1994. **116**: p. 161-168.
72. W. Weaver, J., S.P. Timoshenko, and D.H. Young, *Vibration problems in engineering*. 5th ed 1990 Wiley
73. Narayanaswami, R. and H.M. Adelman, *Inclusion of transverse shear deformation in finite element displacement formulation.* AIAA Journal, 1974. **12**(11): p. 1613-1614.

74. LIN, Y.-H. and Y.-K. TSAI, *Nonlinear vibrations of Timoshenko pipes conveying fluid.* Int. J. Solid Structure 1997. **34**(23): p. 2945-2956.
75. Chu, C.L. and Y.H. Lin, *Finite element analysis of fluid-conveying Timoshenko pipes.* Shock and Vibration, 1995. **2**: p. 247-255.
76. Jaeger, C., *The theory of resonance in hydropower systems. Discussion of incidents and accident ocurring in pressure systems.* ASME Journal of Basic Engineering, 1963. **85**: p. 631-640.
77. Zhang, N., *Dynamic condensation of mass and stiffness matrices* Journal of Sound and Vibration, 1995. **188**(4): p. 601-615.

APPENDIX

Appendix A. Drawing components and structure of experiment

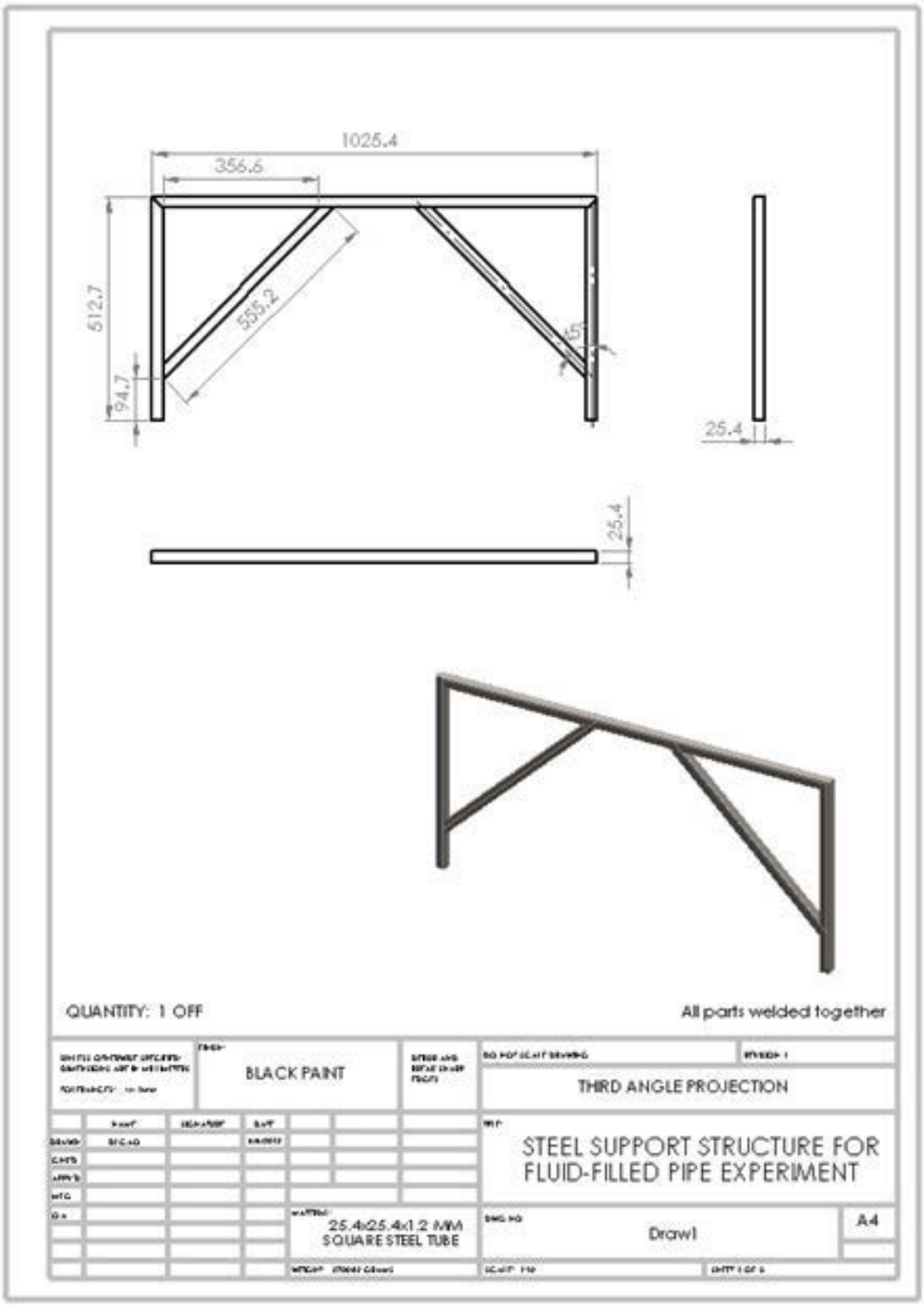

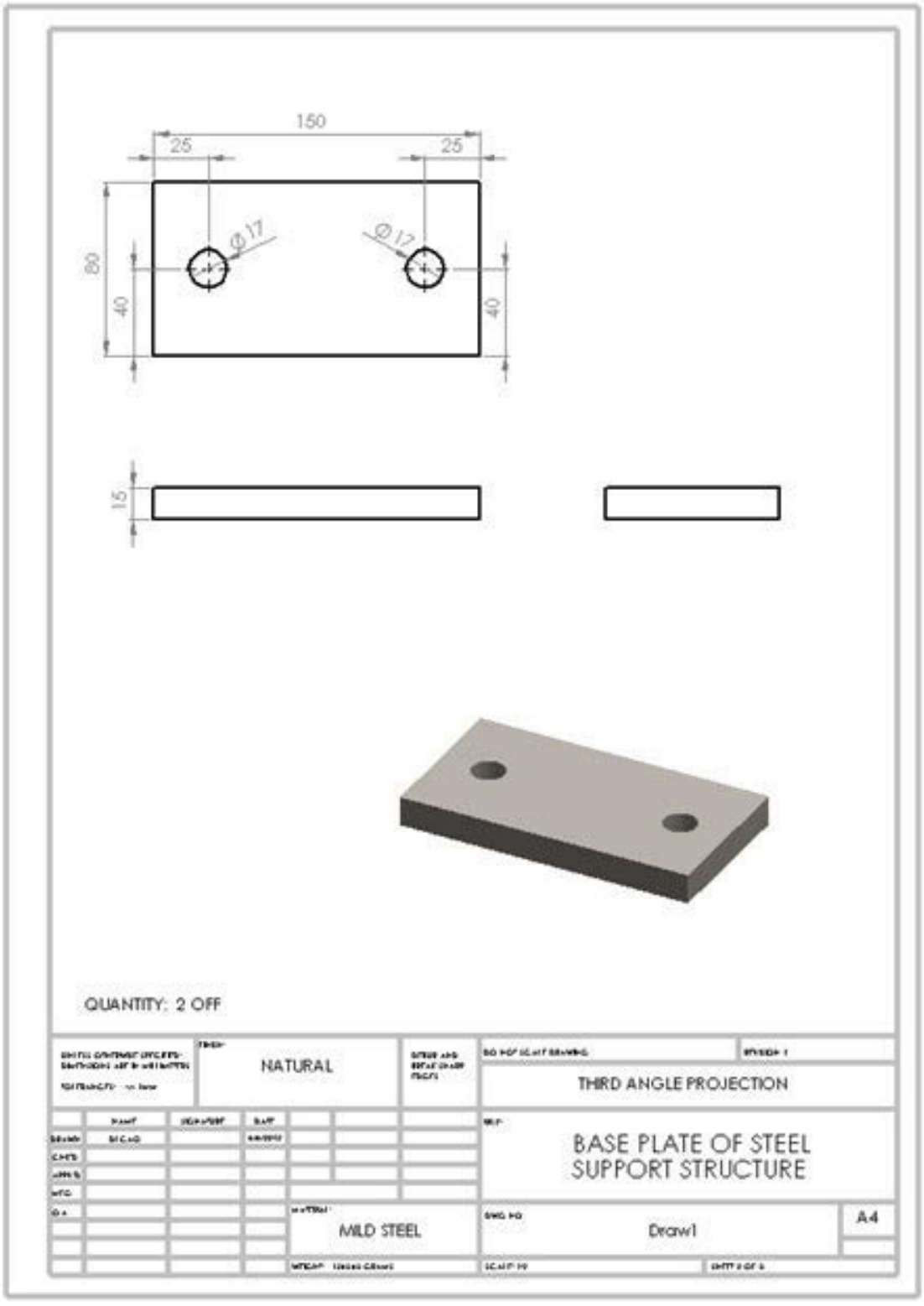
150
25
25
Ø17
Ø17
80
40
40
15
QUANTITY: 2 OFF
NATURAL
THIRD ANGLE PROJECTION
BASE PLATE OF STEEL
SUPPORT STRUCTURE
MILD STEEL
Draw1
A4

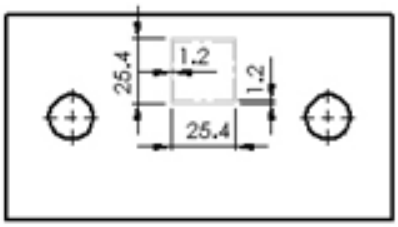

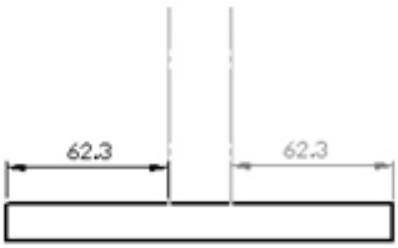

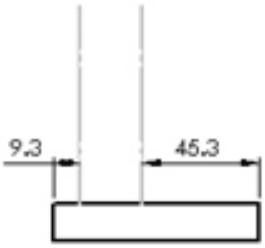

Tube end of support structure are welded on base plate

THIRD ANGLE PROJECTION

THE POSITION OF STEEL SUPPORT ON BASE-PLATE

MILD STEEL

Draw1

A4

Tube end of support structure are welded on base plate

THE POSITION OF SUPPORT STRUCTURE ON BASE-PLATE

MILD STEEL

Draw1

A4

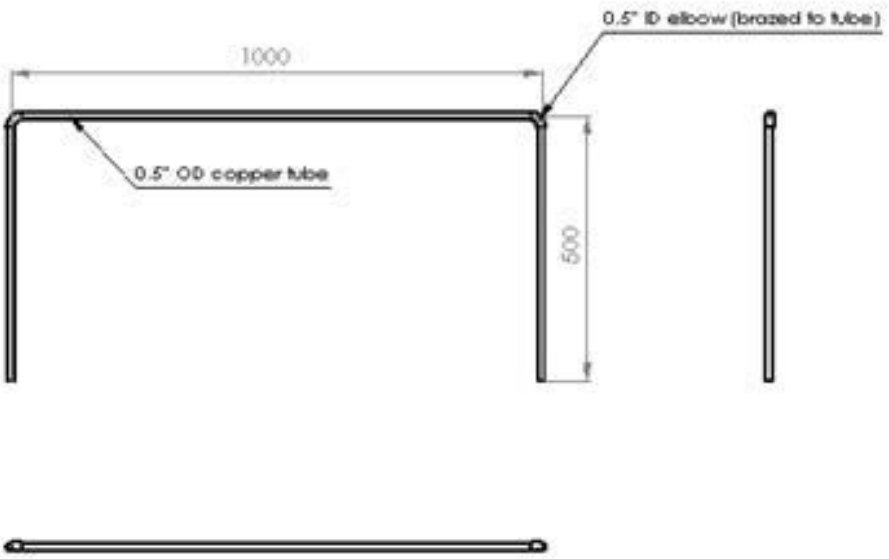

QUANTITY: 1 OFF

All parts welded together

Natural	
	THIRD ANGLE PROJECTION
	FLUID-FILLED PIPE
12.7x1.2 MM CIRCULAR COPPER TUBE	Draw1
	A4

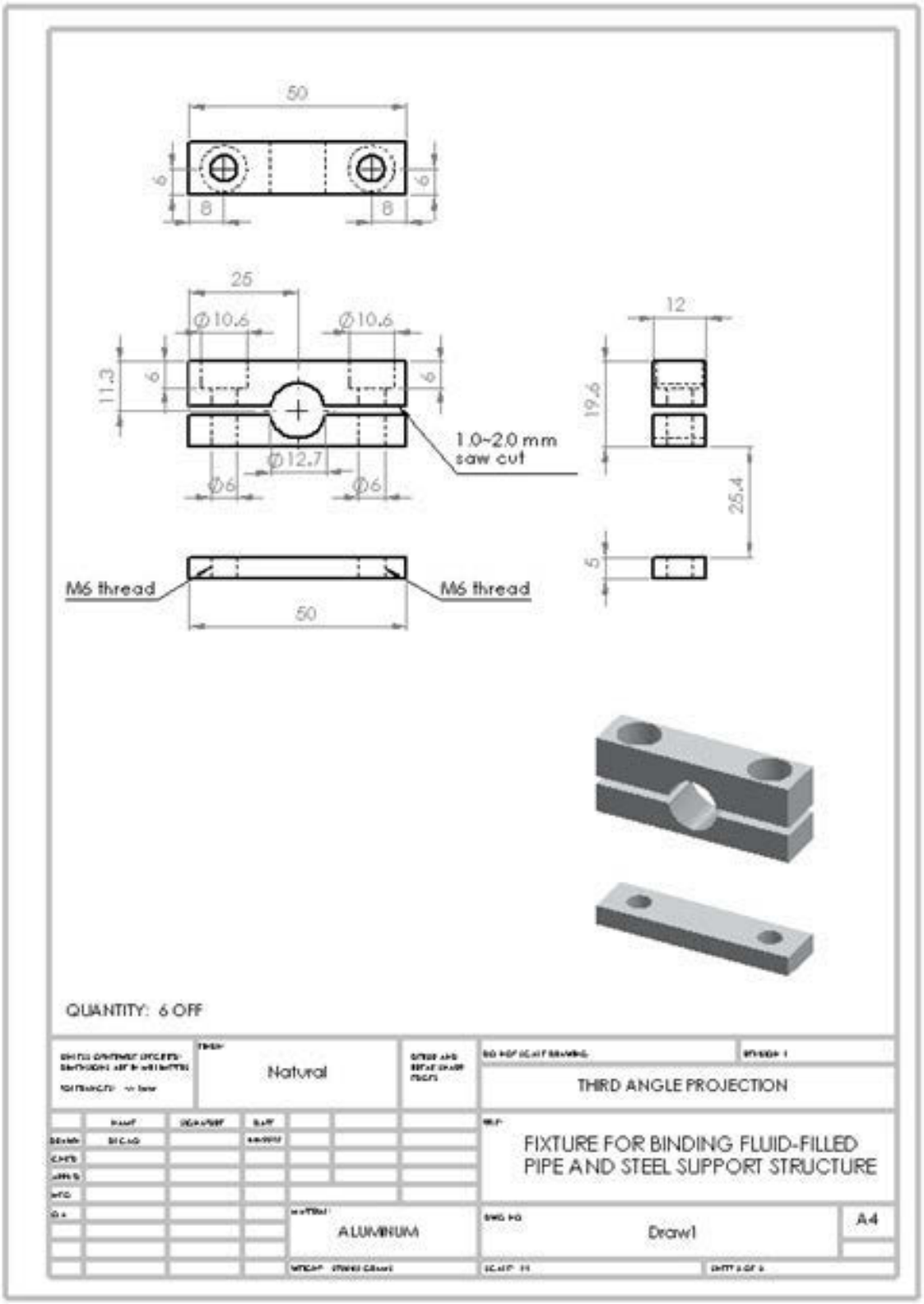
50
6
6
8
8
25
Ø10.6
Ø10.6
11.3
6
6
Ø12.7
Ø6
Ø6
1.0~2.0 mm
saw cut
12
19.6
25.4
5
M6 thread
M6 thread
50
QUANTITY: 6 OFF
Natural
THIRD ANGLE PROJECTION
FIXTURE FOR BINDING FLUID-FILLED
PIPE AND STEEL SUPPORT STRUCTURE
ALUMINUM
Draw1
A4

ITEM NO.	PART NUMBER	DESCRIPTION	QTY.
1	Support structure		1
2	Pipe structure		1
3	Connecter		5

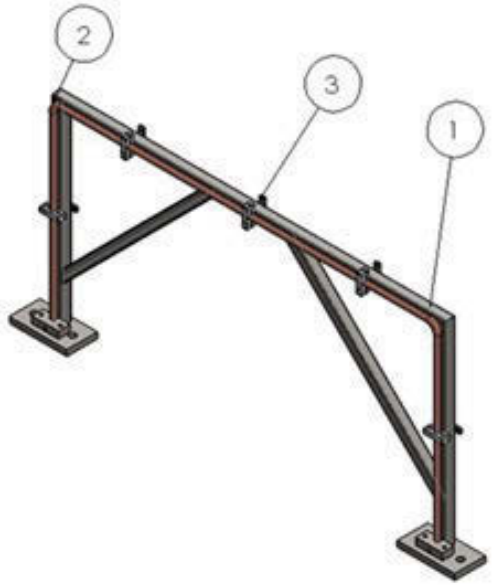

THIRD ANGLE PROJECTION

Combined Structure

Draw1

A4

Appendix B. Specification of Impulse Hammer

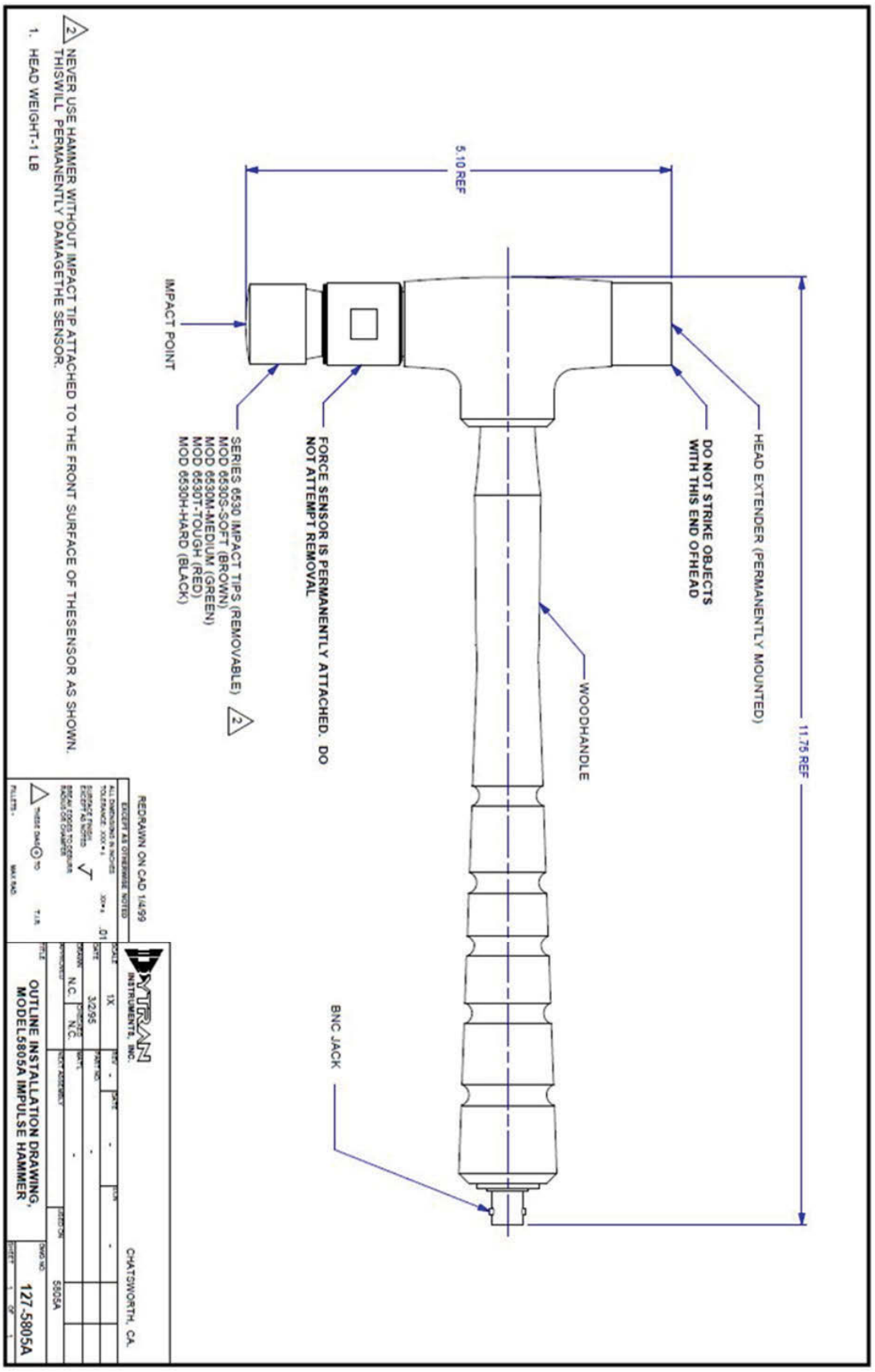

DYTRAN INSTRUMENTS, INC.

SPECIFICATIONS MODEL 5805A 1 POUND HEAD IMPULSE HAMMER

SPECIFICATION	VALUE	UNITS
RANGE, NOMINAL FOR +5 VOLTS OUT	5000	LBS
SENSITIVITY, ±10%	1.0	mV/LB
MAXIMUM INPUT	10,000	LBS
STIFFNESS, FORCE SENSOR	8.0	LB/μ IN
RESONANT FREQUENCY, SENSOR WITH NO IMPACT CAP	>50	kHz
LINEARITY	+/- 2	% FS
F.S. OUTPUT	+5	VOLTS
OUTPUT IMPEDANCE, NOM	100	OHMS
BIAS VOLTAGE, INTEGRAL AMPLIFIER	+7.5 to +9.5	VDC
INPUT CURRENT RANGE [1]	2 to 20	mA
COMPLIANCE (SUPPLY) VOLTAGE RANGE [1]	+18 to +30	VOLTS DC
MATERIAL		
FORCE SENSOR	17-4 PH	ST. STEEL
HAMMER HEAD	STEEL	CAST
HANDLE	WOOD	
WEIGHT, HEAD WITH FORCE SENSOR	1.0	POUNDS
CONNECTOR, AT END OF HANDLE	BNC	JACK

ACCESSORIES SUPPLIED:
(1) 6530S IMPACT TIP, SOFT (BROWN)
(1) 6530M IMPACT TIP, MEDIUM, (GREEN)
(1) 6530T IMPACT TIP, TOUGH, (REF)
(1) 6530H IMPACT TIP, HARD, (BLACK)

[1] Supply power from constant current source power sources only. Do not use with power supply without current limiting, 20 mA maximum. To do so will destroy built-in amplifier.

<From http://www.dytran.com/img/products/5805A.pdf>

Appendix C. Specification of Vibration shaker

PERFORMANCE RATINGS

** Rated output with forced air cooling; Derate 50% for natural convection cooling*

Description	PM25A	PM50A	PM100A	PM250HP	PM500HP
Force Output Displacement	25 pounds Pk* 0.5" Pk-Pk	50 pounds Pk* 0.5" Pk-Pk	100 pounds Pk* 0.5" Pk-Pk	250 pounds Pk* 2" Pk-Pk	500 pounds Pk* 2" Pk-Pk
Velocity	70 in/sec Pk	70 in/sec Pk	70 in/sec Pk	60 in/sec Pk	60 in/sec Pk
Acceleration (bare table) Frequency Range	50 g Pk DC-10,000 Hz	80 g Pk DC-10,000 Hz	106 g Pk DC-7000 Hz	80 g Pk DC-3500 Hz	80 g Pk DC-3000 Hz
Cooling	8 scfm @3" H_2O	13 scfm @3" H_2O	26 scfm @12" H_2O	80 scfm @30" H_2O	80 scfm @30" H_2O
Coil Current & Resistance Suspension Stiffness	4 amps; 2.7 ohms 75 lbs/in	8.5 amps; 1.3 ohms 75 lbs/in	8 amps; 2.6 ohms 75 lbs/in	40 amps; 0.21 ohms 40 lbs/in	38 amps; 0.5 ohms 40 lbs/in
Stray Field - 1" over center	< 20gauss	< 7 gauss	< 8 gauss	< 40 gauss	< 20 gauss
DC Centering				Drives 25 lbs to 1" Pk-Pk with 20% force derating	Drives 50 lbs to 1" Pk-Pk with 20% force derating

MECHANICAL SPECIFICATIONS

Description	PM25A	PM50A	PM100A	PM250HP	PM500HP
Mounting Surface Bolt Holes	Six 10-32 threaded holes at 60° on 2.25" bolt circle (+ center)	Six 10-32 threaded holes at 60° on 2.25" bolt circle (+ center)	Six 10-32 threaded holes at 60° on 2.25" bolt circle (+ center)	Six ¼x28 threaded holes at 60° on 3.50" bolt circle (+ center)	Six ¼x28 threaded holes at 60° on 3.50" bolt circle (+ center)
Moving Element Diam.	2.70"	2.70"	2.70"	4.10"	4.10"
Base Footprint	10" x 7.5"	10" x 7.5"	10" x 7.5"	18" x 14"	18" x 14"
Body Diameter	7"	7"	7"	14¼"	14¼"
Height (to table top)	7½"	9½"	13½"	17¼"	20¼"
Moving Element Axial Resonance	8200 Hz	8000 Hz	6000 Hz	3000 Hz	2800 Hz
Weight, Moving Element	0.50 pounds	0.62 pounds	0.94 pounds	2.6 pounds	5.0 pounds
Weight, Exciter	38 pounds	55 pounds	80 pounds	250 pounds	420 pounds
Weight, Base	7 pounds	11 pounds	15 pounds	25 pounds	25 pounds
Base Type	2-position; rigid	2-position; rigid	2-position; rigid	trunnion	trunnion
Trunnion Base	optional	optional	optional	standard	standard
Cooling Connections	0.5" NPT	0.5" NPT	0.5" NPT	2.0" port	2.0" port

(Ratings & Specifications subject to change without notice 05/97)

<From http://www.mbdynamics.com/assets/datasheets/PMSERIESProductBrief.pdf>